AGGREGATION-DICTATED PHOTOPHYSICS OF CONJUGATED POLYMERS.

BY

ENINGES ASMARE

A **DISSERTATION** SUBMITTED TO

THE DEPARTMENT OF PHYSICS OF ADDIS ABEBA UNIVERSITY

IN PARTIAL FULFILLMENT OF THE REQUIREMENTS FOR THE DEGREE OF **DOCTOR OF PHILOSOPHY IN PHYSICS (POLYMER PHYSICS)**

ADDIS ABEBA

ETHIOPIA

January 30, 2025

ADDIS ABEBA UNIVERSITY

DEPARTMENT OF PHYSICS

The undersigned hereby certify that they have read and recommended to the College of Natural and Computational Sciences for acceptance a thesis entitled "**Aggregation-dictated Photophysics of Conjugated Polymers**" by **Eninges Asmare** in partial fulfillment of the requirements for the degree of **Doctor of Philosophy**.

Dated: **January 30, 2025**

Approved by the Examination Committee

External Examiner: _____

Dr. Christine Steenkamp

Internal Examiner: _____

Dr. Lemi Demeyu

Advisor: _____

Newayemedhin A. Tegegne (Professor of Physics)

Co-Advisor: _____

Tjaart P. J. Krüger (Professor of Physics)

Chairman: _____

Dr. Kenate Nemera

ADDIS ABEBA UNIVERSITY

Date: **January 30, 2025**

Author: Eninges Asmare

Title: **Aggregation-dictated Photophysics of Conjugated Polymers.**

Department: **Physics**

Degree: **Ph.D.** Convocation: **January 30, 2025**

Permission is herewith granted to Addis Abeba University to circulate and to have copied for non-commercial purposes, at its discretion, the above title upon the request of individuals or institutions.

Signature of Author

The author reserves other publication rights, and neither the thesis nor extensive extracts from it may be printed or otherwise reproduced without the author's written permission. The author attests that permission has been obtained for the use of any copyrighted material appearing in this thesis (other than brief excerpts requiring only proper acknowledgment in scholarly writing) and that all such use is clearly acknowledged.

DECLARATION

I hereby declare that this PhD dissertation is my original work, has not been presented for a degree in any other university and that all the sources of material used for the dissertation have been fully acknowledged.

Name: Eninges Asmare

Signature: _____

Place and time of submission:

Addis Abeba University

January 30, 2025

Contents

List of Figures

List of Tables

List of Acronyms

2T-BT-2T – Bithiophene-benzothiadiazole-bithiophene

2T-DPP-2T – Bithiophene-diketopyrrolopyrrole-bithiophene

A – Acceptor

AnE-PVstat – Anthracene-containing poly(phenylene ethynylene)-alt-(phenylenevinylene) statistical

BDT – 4,8-bis(decyl)benzo[1,2-b;4,5-b']dithiophene

BHJ – Bulk hetrojunction

BTIC-CF_3-m – Trifluoromethyl 4,4,10,10-tetrakis(4-hexylphenyl)-5,11-(2-ethylhexyloxy)-4,10-dihydrodithienyl[1,2-b:4,5b]benzodi-thiophene-2,8-diyl)bis(2-(3-oxo2,3-dihydroinden-1-ylidene)malononitrile

BTP-eC9 – 2,2'- [[12,13-Bis(2-butyloctyl)-12,13-dihydro-3,9-dinonylbisthieno[2',3':4',5']thieno[2',3':4,5]pyr
e:2',3'-g][2,1,3]benzothiadiazole-2,10-diyl]bis[methylidyne(5,6-chloro-3-oxo-1H-indene-2,1(3H)-diylidene)
]]bis[propanedinitrile]

CF – Chloroform

CN – 1-chloronaphthalene

CT – Charge transfer

D – Donor

D18-Cl – Poly[(2,6-(4,8-bis(5-(2-ethylhexyl-3-chloro)thiophen-2-yl)-benzo[1,2-b:4,5-b']dithiophene))-alt-5,5'-(5,8-bis(4-(2-butyloctyl)thiophen-2-yl)dithieno[3',2':3,4;2",3":5,6]benzo[1,2-c][1,2,5]thiadiazole)]

DFT – Density functional theory

DIB – 1,4-diiodobutane

DIH – 1,6-diiodohexane

DIO – 1,8-diiodooctane

DTS($PTTh_2$)$_2$ – 5,5'-bis(4-(7-hexylthiophen-2-yl)thiophen-2-yl)-[1,2,5]thiadiazolo[3,4-c]pyridine-3,3'-di-2-ethylhexylsilylene-2,2'-bithiophene

ESP – Eelectrostatic potential

FC – Franck-Condon

FET – Field-effect transistor

FF – Fill factor

FMO – Frontier molecular orbitals

FRET – Förester resonance energy transfer

HOMO – Highest occupied molecular orbital

HR – Huang-Rhys

ICT – Intramolecular charge transfer

IRF – Instrument response function

isoIDITC – 2,2'-((2Z,2'Z)-((4,4,6,6-Tetraoctyl-4,6-dihydro-s-indaceno[1,2-b:7,6-b']dithiophene-2,8-diyl)bis(methaneylylidene))bis(3-oxo-2,3-dihydro-1H-indene2,1-diylidene))dimalononitrile

QY – Quantum yield

L8-BO – 2,2'-((2Z,2'Z)-((12,13-bis(2-ethylhexyl)-3,9-(2-butyloctyl)-12,13-dihydro-[1,2,5]thiadiazolo[3,4-]thieno[2",3":4',5']thieno[2',3':4,5]pyrrolo[3,2-g]thieno[2',3':4,5]thieno[3,2-b]indole-2,10-diyl)bis(methanylylidene)difluoro-3-oxo-2,3-dihydro-1H-indene-2,1-diylidene))dimalononitrile

LCAO – Linear combination of atomic orbitals

LED – Light-emitting diode

LUMO – Lowest unoccupied molecular orbital

MEH-PPV – Poly[2-methoxy-5-(2 0 -ethyl-hexyloxy)-1,4-phenylene vinylene]

MPP – Molecular planarity parameter

OSC – Organic solar cell

P2TI – Poly(bithiophene-isoindigo)

P2TITT – Poly(thieno[3,2-b]thiophene-spaced-bithiophene-isoindigo)

P3HT – Poly(3-hexylthiophene)

PBDTI-DT – Poly(4,8-bis(decyl)benzo[1,2-b;4,5-b']dithiophene-isoindigo)-2-decyltetradecyl

PC_{70} BM – [6,6]-phenyl-C71-butyric acid methyl ester

PCE – Power conversion efficiency

PDA – Poly(diacetylene)

PDOS – Partial density of state

$p-DTS(FBTTH_2)_2$ – 7,7-[4,4-Bis(2-ethylhexyl)-4H-silolo[3,2-b:4,5-b]dithiophene-2,6-diyl]bis[6-fluoro-4-(5-hexyl-[2,2-bithiophen]-5-yl)benzo[c][1,2,5]thiadiazole]

PL – Photoluminescence

PM6 – Poly[(2,6-(4,8-bis(5-(2-ethylhexyl-3-fluoro)thiophen-2-yl)-benzo[1,2-b:4,5-b']dithiophene))-alt-(5,5-(1',3'-di-2-thienyl-5',7'-bis(2-ethylhexyl)benzo[1',2'-c:4',5'-c']dithiophene-4,8-dione)]

PMMA – Polymethyl methacrylate

PPEB – Poly(para-phenylene-ethynylene-butadiynylene)

PSC – Polymer solar cell

PTB7-Th – Poly[4,8-bis(5-(2-ethylhexyl)thiophen-2-yl)benzo[1,2-b;4,5-b']dithiophene-2,6-diyl-alt-(4-(2-ethylhexyl)-3-fluorothieno[3,4-b]thiophene-)-2-carboxylate-2-6-diyl]

o-DCB – 1, 2-dichlorobenzene

OFET – Organic field-effect transistor

OLED – Organic light-emitting diode

OPV – Organic photovoltaic

OPVn – oligo(p-phenylene vinylene)

SDP – Span of deviation from plane

TCSPC – Time-correlated single photon counting

TD-DFT – Time-dependent density functional theory

TDOS – Total density of state

TT – Thieno[3,2-b]thiophene

UV-vis – Ultraviolet visible

Abstract

Improving the PCE in OPVs is among the pioneering researches to satisfy the world energy demand. Recently PCEs of above 19% are recorded by improving morphology of the active layer in OSCs. Molecular aggregation, which was first developed by Kasha, and Jelly and Schiebe, plays a role on the morphology of conjugated polymers. In this work, we study the aggregation photophysics of three copolymers dividing into two objectives. We used three methods - Franck-Condon (FC) analysis, HR factor evolution with temperature, and relative QY calculation - to determine the aggregates types in a benzodithiophene-isoindigo-based **(PBDTI-DT)** copolymer which show that both H- and J-aggregation types present, and the QY calculation clearly indicates dominance of H-aggregates. As a second work the effect of backbone conformation on the aggregation photophysics of isoindigo-based copolymers, namely, **P2TI** and **P2TITT** is studied. **P2TI** was systematically tuned by inserting **TT** into the former resulting in modification of the backbone and was found to affect the planarity due to reduced steric hindrance between the donor and the acceptor units, which was evidenced from the difference in oscillator strength of the first excited state transition. Temperature-dependent PL of the two polymers was well reproduced using two FC progressions, indicating the formation of both H- and J-type aggregates. This was supported by the presence of two emission lifetimes obtained from time-resolved fluorescence measurements. The evolution of the first two vibronic peaks with temperature clearly showed stronger interchain interaction in **P2TITT**.

The very lesson I learned during my PhD is this :

በፊት ሰዎች ሲነግሩኝ ፤ አይ ይሄ እንኳን ፖለቲካ ውስጥ እንጅ አካዳሚክስ ላይ አይኖርም ብዬ ያላመንኩት በታላ ግን ራሴ ያረጋገጥኩት ፤ PhD ለመስራት የሚያስፈልገው ትዕግስ ተመራማሪ መሆን ሳይሆን ትዕግስ ሸንጣ ያክል መሆን መሆኑን ነው።

Chapter 1

Introduction

Current energy sources like oil, coal, and natural gas have two major problems: they have a significant negative influence on the global climate[1] and their amount on Earth is drastically reducing over time. Finding clean and renewable energy sources that can solve the aforementioned issues is therefore essential. Given its abundance, free availability, and carbon-free nature, solar energy is a prominent alternative among other renewable energy sources. The unique qualities of organic solar cells (OSCs), including their light weight, low cost, ease of fabrication, environmental friendliness, and potential for roll-to-roll large area device manufacturing, make them highly intriguing for long-term solar energy harvesting technology.[2] In this regard, among the pioneering researches to satisfy the world energy demand, the primary one is improving the power conversion efficiency (PCEs) in organic photovoltaics (OPVs). Recently certified PCEs of above 19% are recorded by improving morphology of the active layers in OSCs.[3] One way of improving morphology of active layers is adding a donor[3,4] or acceptor[5–7] to a donor-acceptor binary blend in order to form ternary blends. Even in binary blends, solvent and solid additives,[8] processing techniques aiming at facilitating inter-diffusion between donor and acceptor,[9] materials manipulation by a crystallization regulator that optimizes the film crystallization process[10] and molecular design[11] are also found to be able to improve the PCE by providing with desired morphologies.

Establishing structure-property relationships in polymers and blends for photovoltaic applications requires an understanding of the complexity of structures and related quantitative pa-

rameters. If we zoom-in a bulk hetrojunction (BHJ) active layer, we learn that the morphology is dictated by phase-separated structure which is characterized by domain size and purity of donor and acceptor, vertical composition distribution and interaction parameter of polymer/solvent and donor/acceptor. Further zooming-in the phase-separated structure, the molecular aggregation which is characterized by parameters such as stacking distance and percentage of edge-on or face-on orientation appears to play a major role on the morphology.[12] Hence, studying the molecular aggregation and corresponding photophysics in conjugated polymers is essential to improving morphology of OPV active layers with appropriate post-processing techniques.

The molecular aggregation theory was first developed by Kasha,[13–18] and Jelley[19,20] and Schiebe[21,22] on the dye aggregates employing Coulombic dipole-dipole interaction. Following the Kasha model a lot of studies have been conducted to determine the aggregation types formed in polymers using different techniques.[23–42] The aggregate formation and corresponding photophysics on conjugated polymers are studied from the simple dimer to more complex structures. Conjugated polymers may assemble in structures with properties of either J-like[43–48] or H-like[45,47–54] or may interplay between H and J-aggregates due to factors as temperature, additive, concentration or others[30,35,55–58] or as HJ-aggregates[28,32,35,55,58–62] with competing intrachain J-promoting and interchain H-promoting interactions.

Among the different techniques used in the literature to determine the aggregation types formed in polymers, some are spectral shift relative to single molecule spectra,[23,24,27,28,30,32] relative position of the absorbing/emissive excitonic band,[28,32] progression of the first two vibronic peaks with exciton band width[25,26,28,32] or temperature/disorder,[25,28,29,32] emission lifetime[26,28,30,32] and relative quantum yield (QY),[26,27,32,33] from which progression of the first two vibronic peaks with temperature, emission lifetime and relative QY are used in this work.

In this work, the aggregation and photophysics of three copolymers[63–65] are studied. To this end the thesis is organized as follows: In chapter two a review of selected works on molecular packing ever since Kasha developed a head-to-tail and card-pack model is presented. The experimental and computational techniques employed in this work are explained in chapter three. Chapter four is devoted to an investigation on aggregation types in a benzodithiophene isoindigo copolymers using FC analysis on temperature-dependent photoluminescence (PL). In chapter five

the aggregation photophysics of bithiophene-isoindigo-based copolymers are addressed. Chapter six presents the summary of the work and future outlooks.

Problem Statement

Conjugated polymers are applicable in organic light-emitting diodes (OLED), organic field-effect transistors (OFET), and OSCs depending on their photophysical properties and packing types. Studying the aggregation and photophysics of conjugated polymers is important to modulating the synthesis of polymers that could give improved efficiencies of the corresponding applications. On the other hand, identifying the type of aggregation in a polymer enables one to recommend the polymer for a specific type of application. Among the many polymers synthesized at Prof. Wendmagegn Mamo's research group lab, benzodithiophene- and bithiophene-isoindigo-based copolymers have promising PCEs. Hence, in this work three selected conjugated polymers - benzodithiophene- and bithiophene-based copolymers - are characterized using experimental and computational techniques.

Objective

The main objective of this work is to assess the aggregation photophysics of selected copolymers. To achieve this objective two specific objectives were set: investigate the aggregation types in a benzodithiophene-isoindigo copolymer and assess conformation-dictated aggregation photophysics in isoindigo-based copolymers.

Chapter 2

Review on Aggregation Photophysics of Conjugated Polymers

2.1 Semiconducting Properties of Conjugated Polymers

The term 'organic semiconductors' primarily refers to two things: first, that the materials are mostly composed of carbon and hydrogen atoms, with other heteroatoms like sulfur, oxygen, and nitrogen; second, that the materials usually exhibit semiconducting properties, which refers to the ability to absorb and emit visible light as well as a conductivity level high enough to power solar cells, field-effect transistors (FETs), and light-emitting diodes (LEDs). The semiconducting properties of organic semiconductors have a distinct feature different from their inorganic counterpart. In inorganic semiconductors because of their low band gaps thermal excitation can create free charges. In addition, absorption of light at room temperature creates even more free charge carriers due to their large dielectric constant which screens the Coulomb effect between electrons and holes. On the contrary, in the case of organic semiconductors, conductivity is caused by either of the following external factors; injection of charges at electrodes, intentional[66] or unintentional doping and dissociation of excitons which are created by light absorption and bound by mutual Coulomb attraction.[67] This extrinsic conductivity of organic semiconductors is mainly a characteristic feature of the electronic configuration of the carbon atom.

The electronic configuration in the ground state of carbon atom is $1s^2 2s^2 2p^2$ and changes to

$1s^2 2s^1 2p^3$ to form molecules. This configuration is obtained by the excitation of one of the 2s electrons to a 2p state. The valence electrons in $2s^1 2p^3$ could have three different configurations in forming compounds, resulting in sp^3, sp^2 or sp^1 hybrid orbitals. In sp^3 hybridization, also known as tetragonal hybridization, four hybrid equivalent orbitals are produced by the combination of the four electron orbitals. These hybrid orbitals which are oriented toward the corners of a conventional tetrahedron centered on the carbon atom make single bonds with other atoms to form saturated molecules, like methane, CH_4.

In sp^2 hybridization also known as trigonal hybridization, illustrated in Figure 2.1, while one of the original p-orbitals is unchanged, mix up of s, p_x and p_y produce three equivalent hybrid orbitals. The sp^2 hybrid orbitals, lying in the same plane, makes equal angles of 120^o to each other. This arrangement gives rise to the hexagonal ring structure of polycyclic aromatic hydrocarbons. Whereas the p_z orbital which is unchanged by the sp^2 hybridization is known as π-orbital, the hybrid orbitals that are symmetrical both about the molecular plane and the bonding axes, are known as σ-orbitals. In benzene the sp^2 hybrid orbitals of carbon interact with the 1s orbitals of hydrogen and orbitals of other carbon to produce the localized C-H and C-C σ-bonds. On the other hand, the six π atomic orbitals in benzene interact and produce C-C π-bonds making the molecule more stable. σ-electrons and π-electrons differ primarily in that π-electrons are delocalized. For instance, in benzene, the π atomic orbitals of each carbon form six delocalized π molecular orbitals, as the two π atomic orbitals form two π molecular orbitals in Figure 2.1. In other aromatic molecules, there exists similar systems of delocalized π-electrons.[68] Excited states of such π-electron systems, along with their numerous transitions and interactions, give rise to interesting optoelectronic properties of conjugated polymers.

The third configuration, known as diagonal or sp^1 hybridization, is characterized by two unchanged (p_y and p_z) orbitals and two hybrid σ-orbitals that are produced by mixing of s and p_x orbitals. The σ-orbitals are oriented in a direction of 180^o to one another. Linear molecules like acetylene (H-C $\equiv$ C-H) have structure of sp^1 hybridization. The p_y and p_z atomic orbitals (π-orbitals) of each C atom are paired to form two C-C π-bonds in addition to the C-H and C-C σ-bonds.[68]

Knowledge on the energy of molecular orbitals is crucial to understand the optical and electri-

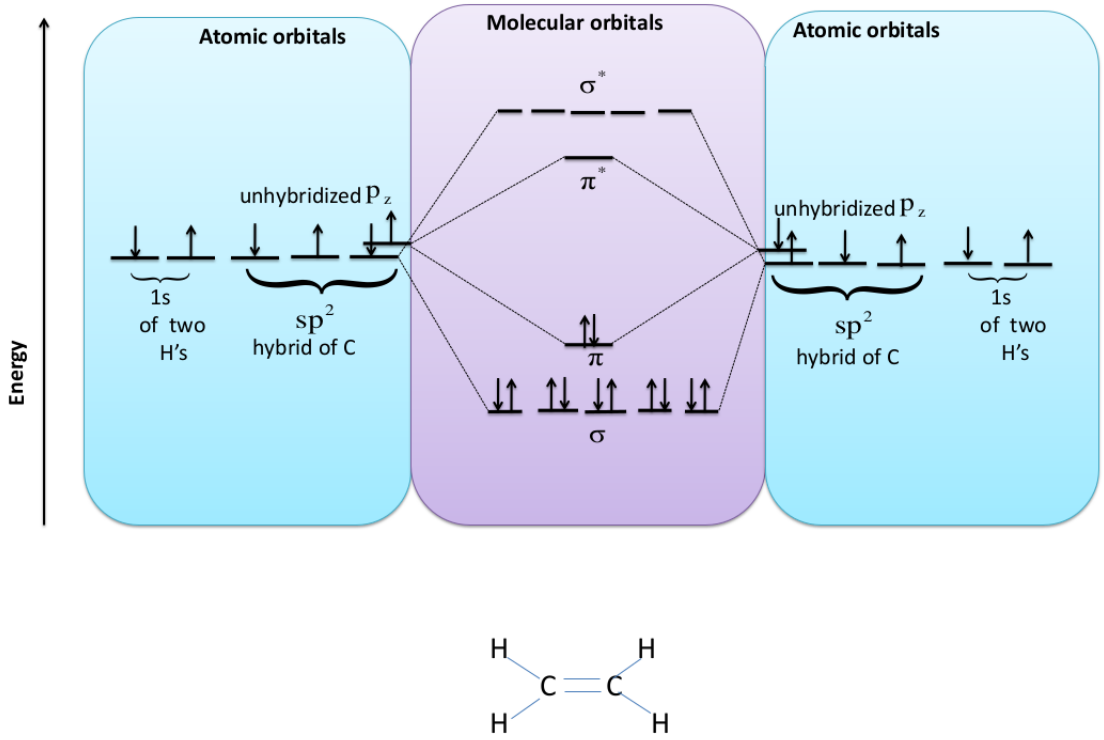

Figure 2.1: Representation of sp^2 hybridized molecular orbitals in forming C_2H_4, one of the electrons from $2s$ of C is excited to $2p$ orbital resulting in $2s^1 2p^3$ configuration.

cal processes in organic molecules. One can use a linear combination of atomic orbitals (LCAO) to approximate a molecular orbital. Take, for instance, the combination of two orbitals, ϕ_a and ϕ_b. These two orbitals may undergo a constructive, $\Psi_+ = c_1\phi_a + c_2\phi_b$, or destructive, $\Psi_- = c_1\phi_a - c_2\phi_b$ (c_1 and c_2 being positive numbers), interference. In constructive interference, the enhanced charge density between the atomic nuclei leads to a bonding character, σ, π. In contrast, in destructive interference the reduced charge density between the nuclei, in which repulsion between the nuclei is not screened by electron density, results in anti-bonding character, σ^*, π^*, see Figure 2.1.

Two essential structural characteristics are required for polymeric semiconductors to be used in OFET and OPV applications. The first is, in order to facilitate appropriate charge transport and optical absorption, π-conjugation of backbone consisting of linked unsaturated units which gives π orbitals extended over the polymer chain. While the second is functionalization of the polymer core with solubilizing substituent, which is necessary to improve solid state core interactions and enable low-cost manufacturing via solution methods. Optical absorption/emission, redox properties, frontier molecular orbital energy levels, and other significant polymer proper-

ties are controlled by the electronic structure of the polymer solution or solid state, which is determined by the degree to which polymer units conjugate or interact.[69]

2.2 Molecular Packing and Photophysics of Conjugated Polymers

2.2.1 Basics on Photophysics

The emission and absorption properties of polymers are easily understood with the help of the Jablonski diagram, Figure 2.2. As summarized in Figure 2.2, absorption (red arrows) of photon excites electrons from S_0 to S_1 or S_2 depending on the photon energy to create closely bound pairs of electron and hole (excitons). Electrons in excited states relax to lowest energy levels before de-exciting to the ground state. Then, the relaxation may be from a higher excited electronic state to lowest excited electronic state or the ground electronic state (internal conversion). It may also be from higher vibrational levels to lowest vibrational level within the same electronic state (vibrational relaxation) or from the singlet state to the triplet state (intersystem crossing). The energy lost due to vibrational relaxation and internal conversion is transferred to vibrational (kinetic) energy. After relaxation, the electrons de-excite from the singlet excited state, S_1, (fluorescence) or from the triplet state, T_1, (phosphorescence) to the ground electronic state. The non-radiative decays, internal conversion ($10^{-11} - 10^{-9}s$) and vibrational relaxation ($10^{-12} - 10^{-10}s$), exceed any radiative transitions, fluorescence ($10^{-10} - 10^{-7}s$) and phosphorescence ($10^{-6} - 10s$), by orders of magnitude according to Valeur and Berberan-Santos.[70]

The likelihood of transitions in absorption/emission between the ground and excited states is dictated by selection rules. Energy, multiplicity, and symmetry - which in centrosymmetric molecules includes parity - are fundamental characteristics of the electronic state. The intensity distribution among electronic transitions are affected by selection rules like multiplicity, symmetry, and parity.[68]

There are even numbers of electrons in a condensed aromatic hydrocarbon. According to the Pauli principle the spin of these electrons are paired and give singlet electronic states in

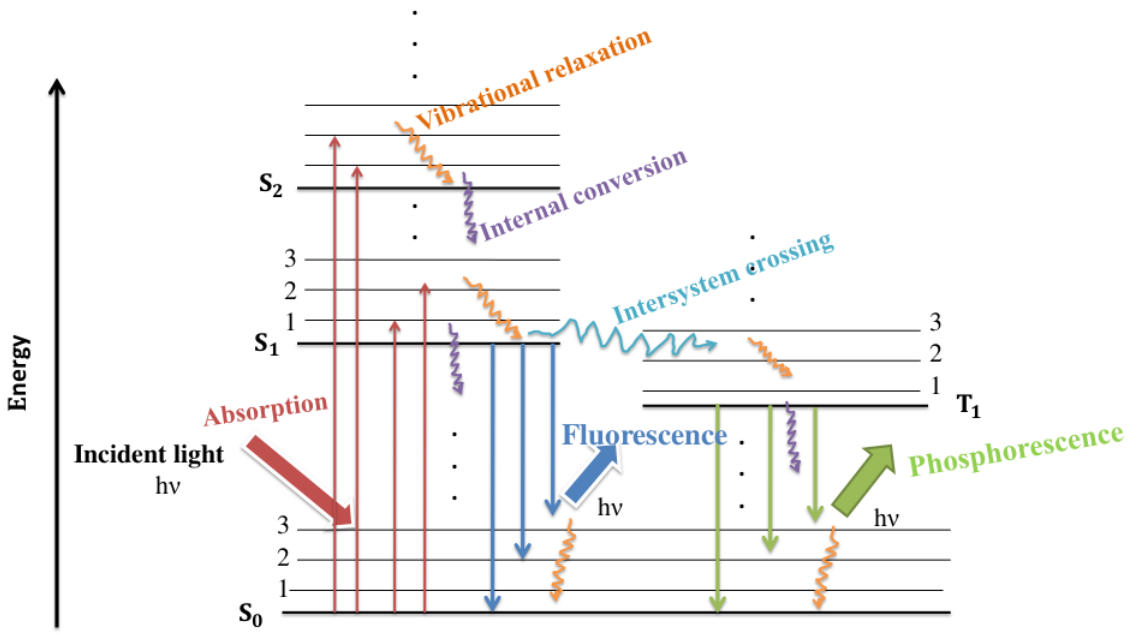

Figure 2.2: Jablonski diagram demonstrating different transitions between S_0 (ground state) and S_1 and S_2 (singlet excited states) or T_1 (triplet excited state) with vibrational levels denoted by 1, 2, 3, ...

unexcited molecules. In the excited electronic state, a singlet state results from the excitation of π-electron without spin change in the molecule. The excited electronic state of a molecule becomes triplet state when an excited π-electron experiences a spin reversal during the transition. For an electronic state, the terms singlet (multiplicity of 1) and triplet (multiplicity of 3) indicate multiplicity, which describes its degree of degeneracy where there is no a perturbing magnetic field. Electric dipole transitions between electronic states with differing multiplicities are spin-forbidden. The probability of transitions between distinct electronic states is also influenced by the symmetry selection criterion. Accordingly, electric dipole transitions that occur between electronic states of the same symmetry are forbidden. Depending on whether the electronic wavefunction in a centrally symmetric system is symmetric or anti-symmetric about reflection in the center of gravity, the states are classified as even (g = gerade) or odd (u = ungerade). The parity selection rule prohibits electric dipole transitions between states that have the same parity. This selection rule permits (prohibits) transitions from the even-parity ground state to the odd (even) parity excited state.

The intensity distribution among the various transitions in absorption and emission is dictated by the relative position of excited-state and ground-state equilibrium geometries demonstrated by

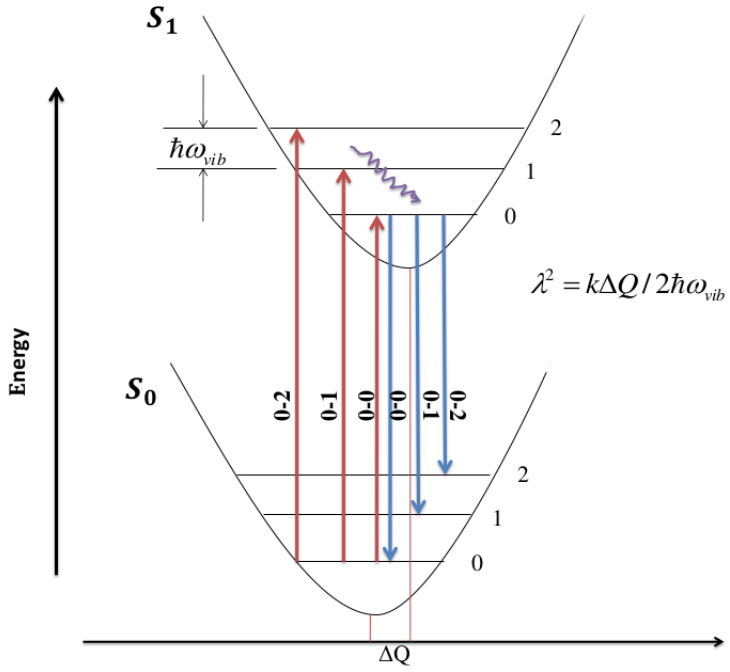

Figure 2.3: Equilibrium position displacement ΔQ of the ground-state and excited-state potentials with possible transitions (absorption in red and emission in blue).

the potential energy surfaces in Figure 2.3. The spectral intensity distribution can be estimated by the FC Principle which assumes all transitions to be vertical and proportional to the overlap integral of the vibrational wave functions involved in the transitions squared, see Figure 2.3. The Born-Oppenheimer approximation, or adiabatic approximation - which itself is predicated on the idea that electronic and nuclear motions can be distinguished, i.e., that they take place in separated time domains - is the foundation of the FC Principle. This is corroborated by the observation that electrons move in molecules with fixed nuclei because mass of electron is significantly smaller than mass of the nucleus. Mathematical derivations of FC analysis derived from Born-Oppenheimer approximation is shown in Section 3.3.

Depending on the integral overlap between states involved in electronic transitions, the relative intensity of pure electronic (0-0) and side-band (0-1,0-2,...) transitions is illustrated in Figure 2.4. In Figure 2.4 three different cases are shown; Figure 2.4 A) shows the intensity distribution in which the Huang-Rhys (HR) factor, which is related to the average number of phonons excited when an electron makes a transition between two electronic states, λ^2 equals to unity. Figures 2.4 B) and C), respectively, represent λ^2 values less than and greater than one. Because $\lambda^2 = \frac{k\Delta Q}{2\hbar\omega} = \frac{E_{relx}}{\hbar\omega}$ where $E_{relx} = \frac{k\Delta Q}{2}$ is relaxation energy or reorganization energy and

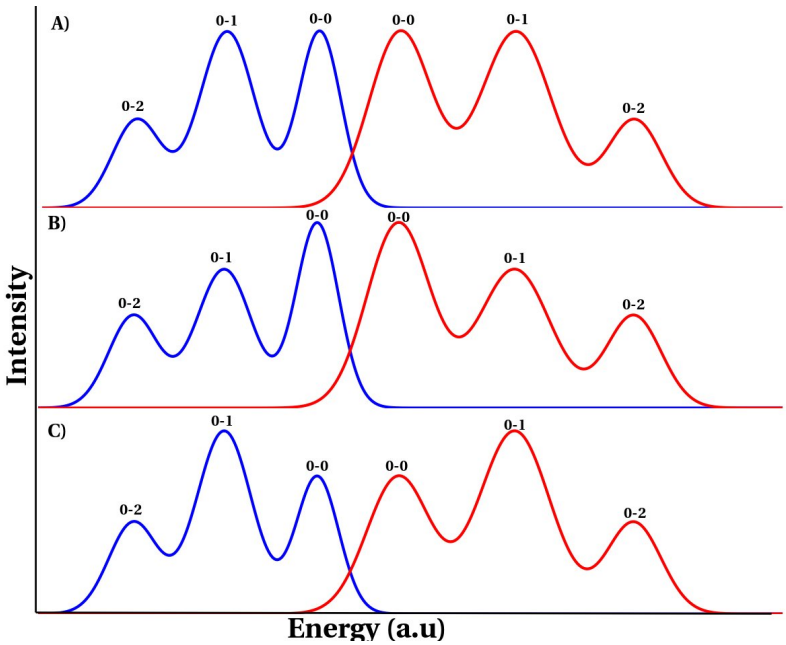

Figure 2.4: Possible intensity distributions in absorption (red) and emission (blue) according to Frank-Condon Principle.

$\hbar\omega$ is vibrational energy, the value of λ^2 reflects on the relative strength of vibrational energy and the corresponding reorganization energy associated with electronic transitions.

Energy and Electron Transfer Reactions

Along with the intrinsic decay mechanisms outlined by the Jablonski diagram, energy and electron transfer reactions are frequently observed in a system consisting of two molecules with differing electronic energy levels. In conjugated polymers, photoexcitation generates singlet excited states whereby the hole and electron are bound by Coulombic attraction. In energy transfer reaction, the excitation energy transfers from the donor component to component. Figure 2.5 illustrates an energy transfer reaction in which the excited donor deexcites to the ground state concomitantly exciting the acceptor. In electron transfer reactions, on the other hand, depicted in Figure 2.6, a charge-separated state is formed from the additional energy of an absorbed photon, in which the acceptor and the donor are, respectively, negatively and positively charged. If the excitation involves the donor whereby an electron is promoted from the highest occupied molecular orbital (HOMO) to the lowest unoccupied molecular orbital (LUMO) by absorption of a photon and the LUMO of the donor is higher in energy than the LUMO of the acceptor,

transfer of electron can take place from the donor to the acceptor.

There are two mechanisms called Förster and Dexter which describe energy transfers,[71] Figure 2.5. In Förster mechanism, which often explains singlet energy transfer, the photoexcited donor deexcites to the ground state concomitantly exciting the acceptor by coupling of transition dipole moments at the acceptor and donor interface. In other words, Förster energy transfer takes place when the photon energy emitted from the donor is equivalent to the excitation energy of the acceptor, or mathematically, $D(S1) \rightarrow D(S0) + h\nu \Rightarrow \ A(S0) + h\nu \rightarrow A(S1)$. Because it depends on the resonance between the absorption of the acceptor and the emission of the donor, the process is also known as Förster resonance energy transfer (FRET). The distance between the acceptor and donor molecules as well as the absorption coefficient of the acceptor and radiative decay of the donor affects FRET. In contrast, due to overlap of the acceptor and donor orbitals, in Dexter energy transfer which is important for triplet-triplet energy transfer reaction double exchange of electrons takes place, bottom of Figure 2.5. The efficiency of this process decreases with the distance between acceptor and donor exponentially. Van Hal[72] observed a singlet-energy transfer reaction in donor-acceptor oligothiophene (nT) moiety of $C_{60} - nT - C_{60}$ triads dissolved in toluene, and a triplet-energy transfer from the fullerene molecule to the oligo(p-phenylene vinylene) (OPVn) molecules in mixtures of OPVn and N-methylfulleropyrrolidine.

According to Marcus theory[73] the transition state formulation can be used to treate the electron transfer reaction labeling the excited donor/acceptor complex (D^*A) and the charge-separated donor and acceptor (D^+, A^-) states as the reactant and product states, respectively, Figures 2.6 and 2.7. Figure 2.7 demonstrates the reactant and product potential energy surface states, the changing geometries being represented by the displacement coordinate. To meet the FC principle and energy conservation criteria, electron transfer must take place at the interface of the two states - reactant state and product state. According to the FC principle, because the nuclei are thought to be frozen for this period, photoexcitation of the D-A causes a transition between the ground and excited states to be vertical. Thermally equilibrated singlet excited state is obtained following vibrational relaxation. This energetically lowest excited state is then used to describe electron transfer process.[72] Figure 2.6 provides a schematic description of the electron transfer from this lowest excited state. Therefore, as shown in Figure 2.7, electron transfer is only

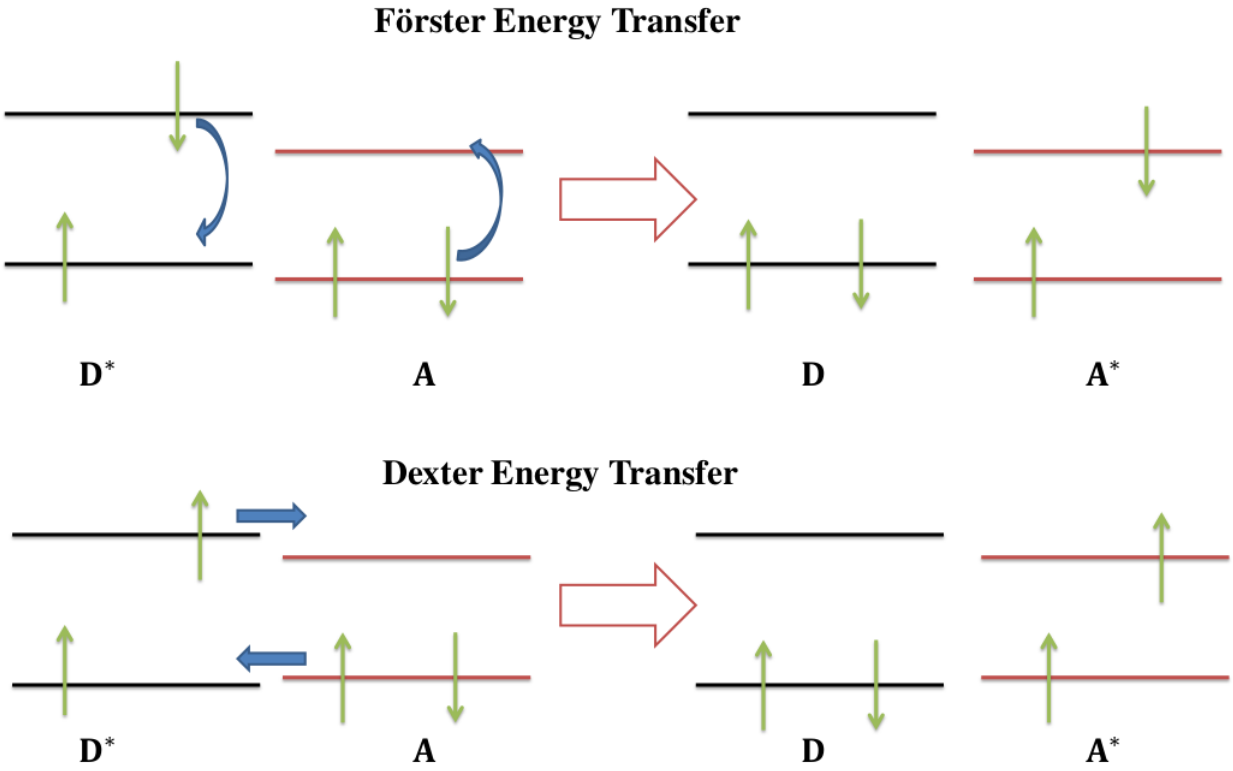

Figure 2.5: Dexter and Förster energy transfer mechanisms, A and D denote acceptor and donor, respectively, while the asterisks represent the corresponding excited states.

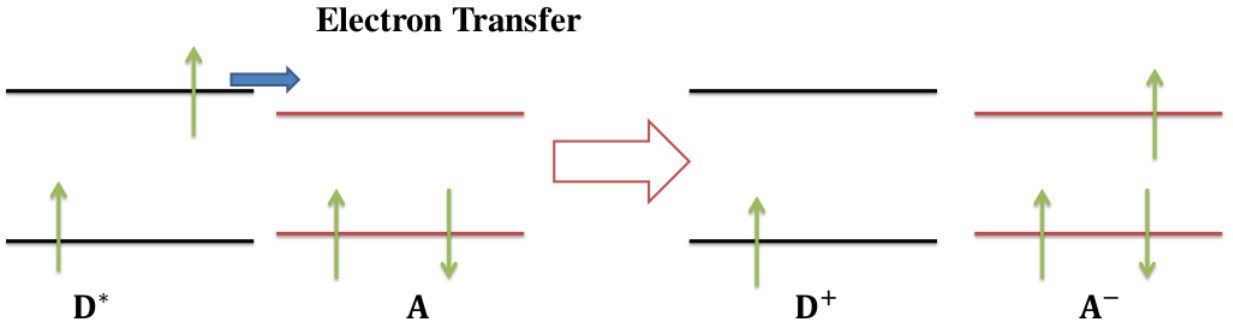

Figure 2.6: Electron transfer mechanism in a donor-acceptor (D-A) copolymer, the asterisk represents an excited state while (+) and (-) denote ions.

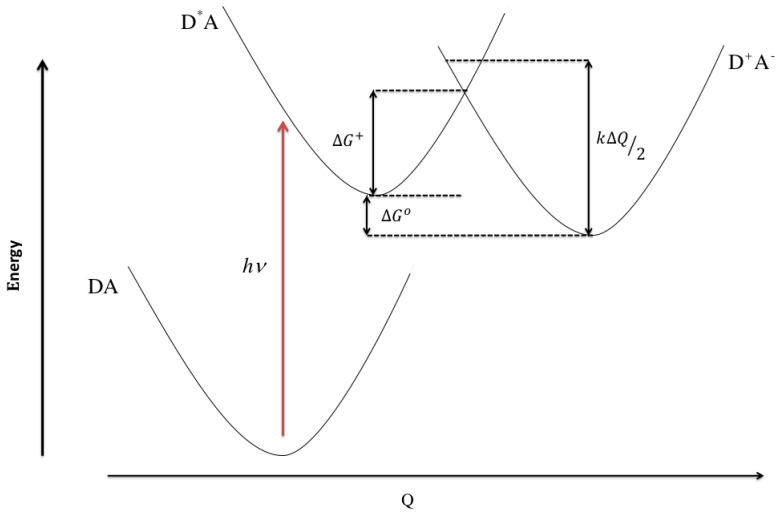

Figure 2.7: Demonstrating potential energy surfaces for ground, excited and charge-separated states. Also shown are Gibbs free energy, ΔG^o, the activation barrier, ΔG^+ and the reorganization energy $k\Delta Q/2$.

possible when thermal fluctuations bring the reactant state's geometry to the value of the nuclear coordinate where the parabolas representing the reactant and product states intersect. Electron transfer is enabled when the nuclei reorganize to form the configuration at which the charge-separated state and the photoexcited D/A complex become energetically degenerate. Electron transfer, according to Marcus, is an activated process with an energy activation barrier ΔG^+ which is a function of the reorganization energy, $k\Delta Q/2$, and Gibbs free energy, ΔG^o:[74]

$$\Delta G^+ = \frac{(k\Delta Q/2 + \Delta G^o)^2}{4k\Delta Q/2}$$

The energy needed to move the reactant and the medium surrounding it to the product state's equilibrium geometry is known as the rearrangement energy. Therefore, isoenergetic electron transfer occurs at the intersection point which represents the energy level and nuclear configuration achieved by the reactant state through vibrational motion.[74] When the reorganization energy equals to the negative of Gibbs free energy, at which the reaction has no activation barrier, a maximum reaction rate is reached.

However, the electronic and optical properties observed in the macroscopic states may not be a direct transformation from isolated molecules. To obtain optimized optical and electronic properties in the macroscopic states, one of the essential techniques is controlling molecular

packing because molecular packing dictates these properties.[75]

2.2.2 Theoretical Developments on Molecular Packing

In a lattice of N molecules the dipole-dipole interaction between excited states causes each state of the isolated molecules to split into exciton band of N-fold. Because of the characteristics of exciton bands optical transitions are possible only to certain exciton band components. For a hypothetical molecular array, Kasha[13–18] proposed three types of orientation of transition dipoles; card-pack, head-to-tail and alternate translational (oblique). In the first type orientation, optical absorption takes place only to the lowest exciton state resulting in red shift absorption of a linear aggregate compared to the monomer unit or isolated species. In the card-pack orientation, the upper exciton state is the allowed exciton level. The absorption of aggregate system blue shifts relative to the unaggregated species. Whereas both the lowest and highest exciton states are allowed exciton levels in oblique arrays of transition dipoles.[14,15]

In addition to the spectral shifts, Kasha used phosphorescence yield, which depends critically on the geometrical orientation of molecules in the aggregate, to distinguish between head-to-tail and card-pack aggregation types. A maximum phosphorescence enhancement is anticipated for card-pack structures because fluorescence from the bottom of the excited singlet band - achieved by thermal re-equilibration following excitation - is prohibited.[17,18] In the head-to-tail arrangement, since the singlet levels with the lowest energy combine radiatively with the ground state, fluorescence emission is enhanced.[18]

The two orientations proposed by Kasha, head-to-tail and card-pack, later on are known as J- and H- (for Hypsochromic shift) aggregates. Coulomb coupling between two molecules is described mathematically by Equation 2.2.1. This equation has been driven for parallel transition dipole moments using dipole-dipole approximation and packing arrangement of one molecule per unit cell.

$$J_C^{pd} = \frac{\mu^2(1 - 3\cos^2\theta)}{4\pi\epsilon R^3} \tag{2.2.1}$$

here μ is the point-dipole moment, R is the distance connecting the molecular mass centers

with slip angle θ, and ϵ is dielectric constant in the medium, as depicted in Figure 2.8. The spectral shifts of the head-to-tail and card-pack arrangements are directly related with the sign of the Coulomb coupling. In accordance with Equation 2.2.1, the Coulomb coupling between two molecules vanishes at $\theta = 54.7$ and changes sign from negative to positive for $\theta < 54.7$ and $\theta > 54.7$, respectively, representing head-to-tail (J) and card-pack (H) arrangements.

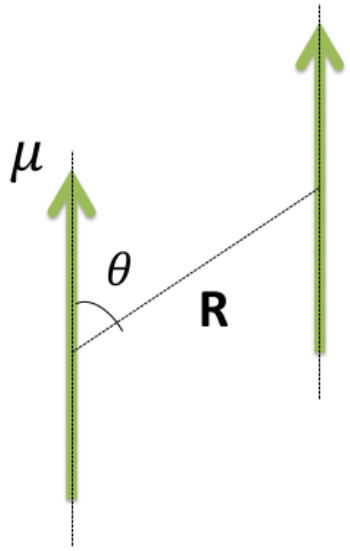

Figure 2.8: Coulomb coupling between two molecules with parallel transition dipole moments.

J-aggregate (after Jelly) was also discovered independently by Jelly[19,20] and Schiebe.[21,22] According to a review by Bricks *et. al*,[46] J-aggregates have characteristic features like strong shift in their emission and absorption spectra to higher wavelength along with spectral sharpening, increase in radiative decay and emission QY compared to the monomers. J-bands are nearly symmetric because there is no discernible vibrational component to their broadening. Their absorption and fluorescence spectra coincide resulting in negligible Stokes shifts, and their similarly narrow width fluorescence spectra show almost resonant behavior. In marked contrast, H-aggregates exhibit opposite behaviors to J-aggregates.

A huge number of studies[23–42] were committed to the transition dipole orientations and related optical properties following Kasha model. In a review on organic molecular aggregates, Ma et.al[48] classified transition dipole orientations based on rotational (X-aggregate) and slip (J or H aggregate) angles between dipole moments, illustrated in Figure 2.9. In this regard, H-aggregate exhibits positive Coulomb coupling due to cofacial, parallel molecular stacking with slip angle

greater than 54.7^o, at which the Coulomb coupling vanishes as supported by Equation 2.2.1. As the slip angle decreases below 54.7^o the system changes from H-aggregate to J-aggregate giving negative Coulomb coupling. According to theoretical studies, in X-aggregation, the splitting in energy level of the two lowest excited states can be reduced due to rotation of adjacent transition dipoles and this can optically permit the transition from both excited levels to the ground state. The X-aggregates' spectral signatures can resemble those of monomers, and the optical splitting becomes negligible at rotation angles of 90^o.[48] The intriguing X-aggregation on the packing of distyrylbenzene derivatives in crystal modes was initially noted by Bartholomew *et al.*[76] in 2000. In the crystal of 1,4-bis(2,2-diphenylethenyl)benzene, one of the distyrylbenzene derivatives, the benzene rings of neighboring molecules create a stacking mode of edge-to-face, indicating that the C–H - - π interactions help generate a cross-stacking mode.

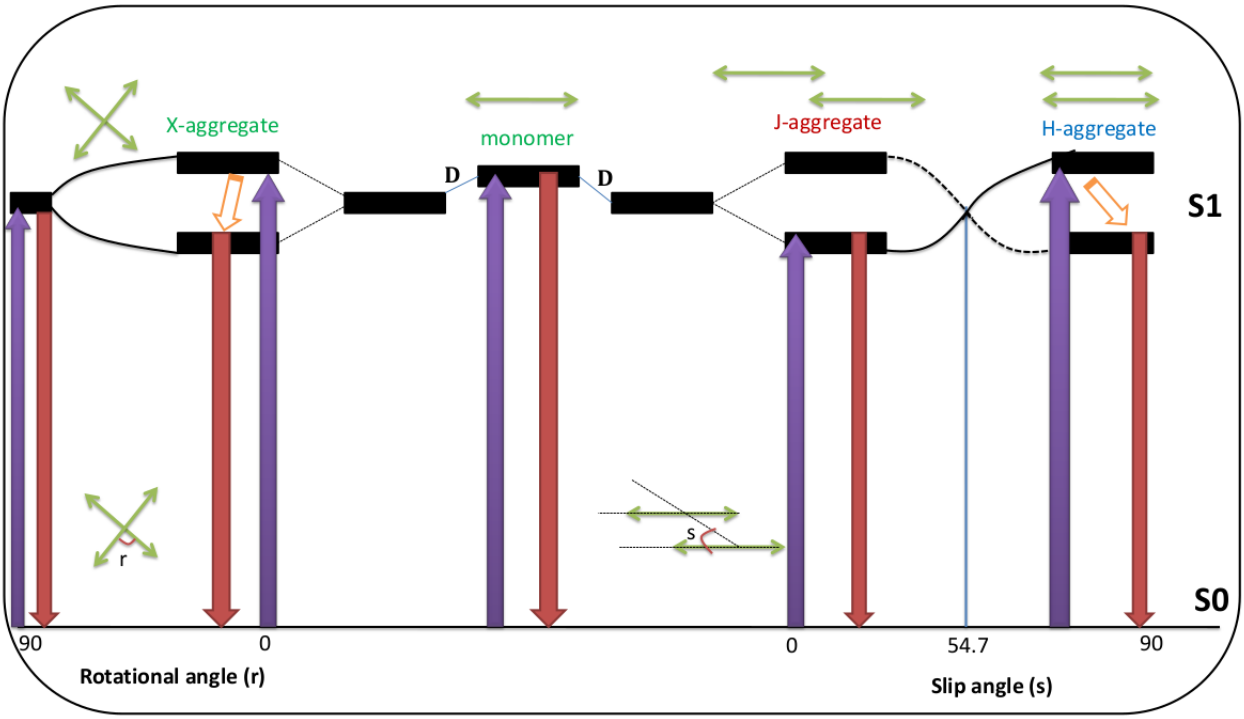

Figure 2.9: Molecular aggregates (X, J and H) and exciton band splitting due to dipole-dipole Coulomb coupling, gas-to-crystal frequency shift in units of energy is denoted by D.

In a much more intense review aiming to expanding the Kasha theory by addressing the limitations by incorporating vibronic and intermolecular charge transfer (CT) mediated couplings, Hestand and Spano[32] explained the aggregation types, the corresponding photophysical properties and techniques to differentiate between each type theoretically with the help of Frenkel

exciton Hamiltonian describing delocalized excited states as molecular excitons. The Frenkel exciton Hamiltonian, describing linear aggregates consisting of N-coupled chromophores with packing modes of one molecule in a unit cell, is given by Equation 2.2.2.[32]

$$H_{ex} = E_M + D + \sum_{m,n} J_{m,n}|m\rangle\langle n| \tag{2.2.2}$$

where, E_M is the $S_0 \rightarrow S_1$ transition energy of monomer unit and D is the gas-to-crystal frequency shift in units of energy, while $J_{m,n}$ denotes the Coulomb coupling of the molecules n and m. Here the ket $|m\rangle = |g_1, g_2, ..., e_m, ...g_M\rangle$ stands for the mth chromophore that is excited to S_1 electronically while every other chromophores is in their ground electronic states, S_0.

Applying boundary conditions that are periodic, the wavelike excitons each with a wave number k are eigenstates of H_{ex}.

$$|k\rangle = \frac{1}{\sqrt{N}} \sum_n e^{ikn}|n\rangle \quad k = 0, \pm 2\pi/N, \pm 4\pi/N, ..., \pi$$

From Equation 2.2.2 follows E_k, which is the energy of the k^{th} exciton,

$$E_k = E_M + D + J_k$$

here $J_k \equiv \sum_n J_{m,n} cos(k(n-m))$ and when retaining only nearest neighbor coupling changes to $J_k = 2J_C cosk$. For linear aggregates this is a good approximation. Following identification of the bright exciton to be $k = 0$ and located at the top and bottom bands in H- and J-aggregates, respectively, the energy dispersion curve in Figure 2.10 illustrates the Kasha spectral shifts.

Assigning H- and J-aggregates is typically dependent on the relative blue- or red-shift of the aggregate absorption compared to, $E_M + D'$ which denotes the peak of the monomer in solution, with D' representing the gas-to-solution frequency shift in unuts of energy. This clearly shows that the assigning H/J-aggregate based on Kasha depends on the condition

$$|D - D'| < 2|J_C|$$

here $D - D'$ represents the solution-to-aggregate spectral shift in units of energy. The exciton

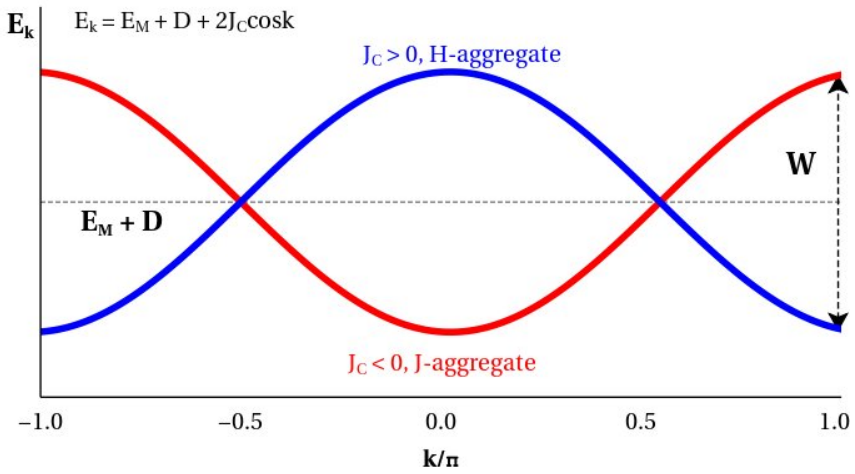

Figure 2.10: Dispersion curves of energy for H- and J-aggregates, $W = |J_{k=0} - J_{k=\pi}| = 4|J_C|$ is the free exciton bandwidth in the limit of nearest neighbor coupling.

blue-shift might be less than the solution-to-crystal shift because $D - D'$ is likely a negative quantity. In weakly coupled H-aggregates this could lead to inaccurate assignment giving an overall red-shifted spectrum which is a property of J-aggregate. For example, in the case of P3HT, as reported by Brown *et al.*, while the molecules are cofacial and analogous to H aggregates, a significant red shift was observed due to enhanced intrachain planarization.[77] Other examples include the aggregates formed in lutein, lutein diacetate, perylene diimide dimers and nonfluorescent squaraine aggregates. Zsila *et al.*[78] reported the formation of head-to-tail J-aggregate assemblies in lutein diacetate and card-packed H-aggregates in lutein depending on the spectral shifts. However, Spano later on, explaining that these different spectral line shapes arises from weakly and strongly coupled H-aggregates, showed the spectral line shapes for both lutein diacetate and lutein are characteristic of H-aggregates.[51] On the other hand, Margulies *et al.* reported perylene diimide dimers form H-aggregates while the first vibronic peak is redshifted.[79] Nonfluorescent squaraine aggregates reported by Zhang *et al.* to form J-aggregate[80] was later revealed to be a red-shifted H-aggregate by Sanyal *et al.* as the lowest energy excited state is optically dark.[81]

Band curvature is another method of differentiating between H- and J-aggregates. The band curvature, given by Equation 2.2.3, is calculated as the second derivative of E_k in relation to k.

$$\omega_c \equiv \frac{1}{2}\frac{d^2 E_k}{dk^2} \mid_{k=k_{min}} \tag{2.2.3}$$

where $k_{min} = 0$ and $k_{min} = \pi$ for J-aggregate and H-aggregate, respectively. As one can observe in Figure 2.10, the band curvature is negative in H-aggregates and positive in J-aggregates. This is because the $k = 0$ exciton defines the band top and band bottom in H-aggregate and J-aggregate, respectively. The characteristic of emission in H- and J-aggregates is different as, according to Kasha, the origin of emission is the lowest energy excited state. In this regard, in J-aggregates the radiate decay rate is enhanced and there is ideally no Stokes shift. In contrast, the $k = \pi$ exciton in H-aggregates is populated from the k = 0 exciton by rapid intraband relaxation, then, either vibronic coupling or symmetry-breaking disorder must exist for emission to occur. This shows the origin of absorption and emission are greatly influenced by the band curvature. Under the nearest neighbor approximation, the band curvature evaluated at the minimum band simplifies to $\omega_c = -J_C$ and $\omega_c = J_C$, in H- and J-aggregates, respectively.

The Kasha model is restricted to Coulomb coupling between chromophores and does not take into consideration the vibronic fine structure that is ubiquitous in many aggregating chromophores. The Frenkel-Holstein Hamiltonian which describes the delocalizing effect of electronic coupling takes the form of Equation 2.2.4 when written for excited chromophores in the local basis set. Among the N chromophores comprising the system this expression includes only one excited chromophore.

$$H_{FH} = \omega_{0-0} + D + \sum_{m,n} J_{m,n}|m\rangle\langle n| + \omega_{vib}\sum_{n} b_n^\dagger b_n + \omega_{vib}\sum_{n}\{\lambda(b_n^\dagger + b_n)\lambda^2\}|n\rangle\langle n| \qquad (2.2.4)$$

While the first three terms of Equation 2.2.4 represent the Frenkel exciton Hamiltonian, the fourth one accounts for intramolecular vibration of energy ω_{vib}. In this case, a vibrational quantum is created (annihilated) within the nth chromophore having nuclear potential of S_0, that is assumed to be harmonic, by the operator $b_n^\dagger(b_n)$. The remaining terms indicate the shift of the excited state nuclear potential, S_1, from the ground state nuclear potential, which is measured by the HR parameter, λ^2.

The homogeneous absorption spectrum $A(\omega)$ is obtained by adding up all of the electronic transitions of the aggregate Hamiltonian from the vibrationless ground state $|G\rangle$ to each of the excited state eigenstates, $|\Psi_i\rangle$.

$$A(\omega) = \frac{1}{N\mu^2} \sum_i f_i W_{LS}(\omega - \omega_i)$$

here f_i denotes the oscillator strength corresponding to $|G\rangle \rightarrow |\Psi_i\rangle$ transition

$$f_i = \omega_i |\langle \Psi_i | \hat{M} | G \rangle|^2$$

while $W_{LS}(\omega)$ represents the line shape function. Division by μ^2 makes the 'reduced' spectrum dimensionless. Moreover, the spectrum is divided by N to normalize it to the number of chromophores.

According to Kasha's rule, emission is considered to originate from the lowest energy exciton $|\Psi_{em}\rangle$ in analyzing the PL spectrum. At temperatures low enough to exclude emission from exciton states that are thermally excited, a clear vibronic development can be seen in the PL spectrum.

$$S(\omega) \approx \sum_{\nu_t=0,1,2,...} (\omega_{em} - \nu_t \omega_{vib})^3 I^{0-\nu_t} W_{LS}^{PL}(\omega - \omega_{em} + \nu_t \omega_{vib})$$

where $0-\nu_t$ PL line strengths which describe the $|\Psi_{em}\rangle$ to ground electronic states emission are defined as follows, provided that the electronic ground states consist of a total of ν_t vibrational quanta, $\nu_t = 0, 1, 2, ...$

$$I^{0-0} \equiv \frac{1}{\mu^2} |\langle \Psi_{em} | \hat{M} | G \rangle|^2$$

$$I^{0-1} \equiv \frac{1}{\mu^2} \sum_{n=1}^{N} |\langle \Psi_{em} | \hat{M} | g; 0_1, 0_2, ..., 1_n, ..., 0_N \rangle|^2$$

$$I^{0-2} \equiv \frac{1}{\mu^2} \{ \sum_{n=1}^{N} |\langle \Psi_{em} | \hat{M} | g; 0_1, 0_2, ..., 2_n, ..., 0_N \rangle|^2 + \sum_{m,n=1_{m>n}}^{N} |\langle \Psi_{em} | \hat{M} | g; 0_1, 1_m, 0_{m+1}, ..., 1_n, ..., 0_N \rangle|^2 \}$$

Summations over each potential terminal state with a total of ν_t vibrational quanta dispersed across N chromophores are involved in the $0-\nu_t$ line strengths in every scenario.

Incorporation of the vibronic coupling enables distinguishing between H and J aggregates with vibronic signatures other than spectral shift which might not be reliable for some cases as discussed above.[62] In J-(H-) aggregates, the line strengths of the vibrationless, A_1, and

first vibronic, A_2, peaks in the absorption spectrum are represented by the ratio A_1/A_2, which decreases (increases) as the exciton bandwidth decreases. On the other hand, the PL ratio, I_{0-0}/I_{0-1} in J-aggregates is N/λ^2, with N representing the number of chromophores and λ^2 denoting the HR factor of a monomer unit, and this ratio is zero in H-aggregates at sufficiently low temperatures and no disorder which enables emission to originate only from the lowest energy state. This is explained in terms of enhancement of I_{0-0} emission in J-aggregates and symmetry forbidden of I_{0-0} emission in H-aggregates. The PL ratio has also an opposite relation with increasing exciton coherence number, N_{coh}, in H- and J-aggregates, with a decreasing and an increasing trend, respectively. And this results in an increasing (decreasing) PL ratio in H- (J-) aggregates as the temperature and energetic disorder rises.[32] In relation to the enhancement in J-aggregates and suppression in H-aggregates of I_{0-0}, emission QY and emission lifetimes are also other factors used to distinguish between J- and H-aggregates.

The successful expansion of the exciton theory for H- and J-aggregates by incorporating vibronic and intermolecular CT mediated couplings allowed for a better understanding of the photophysics of conjugated molecules arranged in a variety of architectures.[32] The presence of both long- and short-range couplings simultaneously allows for explanation of a wide range of photophysical properties, some of which cannot be explained in the context of the basic Kasha model.[82,83] Importantly, the vibronic signatures that were first driven for the Coulomb-coupled aggregates remain valid for identifying H- and J-aggregates based on the spectral ratios A_1/A_2 and I_{0-0}/I_{0-1} when Coulomb and CT-mediated couplings both present. The relative position of the $k = 0$ band, which is the real distinction between H- and J-aggregates, defining the band maximum/minimum in H- (J-) aggregates also works whether the coupling source is CT-mediated, Coulombic or a combination of both.

In some cases, even though the proper H-like vibronic signatures are observed, such as the position of bright exciton being at the band top, that clearly defines H-aggregate, the CT-mediated interaction may cause a resultant red-shift of every exciton irrespective of the value of k. This would produce an oxymoronic red-shifted H-aggregate, most likely because of nonresonance dispersion forces.[51,79–81] In addition to influencing the type of optical response - H-like, J-like, or a hybrid - Coulombic and CT-mediated couplings also have a significant effect on exciton

dynamics. Depending on whether the two coupling sources interfere constructively (HH) or destructively (HJ), the exciton mobility is enhanced or suppressed, respectively.[84,85]

In expanding Kasha model apart from addressing the limitations, there are also efforts committed to address more complicated architectures. The aggregates in systems such as in Figure 2.11, which gives rise to polarization dependence absorption due to packing modes of two or more molecules per unit cell, support two types of transitions. 1) to the $k = 0$ exciton with an oscillator strength proportional to $|\mu_1 + \mu_2|^2$ and polarized normal (parallel) to the aggregate axis in H-type (J-type) aggregates, top right of Figure 2.11 (bottom left of Figure 2.11). 2) to the $k = \pi$ exciton with oscillator strength proportional to $|\mu_1 - \mu_2|^2$ and polarized parallel (normal) to the aggregate axis in H-type (J-type) aggregates bottom right of Figure 2.11 (top left of Figure 2.11). Many aggregates and crystals with herringbone-packed have been found to exhibit strong polarization-dependent emission and absorption spectra.[86–94]

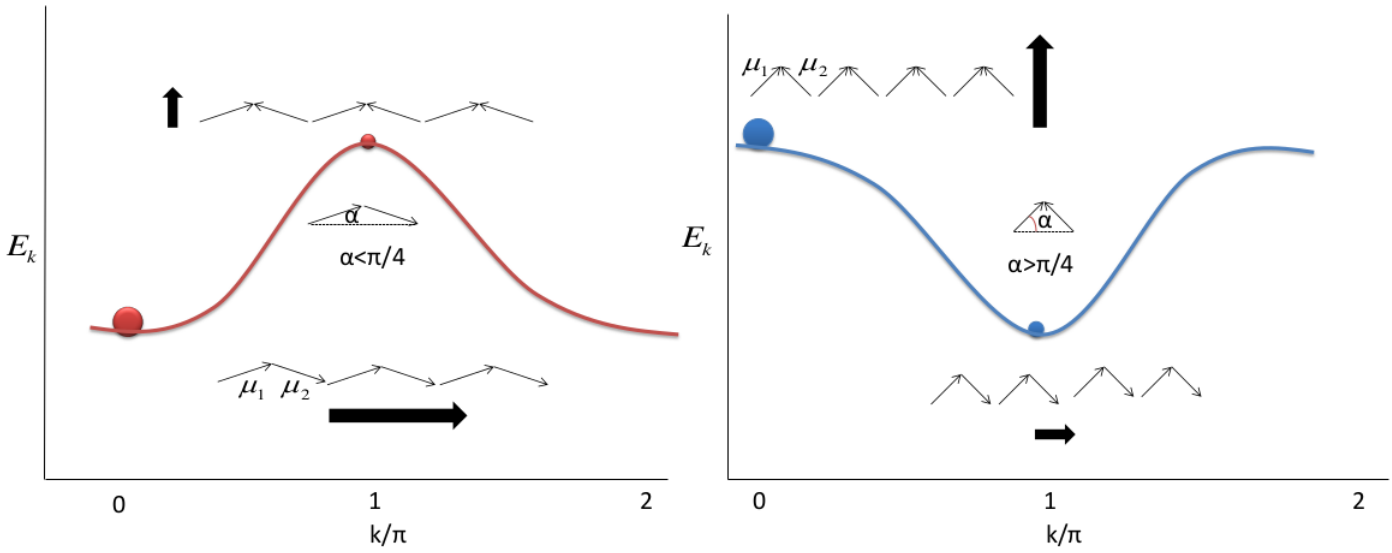

Figure 2.11: Dispersion curves of exciton (left) for J- and (right) H-type aggregates illustrating two molecules per unit cell.

Muccini *et al.*[95] found that the electronic coupling with completely symmetric modes results in the activity of electronic false origins in the polarized absorption spectra which, inturn, brings about notable deviations from the FC coupling expectations in the intensity of vibronic bands. These experimental spectra can be consistently interpreted in terms of a special vibronic coupling called Herzberg-Teller coupling.[95,96] The transition moment $\mu_{gp,mq}$ between vibronic states g_p

and m_q is defined as

$$\mu_{gp,mq} = \langle g_p(Q)|\mu(Q)|m_q(Q)\rangle \tag{2.2.5}$$

Expanding the electronic transition moment $\mu(Q)$ in the nuclear coordinates as a Taylor series about the equilibrium configuration Q_0 leads to the vibronic transition moment given by Equation 2.2.6.[95]

$$\mu_{gp,mq} = \langle g_p(Q)|\mu(Q_0)|m_q(Q)\rangle + \langle g_p(Q) \sum_k \left(\frac{d\mu(Q)}{dQ_k}\right)_{Q_0} Q_k|m_q(Q)\rangle + ... \tag{2.2.6}$$

The first term of Equation 2.2.6 represents the Franck-Condon coupling, where the electronic transition moment m(Q) is independent of the nuclear coordinates and the polarization of the transition is that of the electronic origin m. The Herzberg-Teller vibronic coupling is represented by the second term in Equation 2.2.6. In this case, the electronic transition moment is dependent on the nuclear coordinates and the Condon approximation is relaxed. Two electronic excited states couple through molecular vibration in the Herzberg-Teller mechanism, causing the oscillator strength of the higher excited electronic state to be borrowed to the vibronic level of the lower excited electronic state. Hestand and Spano[32] found that near the origin of the polarized absorption of oligophenylenevinylene and oligothiophene crystals, and the PL spectrum of H-aggregates in crystalline distyrylbenzene, had peaks originating from Herzberg-Teller coupling.

The observation of similar photophysical properties between a linear through-space coupled J-aggregate molecules and a single through-bond coupled conjugated polymer chain of monomers due to the positive band curvature at the k = 0 point common to both systems,[29] enables to handle polymer π-stacks as a two dimensional aggregate, where J-like intrachain components and H-like interchain components compete. Segregated HJ-aggregates manifest such competition in conjugated polymer π stacks, as shown in Figure 2.12. In these stacks, chains of single polymer can be thought of as J-chains, where repeat-unit chromophores interact through covalent coupling, while neighboring polymers interact with one another through H-promoting Coulomb coupling. The free-exciton energies for an $N_x \times N_y$ HJ-aggregate with $N_x, N_y > 2$ are dependent

on the wave vectors k_x, k_y,

$$E(k_x, k_y) = E_M + D + 2J_{intra}cosk_y + 2J_{inter}cosk_x \tag{2.2.7}$$

here $k_{x,y} = 0, \pm 2\pi/N_{x,y}, ..., \pi$. If $J_{inter} = J_{intra}$, in what is known as null aggregate, the bright exciton resides exactly in the middle of the band resulting in no exciton-induced spectral shift.

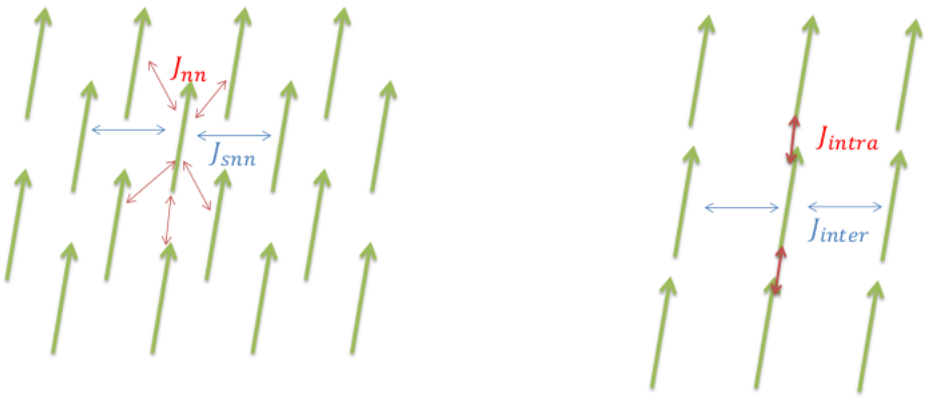

Figure 2.12: Segregated HJ-aggregate demonstrating one molecule per unit cell, (left) J-type nearest neighbor and H-type second-nearest neighbor interactions, and (right) H-promoting interchain and J-promoting intrachain interactions.

In the literature a lot of materials are modeled as HJ-aggregates, including PDA,[28,55] P3HT,[26,28,55] PPEB,[30] MEH-PPV,[28,58,59,61] 2T-DPP-2T and 2T-BT-2T,[62] PTB7-Th[34] and AnE-PVstat[60] to mention just a few. Materials modeled as HJ-aggregates might undergo interplay between J- and H-aggregates. According to Yamagata *et al*,[55] in PDA, the H to J transition occurs at a temperature where $kT = \Delta E$, where k is Boltzmann constant and ΔE is the interchain splitting. In contrast, in P3HT, H or J behavior is discovered to be tunable by changes in morphology. The primary exciton coupling of P3HT nanofibers changed primarily from H-aggregation (interchain) for low molecular weight to primarily J-aggregation (intrachain) coupling for high molecular weight, according to Baghgar *et al*,.[26] Eder *et al*.[30] observed the switching between J- and H-type aggregates by swelling and drying of the film in a matrix, with the aim of researching the electrical coupling in PPEB. By transporting a acetone/chloroform saturated nitrogen vapor onto the polymer thin film, the film in the matrix was annealed. As a result of this the single conjugated polymer chains diffused and the film swelled, enabling them aggregate with one another to form mesoscopic objects composed of several conjugated polymer chains with the characteristic

J-aggregate. The dry aggregate, on the other hand, demonstrates every characteristic of H-type aggregation. According to Ziffer *et al.*,[34] in thin films of PTB7-Th the aggregation behavior changes from a typical H-like to an unusual HJ-like due to change in orientation of fluorine atom in thieno[3,4-b]thiophene unit with respect to the benzodithiophene unit. This indicates significant differences in interchain coupling between polymer chains and intrachain exciton coupling along the polymer backbone. Additionally, Wang *et al.*[58] observed that intrachain excitons with J-like features dominated the PL emission in MEH-PPV films without annealing, while H-aggregate behavior (interchain interaction) dominated for films annealed at 420 and 520 K.

2.2.3 Ways of Differentiating Between Aggregation Types

In this subsection we discuss the reliable ways used in the literature to distinguish between the different aggregation types. Differentiating between the aggregation types in conjugated polymers is not a simple task as there is a competition between H-promoting interchain and J-promoting intrachain interactions. As was previously mentioned, one method of distinguishing between the different types of aggregation is to use the aggregate absorption peak shift in solution or thin film with respect to the monomer peak. However, in H-aggregates that are weakly coupled this method is not reliable, where the gas-to-crystal frequency shift can overcome the exciton blue-shift, resulting in an overall red-shifted spectrum leading to an incorrect assignment. In this case people use other supporting techniques, in addition to absorption spectral shift, such as stokes shift[23] and fluorescence efficiency,[27] for example.

The relative position the bright exciton that it the nodeless exciton in the exciton band, which is unaffected by the source of coupling - be it Coulombic, CT-mediated or a combination of both is a genuine distinguishing factor between H and J aggregation types. Additionally, the vibronic fingerprints for categorizing H- and J-aggregation based on the spectral ratios $R_{abs} = A_{0-0}/A_{0-1}$ and $R_{PL} = I_{0-0}/I_{0-1}$ continue to be valid when both Coulomb and CT-mediated couplings are present. These signatures were initially derived for Coulomb-coupled aggregates.[32] In general, progression of the first two vibronic peak ratios with exciton bandwidth or temperature/disorder, emission lifetime and relative QY are the criteria used to distinguish between the aggregation types. Some of the works on aggregation types in conjugated polymers using these technique are

summarized below.

Yamagata *et al.*[25] highlighted that at $T = 0K$ without disorder, $0-0$ peak in the PL spectrum is absent in H-aggregates. This is because in H-aggregates the nodeless bright exciton the exciton band lies at the top. However, rising temperatures causes the $k = 0$ exciton which lies the top of the lowest energy vibronic band to thermally activate, increasing $0 - 0$ emission. Conversely, in J-aggregates in the absence of disorder, $0 - 0$ emission is amplified - also known as superradiant - and decreases with rising temperature because the $k = 0$ exciton population is being depleted. On this basis, temperature-dependent PL has been used to infer the aggregation types formed in conjugated copolymer.[29,34,55,58,60,61] In their study on AnE-PVstat copolymer, Saaidia *et al.*[60] found that the PL ratio, I_{0-0}/I_{0-1}, significantly exceeds unity, indicating intrachain through-bond interactions (unconventional J-aggregates), and that increases with rising temperature of the solution, indicating H-aggregate behavior (interchain interactions). They were able to use the HJ-aggregate model because of this observation. Both J- and H-like behaviors were shown to exist at room temperature when the $0 - 0$ to $0 - 1$ PL ratio was studied in relation to temperature within this framework of the HJ-aggregate model. In MEH-PPV films, Wang *et al.*[58] also employed temperature-dependent PL. Intrachain excitons exhibiting J-like characteristics dominated the PL emission in the films that were not annealed; the I_{0-0}/I_{0-1} PL ratio decreased as the temperature increased. The H-like behavior (interchain interaction) predominated in MEH-PPV films that were annealed at temperatures of 420 and 520 K, leading to an increase in the I_{0-0}/I_{0-1} PL ratio as temperatures rose. Additionally, Spano and Silva[28] found that as temperature or disorder increased, the ratio of the PL spectrum, I_{0-0}/I_{0-1}, increases in H-aggregates and declines in J-aggregates.

The other techniques to distinguish between the aggregation types include QY[26,27,31] and emission decay rate/lifetime.[26,28–30,55] Baghgar *et al.*[26] identified low QYs as a characteristic of H-aggregates and an increased PL decay rate to J-aggregate character while investigating the impact of polymer chain folding on the transition from J- to H-aggregate behavior in P3HT nanofibers with high and low molecular weight. Similarly, Deng and colleagues[27] assert that when compared to isolated chromophores, H-aggregates cause a significantly lower fluorescence efficiency in addition to red-shift in fluorescence and blue-shift in absorption spectra, whereas

J-aggregates cause both fluorescence and absorption spectral red-shifts along with a significantly higher fluorescence efficiency. On the other hand, Spano and Silva[28] reported that in H- (J-) aggregates, the ratio in the absorption spectrum of the first two vibronic peaks, A_{0-0}/A_{0-1}, decreases (increases) with exciton bandwidth. They further support this by comparing the radiative decay rate claiming that the excited-state radiative decay rate is suppressed in an H-aggregate and enhanced in a J-aggregate. Eder *et al.*[30] also assigned long (short) lifetimes as characteristics of H- (J-) type coupled chromophores. Yamagata and Spano[29] while comparing similarities in the photophysical properties between J-aggregates and single chain polymers, attribute properties such as enhanced radiative decay rates to a single molecule and red-shifted absorption spectrum with increasing chain length to J-aggregate characteristics.

2.3 Aggregation and Morphology Dictating Improvement in PCE of OSCs

2.3.1 Aggregation and Polymer Structure Correlations

Although some molecules predominantly tend to form one type aggregation, for example, as reviewed by Wurthner *et al.*[43] and Bricks *et al.*[46] a variety of dyes including porphyrins, cyanines, perylene bisimides and phthalocyanines form J-aggregates, whereas oligothiophene nanostructures,[50] carotenoid assemblies[51] and P3HT[54] form H-aggregate, subtle structural changes of a polymer could have a significant impact on the aggregation type to be formed. Kim *et al.*[24] designed and synthesized four quaterthiophene derivatives with end-groups composed of dicyclohexyl butyl, dicyclohexyl ethyl, cyclohexyl butyl and cyclohexyl ethyl and observed that in thin films of cyclohexylated quaterthiophenes the absorption peaks were blue-shifted compared to the solution which could be explained by molecular packing structure that leads to H-aggregate formation. On the contrary, in dicyclohexylated quaterthiophenes thin films the absorption peaks were red-shifted relative to the solution, which could be well explained by J-aggregation. The aggregation type formed by a polymer could be tuned by changes in the polymer structure due to a variety of techniques such as varying side chains, additives, temperature, annealing and others.

Eder *et al.*[30] were able to tune between J-type and H-type coupling by side chain engineering on PPEB. They varied the side chains between hexyloxy, 2-ethylhexyloxy and cholestenol substituted benzyloxy. They found that various side chains have significant impact on the photophysics of isolated aggregates but have no effect on the photophysics of the materials at the single-molecule level when comparing the photophysics of the three PPEB derivatives in single-molecule and isolated aggregate form. They also conclude that changing the side chains from 2-ethylhexyloxy to hexyloxy switches the dominant coupling from J-type to H-type. However, as demonstrated by the lack of variations between the single-molecule and isolated aggregation forms, the large side chain - cholestenol substituted benzyloxy - prevents any type of electronic coupling.[30] The way the side-chains get connected also affect the aggregation in addition varying the side chains. With a difference only in the connectivity of the side-chains - acyclic or macrocyclic- on BDT derivatives, McDearmon *et al.*[33] developed building block of macrocyclic benzodithiophene and compared the resulting polymers properties to analogous acyclic derivatives. The macrocyclic BDT building block was observed to modify aggregation in conjugated polymers by decreasing interchain interactions, leading to enhanced PL both in the solid state and solution. Apart from side chains and their connectivity, orientation of atoms in molecules has also an effect on molecular aggregations. According to Ziffer *et al*,[34] the optical characteristics of diluted solutions and thin films show that the orientation of fluorine atom on the thieno[3,4-b]thiophene unit relative to the benzodithiophene unit does, in fact, affect electronic properties of aggregated polymer chains in PTB7-Th in the excited state. Significant differences in interchain coupling between polymer chains and intrachain exciton coupling along the polymer backbone are indicated by their demonstration that this subtle change along the polymer backbone causes thin films to change from an unusual HJ-like to typical H-like aggregate behavior. Single PTB7 strands in solution with strong self-aggregation caused similar absorption spectra between the dilute solution and thin film in the orientation with HJ aggregation. In contrast, the orientation with H aggregation showed a distinct blue shift and shape change between its dilute solution and thin film absorption spectra, indicating that the polymers are not forming ordered aggregates in solution.

Structural tuning by varying conjugation length can also induce aggregation types. Designing

dimers of oligo(phenylene-butadiynylene) with conjugated units of 6 and 12 benzene rings long and spaced by a biphenylene unit, 4.6 $\mathring{A}$ apart on average, Eder *et al.*,[35] showed that 12-ring oligomer show a clear characteristic of J-aggregate with only weakly visible H-aggregate. In contrast, the short dimer a a more pronounced H-type coupling was observed. In addition, Yamagata *et al.*[55] found that J-aggregate property is induced by longer conjugation length, which results in long range intrachain order and weaker interchain interactions, contrary to H-aggregate behavior induced by short range intrachain order resulting in stronger interchain coupling. Molecular weight is also found to affect molecular aggregate due to structural effect as reported by Baghgar *et al.*[26] on P3HT nanofibers. It is shown that the primary exciton coupling changes from interchain to intrachain for low and high molecular weight P3HT nanofibers. These results are described by a structural image wherein high molecular weight P3HT chains fold inside the lamellae, improving chain planarity and potentially reducing the slip-stacking of thiophene rings in the subsequent lamellar packing. In line with an increase in J-aggregate character, there was also a noticeable rise in the overall PL decay rate with increasing molecular weight.

Yamagata and Spano[55] reported that temperature could also affect the aggregation type formed in polymers taking the case in PDA dimers in which they observed that one type of coupling prevails below certain temperature and other coupling type prevails above it. In the framework of the HJ-aggregate model on AnE-PVstat,[60] an investigation on the development of the $0-0$ to $0-1$ PL ratio with temperature revealed the existence of J- and H-like properties at room temperature. As the temperature rises, interchain intermolecular interaction decreases, causing H-aggregates to dissociate, providing yet another illustration of how temperature influences the types of aggregations. The effect of temperature on aggregation types was further extended by Zhao *et al*[57] to compare the amount of aggregation formed in $DTS(PTTh_2)_2$ by different solvents with different boiling points. Making films of $DTS(PTTh_2)_2$ from two solvents, chlorobenzene and thiophene, and drying for several hours, they observed that the total amount of J- and H-aggregation increased using chlorobenzene with more J-aggregation. This is attributed to the higher boiling point of chlorobenzene. In other words, time of film forming is extended in a solution with high boiling point facilitating J-aggregation formation because in terms of thermodynamics J-aggregation is the more stable stacking style and molecules tend to stack-

ing in J-aggregation. Consequently, J-aggregation will be improved more than H-aggregation in chlorobenzene. In addition to solvents, additives are also found to affect the stacking style of $DTS(PTTh_2)_2$. It has been found that additives with (without) properties of selectively dissolving side chains promote H-aggregation (J-aggregate) formation. In BTIC-CF 3 -m[97] it is also found that the coexisting J- and H-aggregations can easily be controlled by using different additives. Two common additives, DIO and CN, support the formation of J- and H-aggregation, respectively.

In a study dealing with the effect of thermal annealing on conformation of MEH-PPV, Hu *et al.*[61] reported that the conformation of MEH-PPV which dictates the aggregation depends on the matrix used and whether or not the samples are annealed. They compared this effect for two matrices, PMMA and polystyrene with MEH-PPV:matrix weight ratios of 1:100 and 1:1000. Similar to as-cast neat film, the conformation of the as-cast MEH-PPV/PMMA film from 1:100 solution displayed J-like PL emissions. While neat film showed no J-aggregate-like emissions after being annealed at 160 ℃, and PL of MEH-PPV/PMMA showed both H- and J-aggregate characteristics after annealing at the same temperature. Conversely, the as-cast and annealed conformation of the 1:1000 solution blends of MEH-PPV/PMMA exhibited an oligomer-like emission that was insensitive to the annealing or measurement temperatures. But when the host matrix was changed to polystyrene, the as-cast film mostly had an extended conformation and showed oligomer-like emissions, regardless of the weight ratio of MEH-PPV: polystyrene. The conformation transition in MEH-PPV/polystyrene blends from extended to aggregated during thermal annealing was proven by the observation of both J- and H-like as well as relatively weak oligomer-like emissions after annealing at 160 ℃. In MEH-PPV/PMMA blends this was unlikely to have happened during thermal annealing. Consequently, photophysical characteristics of conjugated polymer chains can be significantly altered by choosing host matrices with the right annealing procedures. As it has been widely argued, because polystyrene is a good solvent matrix and PMMA is not polymer chains can form more extended conformations in polystyrene than in PMMA. Another work by Ou *et al.*[56] on single molecules of MEH-PPV in PMMA matrix shows how thermal annealing causes the molecules to transform from collapsed conformations to highly ordered, extended rod-like forms. Because transition happens as the annealing temperature

rises over 100 ℃a temperature approaching the glass transition temperature T_g of the matrix is optimal for the optimization and control of polymer films. Wang *et al.*[58] also investigated how thermal annealing affected MEH-PPV aggregation. They reported that intrachain excitons with J-like characteristics dominated the PL emission in the films without annealing, while H-like behavior (interchain interaction) predominated for MEH-PPV films annealed at temperatures of 420 and 520 K.

2.3.2 Optimizing Morphology to Improve PCE of OSCs

In order for an OPV cell to effectively convert solar energy into electrical energy, it is necessary to optimize the processes; absorption of light, diffusion and dissociation of exciton, charge transport, and charge collection, Figure 2.13. In active layers, donor materials absorb photons and create excitons which are tightly bonded electron-hole pairs, top-left of Figure 2.13. Subsequently, the excitons diffuse towards the D:A interface, whereby the driving forces split the excitons into electrons and holes, top-right of Figure 2.13. Note here that if the domain size in the active layer is comparable to the exciton diffusion length, the charge generation efficiency maximizes. Furthermore, in conjugated polymers, enhancing interchain coupling, establishing intercrystallite connectivity, and promoting intrachain transport are all required to improve charge transport, bottom-left of Figure 2.13. In other words, effective charge transport is facilitated by both the pre-aggregation in solution and the short-range ordered aggregation in the film.[12]

Mathematically, we use Equation 2.3.1 to calculate the PCE of solar cells.

$$PCE = \frac{V_{OC} \times J_{SC} \times FF}{P_{in}} \tag{2.3.1}$$

where P_{in} is the incident power, FF is fill factor, J_{SC} is short circuit current density and V_{OC} is open circuit voltage.

However, this has come at the expense of V_{OC} novel low band gap materials have been designed and synthesize to improve J_{SC}. On the contrary, if the band gap of the light-absorbing material is increased to increase the device's V_{OC}, J_{SC} will decrease, and vice versa. It is therefore detrimental that there needs to be a compromise between V_{OC} and J_{SC}. While increasing the film

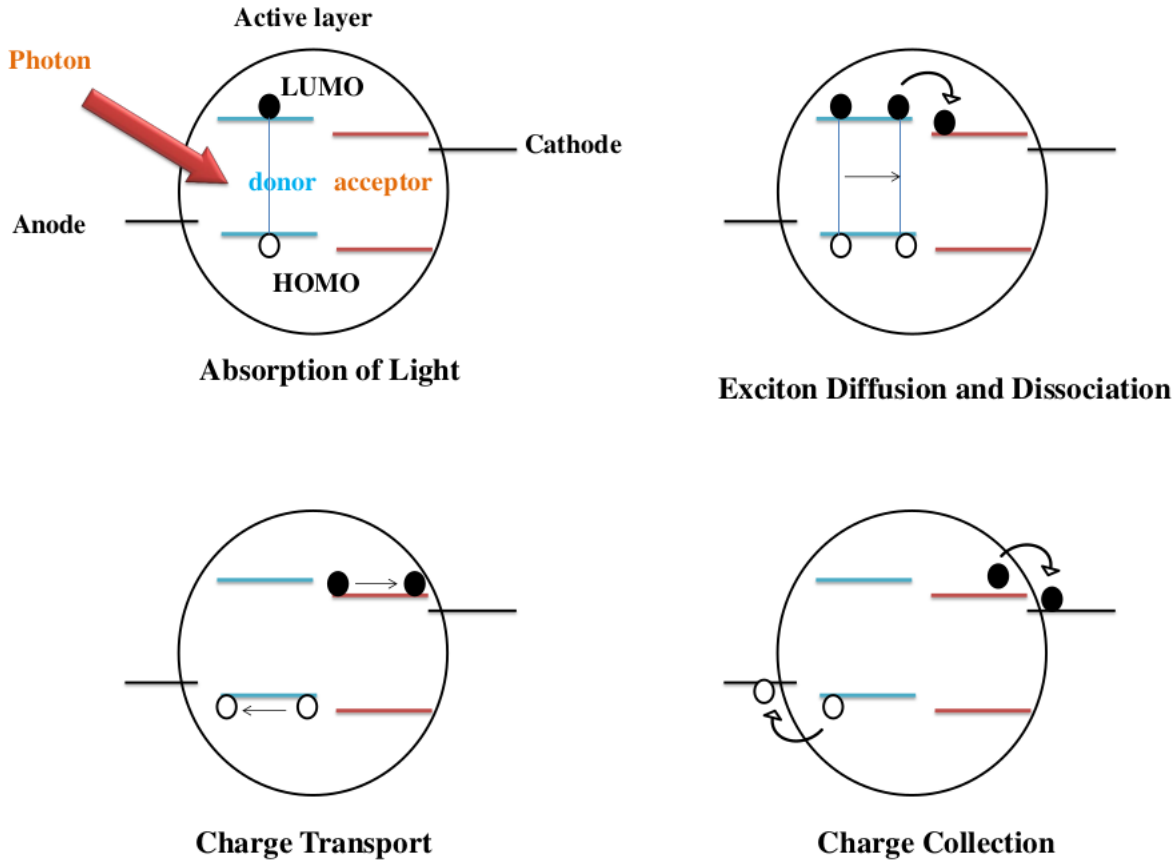

Figure 2.13: Working principle of OPV cell

thickness by processing parameter adjustments might also increase the value of J_{SC}; however, this usually results in a concomitant decline of FF which results in no improvement on PCE. As a result, the FF is essential to enhancing PCE for OPVs. FF is affected by features such as domain size and purity, $\pi - \pi$ stacking distance and orientation, and more when seen from the perspective of a device or material design.[98] By optimizing the domain size to suppress recombination rate, a device can achieve high FF with an effective carrier extraction. It is also conceivable that improving domain purity while keeping the optimal domain size could result in better FF and PCE. This was achieved by ternary system as reported by Zhang *et al.*[99] adding a high crystalline tendency small molecule $p - DTS(FBTTH_2)_2$ into $PTB7 - Th : PC_{71}BM$. In contrast, the transporting direction and speed are determined by the $\pi - \pi$ stacking orientation and $\pi - \pi$ stacking distance, respectively. Because conjugated polymers have a substantial π-conjugated structure, π-orbital overlap impacts charge transport which occurs along the backbone of conjugated polymer at the fastest rate. The molecular packing information is reflected in the

molecular spacing, like lamellar spacing and $\pi - \pi$ stacking distance.

Theoretically it is possible to increase the FF of an OPV device and promote mobility by decreasing the $\pi - \pi$ stacking distance in thin films. As shown in Figure 2.14, the out-of-plane and in-plane molecular self-aggregation information determines the three stacking modes - face-on, flat-on and edge-on - that are frequently included in the texture orientation. The molecular orientation will be edge-on when the lamellar stacking is perpendicular and the $\pi - \pi$ stacking is parallel to the substrate. In contrast, molecules are orientated face-on when the the lamellar stacking is parallel and $\pi - \pi$ stacking is perpendicular to the substrate. While edge-on molecular order is preferable for FETs because the in-plane direction is the efficient charge transport pathway, face-on molecular order is generally better for polymer solar cells (PSCs) because the out-of-plane direction is the effective charge transport pathway.[12]

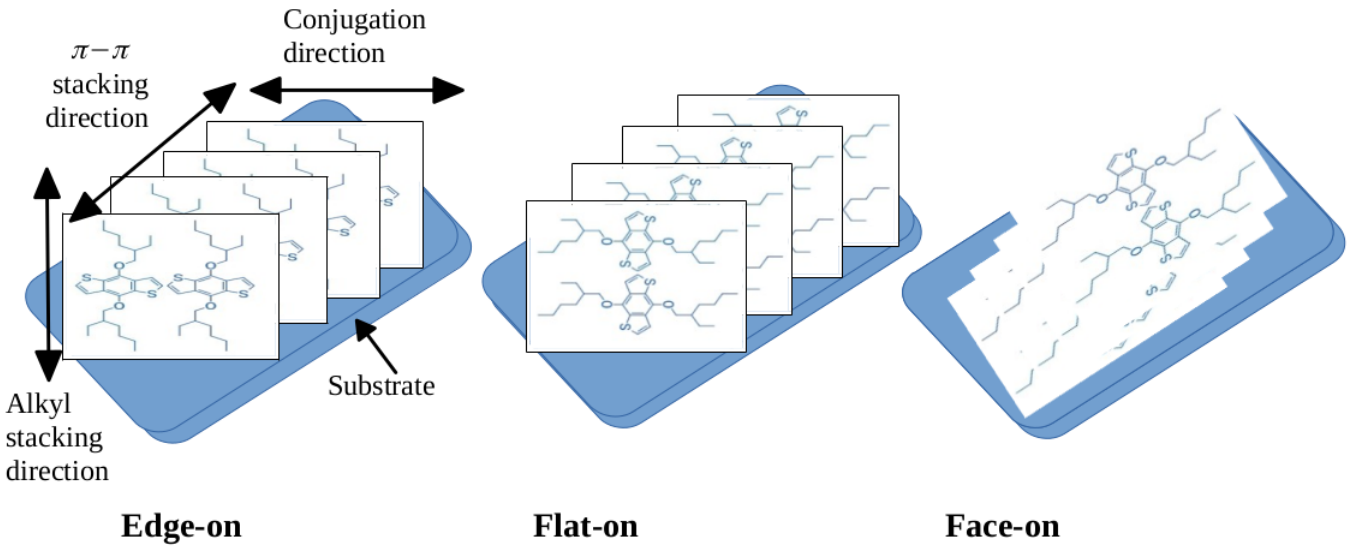

Figure 2.14: The three stacking modes

Enhanced device performance and reduced carrier recombination probability are generally attributed to higher phase purity in the blend, which promotes effective exciton dissociation and charge transport. Tuning domain size and purity can be achieved by a ternary blend systems. Ternary blend via donor alloy[3,4] and acceptor alloy[5–7,100,101] strategies elevate energy of CT state in ternary OSCs. These strategies also minimize the energy loss for generation of charge and enhance the hybridization between CT state and localized excited state which, in turn, reduces the nonradiative energy loss and have a substantial influence on photoelectronic properties, blend

nanomorphology and intermolecular $\pi-\pi$ stacking, leading to superior photovoltaic performance. The ternary OSCs, when combined with the ideal morphology, provide an impressive PCE of more than 19% with a markedly enhanced open-circuit voltage (V_{OC}) without sacrificing FF and short-circuit current density (J_{SC}) when compared to the binary ones.[4,5] Examples of such ternary OSCs include donor alloy of PM6:D18-Cl with L8-BO as the acceptor and BTP-eC9:isoIDITC acceptor alloy with PM6 donor, as reported by Gao *et al.* and Chen *et al.,* respectively. By adding a second donor into a D:A blend, Zhu *et al.* effectively exhibited a show-case of 19.3% average efficiency. This improvement in device performance was achieved by double-fibril network morphology. This morphological scheme facilitates exciton diffusion and charge carrier transport by forming double-fibril network of a multi-length with both high-quality donor and acceptor crystallites.[3]

A thorough and comprehensive understanding of the aggregated structure of polymers in both solution and solid phases is necessary for the morphological optimization of the active layers in PSCs. The aggregated structure of active layer components and the interaction between each component affects the final morphology. Plot of structural complexity schematic of aggregated structure in PSCs is shown in Figure 2.15. The schematic diagram illustrates the multiscale structure of conjugated polymers, ranging from the donor polymer aggregated structure to the most complex BHJ morphology. The bulk-heterojunction (BHJ) active layer exhibits an aggregated structure at various length scales. On a broader scale, the phase-separated structure of blend films is significantly influenced by the miscibility of acceptor and donor materials. The domain purity is typically low for hyper-miscibility systems, leading to insufficient exciton dissociation. The acceptor component in the mixed phase is frequently quenched to the percolation threshold in hypo-miscibility systems, where blends of polymer:small molecule are most suited for domain purity. In hypo-miscibility systems optimizing the vertical phase separation structure can also improve performance of the device.[12]

The film casting process involves various factors that affect the polymer molecular arrangement and active layer's multilevel self-assembly structure. These factors include solvent volatilization rate, material solubility, solvent additives, casting conditions, and post-deposition treatments. Specifically, these factors affect properties like ordering and orientation, molecular con-

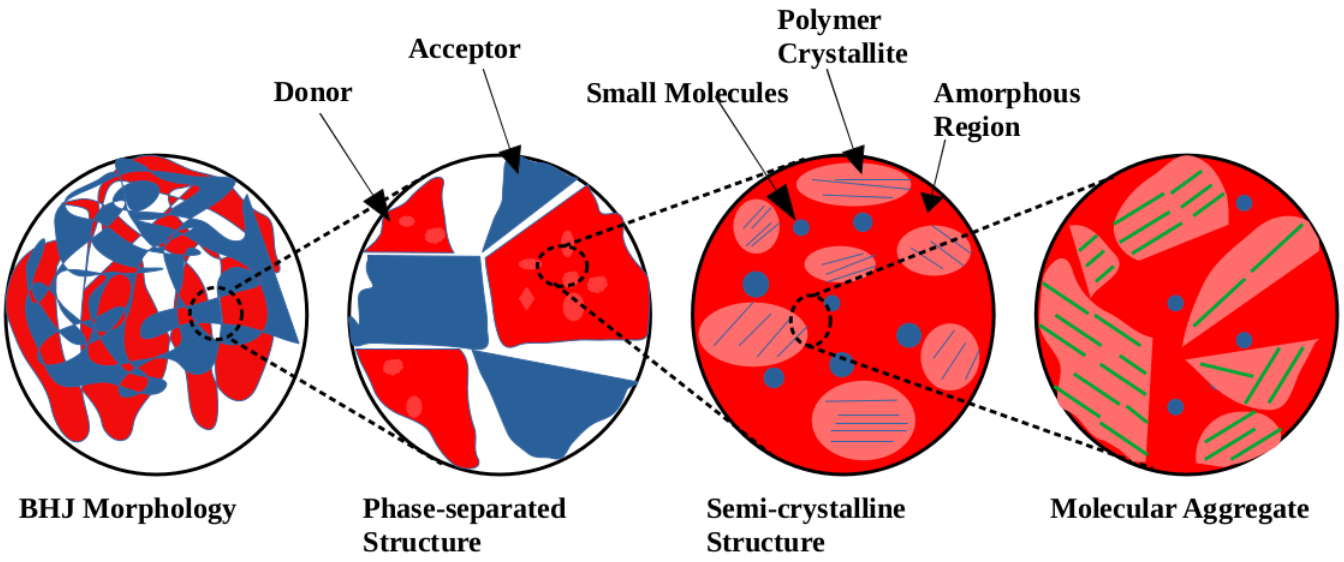

Figure 2.15: Schematic diagram representing the aggregated structure, semicrystalline and phase-separated structures, and BHJ morphology.

formation, crystalline and amorphous regions as well as domain size and purity. These properties, in turn, are closely related to light-harvesting, exciton generation and dissociation, and charge transport in PSCs.[12] Conjugated polymer film morphology is dependent on spin-casting speed, choice of solvent, and polymer concentration.[102] Macroscopic morphology and structure revealed a considerable dependency on solvent molecule structure: for example, Kar *et al.*[103] showed in linear solvents, core-substituted naphthalenediimide forms a fibrillar network, whereas in cyclic solvents, it displays nanoscale spherical particles. The aggregate formation of the blend produces a synergistic impact in one type of solvent and absence of this impact in another solvent due to unbalanced crystallization of acceptor and donor in the latter case, according to another study on H-aggregate donor and J-aggregate acceptor by Jiang *et al.*.[104] By selectively dissolving either components in the active layer, additives also play a role in tuning morphology resulting in altered donor-acceptor interface density and domain size. Lou *et al.*,[105] for example, demonstrated a case in which DIO selectively dissolves $PC_{71}BM$ which facilitates integration of $PC_{71}BM$ into PTB7 resulting in greater donor-acceptor interface density. The active-layer morphology was also shown to be determined by temperature-dependent aggregation properties polymer donors in solution.[106]

In a study on $DTS(PTTh_2)_2 : PC_{70}BM$ aiming at improving photovoltaic efficiency by balancing H- and J-aggregations, Zhao *et al.*[57] concluded that optimizing morphology by precisely

controlling H- and J-aggregations has been found to be the key factor in improving the efficiency of organic solar cells. On the one hand, because J-aggregation requires less energy to excite, it is beneficial for producing more excitons. H-aggregation, on the other hand, encourages exciton dissociation because of two reasons: it provides excitons longer lifetime as well as stronger driving force of dissociate. Additionally, the two stacking modes complementary light absorption is beneficial for maximum light absorption.

Chapter 3

Materials and Methods

This chapter is devoted to list the materials and explain the experimental and computational methods used in this study.

3.1 Materials

Polymers and solvents

Polymers

Three copolymers whose synthesis are reported in Refs. 63–65 and their corresponding chemical structures depicted in Figures 3.1 and 3.2 are studied in this work. The three copolymers consist of benzodithiophene (BDT), bithiophene and thienothiophene-spaced-bithiophene as donors and isoindigo with 2-decyltetradecyl side chain as a common acceptor, denoted respectively, as **PBDTI-DT**, **P2TI** and **P2TITT**.

Solvent

The solvent used in this study to prepare the solutions and thin film of polymers is 1, 2-dichlorobenzene (o-DCB), while chloroform (CF) and other solvents like acetone, isopropanol, dichloromethane, ammonia, hydrogen peroxide, and deionized water were also employed as cleaning agents.

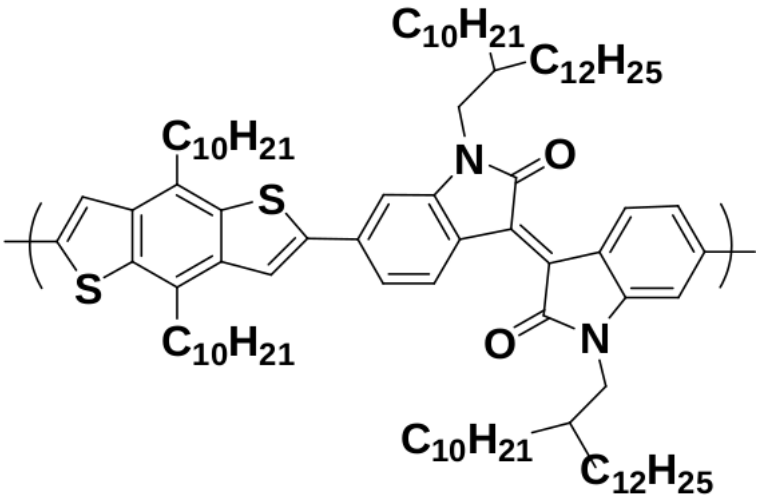

Figure 3.1: Chemical structure of **PBDTI-DT**

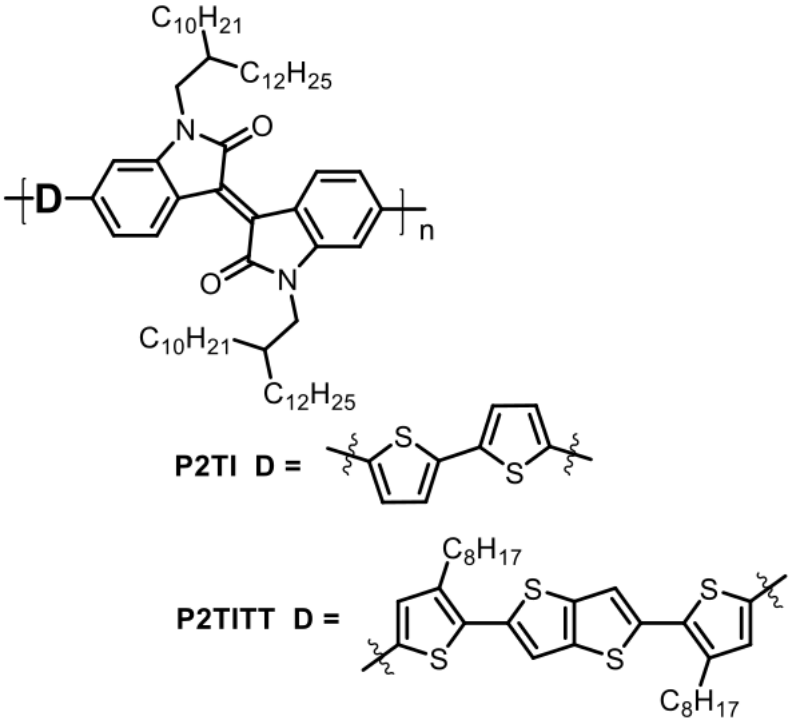

Figure 3.2: Chemical structures of **P2TI** and **P2TITT**

3.2 Experimental Methods

Solution Preparation

The solutions of the copolymers were prepared using o-DCB as a solvent at an average concentration of 0.02 mg/ml.

Thin Film Preparation

The thin films were prepared by spin-coating the polymer solutions on glass substrates at 1000 rpm, followed by annealing at 80 ℃ for 10 minutes to dry out the solvent.

Steady State UV-vis Spectra

UV-Vis spectra were among the experimental techniques employed in this work to study the photophysics of the polymers. Steady state room temperature UV-Vis absorption spectra in solution and spin-coated thin film were measured using an Edinburgh Instruments DS5 UV–Vis spectrophotometer for **PBDTI-DT** and a Perkin-Elmer Lambda 19 UV–Vis/NIR spectrophotometer for **P2TI** and **P2TITT**.

Steady State and Temperature-dependent Photoluminescence

The aggregation of polymers can be inferred from the progression of vibronic peak ratios with temperature. To this end the PL spectra of the polymer solutions were recorded while exciting the solutions with light at their absorption maxima in the lower-energy region (below 2.5 eV) using a HORIBA Jobin Yvon Fluoromax-4 spectrofluorometer. To control the temperature during the PL measurements, a Thermo Scientific NESLAB RTE-7 circulating bath was used, allowing the temperature to be varied from -10 to 90 ℃ for **PBDTI-DT**, and from -5 to 85 ℃ for **P2TI** and **P2TITT**.

Raman Spectra

The Raman spectra of **PBDTI-DT** were recorded using a WITEC α-300 spectrometer with a laser excitation source operating at 532 nm.

Relative Quantum Yield

The relative QY (ϕ_s) of **PBDTI-DT** was calculated using rhodamine 101 as a reference, which was diluted to an optical density (A) of below 0.1 to avoid self-absorption. The QY was then calculated using the following equation in five different concentrations:

$$\phi_s = \phi_r \left(\frac{\nabla(s)}{\nabla(r)} \right) \left(\frac{\eta_s^2}{\eta_r^2} \right), \tag{3.2.1}$$

where the subscripts s and r denote the sample and reference, respectively. The symbols ϕ, ∇, and η are the fluorescence QY, the gradient from the plot of integrated fluorescence intensity vs $\mathbf{1 - 10}^{-A}$, and the refractive index of the solvent, respectively.

Emission Lifetimes Measurement

The emission lifetimes of the two copolymers, **P2TI** and **P2TITT**, were measured in solution (0.02 mg/mL) and as thin film (15 mg/mL) using a home-built time-correlated single photon counting (TCSPC) experimental setup, as described by Kyeyune *et al.*[107] The TCSPC setup was equipped with a supercontinuum picosecond pulsed laser source (SuperK EVO, NKT Photonics). An optically narrow excitation beam at 633 nm was produced by sending the laser beam through a 632.8 nm band-pass filter (FLH633-1, Thorlabs). The excitation beam was reflected by a dichroic mirror (FF649-Di01-25×36 Semrock Brightline) into a water-immersion objective (Nikon CFI NIR Apochromat 60×, NA 1.0). Fluorescence from the sample was measured by a single-photon avalanche diode (COUNT-T100, Laser Components) coupled to a Becker & Hickl GmbH TCSPC module (SPC-130 EM) by focusing through a 75-µm pinhole and fluorescence filter (FELH0650, Thorlabs) to block scattered excitation light. Each sample was measured for 60 seconds.

3.3 Computational Methods

Density Functional Theory Calculations

The ideas of theoretical and quantum chemistry are incorporated into practical computer programs to perform computational chemistry, which is used to assess the structural properties of various molecules. Density Functional Theory (DFT) is one of the increasingly popular techniques for the calculation of molecular structure.[108] DFT focuses on the electron density ρ rather than considering the electron wavefunction Ψ. The energy of the molecule which is constructed from superposition of "Kohn–Sham-orbitals" is written as a function of the electron density, which in turn, is a function of position. These orbitals are calculated by solving Kohn–Sham equations, Equation 3.3.1, iteratively and self-consistently. And these orbitals are different the common spatial electron orbitals. DFT theory is a powerful technique and is still being under further development.

$$\left(-\frac{\hbar^2}{2m}\Delta^2 + v_{eff}(r)\right)\varphi_i(r) = \epsilon_i\varphi_i(r) \tag{3.3.1}$$

Here ϵ_i is the orbital energy of the corresponding Kohn–Sham orbital $\varphi_i(r)$, $v_{eff}(r)$ is the Kohn–Sham potential, and the density for an N-particle system is

$$\rho(r) = \sum_{i}^{N} |\varphi_i(r)|^2$$

It is used to calculate different compounds' energies, dipole moments, and thermodynamic characteristics. In the case of solid organic materials in particular, aggregation may have large influence on the spectrum but is more challenging to predict using time-dependent density functional theory (TD-DFT) than single-molecule spectra, particularly when charge-transfer transitions between molecular units are present. When there is considerable charge-transfer character or a significant degree of conjugation, an artificial redshift is introduced into the TD-DFT spectra of even single molecules.[109,110] In this study DFT and TD-DFT calculations were conducted to support experimental characterizations on selected polymers.

DFT calculations were employed in the gas phase to optimize the backbone geometry, and calculate frontier molecular orbitals, and Raman spectra of the **BDTI** oligomers ($n = 1 - 3$) using Gaussian 16/C01.[111] The calculations were executed using the B3LYP hybrid functional and 6-31G(d,p) basis set after reducing the alkyl side chain lengths to single methyl units as their contribution to the electron density of the polymer is negligible.[112] The excited-state analysis together with the UV-Vis absorption of the oligomer were studied using TD-DFT with the CAM-B3LYP functional and 6-31G(d,p) basis set. On the other hand, DFT calculations to optimize the backbone geometry and calculate the frontier molecular orbitals (FMOs) on three units of **P2TI** and **P2TITT** were carried out using the B3LYP hybrid functional and 6-31g(d) basis set. The excited-state properties and the UV-Vis absorption spectra of the oligomers were analyzed using CAM-B3LYP functional and 6-31g(d) basis set. For the density of states (total/partial density-of-state (TDOS/PDOS)) calculations on three units of **P2TI** and **P2TITT**, the CAM-B3LYP functional was used instead. Geometry optimization and frequency calculations were performed until a stationary point was found for both calculations in all cases.

The Franck-Condon Analysis

Intensities of vibronic transitions can be described by the FC Principle. In quantum mechanical formulation FC principle is stated as follows: the strength of a vibronic transition is directly related to the square of the overlap integral between the vibrational wavefunctions of the initial and final states involved in that transition. This principle is based on the Born-Oppenheimer approximation. The overall energy comprises both electronic and vibrational components, while the total wavefunction is derived by multiplying the electronic wavefunction with the nuclear wavefunction. According to Born-Oppenheimer approximation separation of the electronic, r, and nuclear, R, wavefunctions are separable.

$$\Psi(r, R) = \phi_e(r, R)\chi_\nu^e(R) \tag{3.3.2}$$

where r is the electronic coordinate and R the nuclear coordinates. The index e corresponds to an electronic state, while ν is the vibrational quantum number.

The dipole moment operator is

$$\hat{\mu} = -e\sum_i r_i - e\sum_k Z_k R_k = \hat{\mu}_e + \hat{\mu}_N$$

With the consideration of only one vibration, the dipole matrix element for a transition between electronic state g with vibrational level m and electronic state e with vibrational level n is given by,[113]

$$\begin{aligned}
\tilde{\mu} &= \langle \phi_e(r,R)\chi_n^e(R)|\, \hat{\mu}_e + \hat{\mu}_N \,|\phi_g(r,R)\chi_m^g(R)\rangle \\
\tilde{\mu} &= \langle \chi_n^e(R)|\, \langle \phi_e(r,R)|\, \hat{\mu}_e \,|\phi_g(r,R)\rangle \,|\chi_m^g(R)\rangle \\
&\quad + \langle \chi_n^e(R)|\, \hat{\mu}_N \,|\chi_m^g(R)\rangle \,\langle \phi_g(r,R)|\phi_e(r,R)\rangle \\
\tilde{\mu} = \langle \chi_n^e(R)|\, \langle \phi_e(r,R)|\, \hat{\mu}_e \,|\phi_g(r,R)\rangle \,|\chi_m^g(R)\rangle &= \langle \chi_n^e(R)|\, \hat{\mu}_{eg}(R) \,|\chi_m^g(R)\rangle
\end{aligned}$$

$\hat{\mu}_{eg} = \langle \phi_e(r,R)|\, \hat{\mu}_e \,|\phi_g(r,R)\rangle$ is the electronic dipole moment.

The transition dipole moment between electronic state g with vibrational level m and electronic state e with vibrational level n, according to the Condon approximation, is

$$\tilde{\mu}_{gm,en} = \mu_{eg}^0 \,\langle \chi_n^e(R)|\chi_m^g(R)\rangle$$

The absorption cross section is directly related to the square of this transition dipole moment,

$$\sigma \propto |\tilde{\mu}_{gm,en}|^2 = \left|\mu_{eg}^0\right|^2 \times FC$$

Using the model of displaced harmonic oscillator and with the assumption of population of the zero vibrational level in the ground state, Franck - Condon integrals can be worked out analytically. The vibronic transition 0-n, which dictates the probability of each vibronic

transition, has FC integral:

$$F_{0n} = \frac{e^{-S}S^n}{n!}$$

where, $S = \frac{1}{2}\frac{m\omega}{\hbar}(\Delta Q)^2$ with m denoting the reduced ionic mass.

$$S = \frac{k\Delta Q}{2\hbar\omega} = \frac{E_{relx}}{\hbar\omega}$$

The Huang-Rhys factor, S, denotes the average number of phonons generated by the vibronic transitions. E_{relx} is relaxation energy or reorganization energy. For a single-mode vibrational progression, the value of S can be calculated from experimental spectra using $I_{0-1}/I_{0-0} = S$, where I_{n-m} represents the amplitude of the transition between vibrational level n and m.

Franck–Condon (FC) analysis was used to estimate the spectral intensity distribution of the PL of **PBDTI-DT**, **P2TI** and **P2TITT**. In this regard, temperature-dependent PL spectral profiles of these copolymers were fitted with two progressions for J- and H-type aggregates given in Equations. 3.3.3 and 3.3.4, respectively.[59,114,115]

$$I_J(\hbar\omega) \propto (\hbar\omega)^3 n^3 exp(-S)\left(\sum_{m=0}\frac{S^m}{m!}\Gamma(\hbar\omega - E_0 + mE_p)\right) \tag{3.3.3}$$

$$I_H(\hbar\omega) \propto (\hbar\omega)^3 n^3 exp(-S)\left(\alpha\Gamma(\hbar\omega - E_0) + \sum_{m=1}\frac{S^m}{m!}\Gamma(\hbar\omega - E_0 + mE_p)\right), \tag{3.3.4}$$

where n is the real part of the refractive index at photon energy $\hbar\omega$, S is the HR factor, which gives a measure of the coupling between the electronic transition and a phonon mode, m denotes the vibrational level, E_0 is the 0-0 transition energy, E_p is the phonon energy, and Γ is a Gaussian line shape with constant width. The parameter α is the exciton coherence number which appears only in the modified Franck - Condon model and denotes the competition between intrachain and interchain exciton coupling. It is a function of disorder and dictates the intensity of I_{00}, which is absent for a perfectly ordered H-aggregate at 0 K.

Chapter 4

Investigation into Aggregation Types in a Benzodithiophene-Isoindigo Copolymer

4.1 Introduction

Incorporation of an electron-deficient moiety in the backbone of an electron-donating polymer to produce a donor-acceptor (D-A) copolymer has been found to be a successful technique to produce low-band gap polymers. Isoindigo has found broad application in the synthesis of low-band gap polymers as acceptor units because of its highly planar structure, which favors good charge carrier mobility. Results from reports on isoindigo-based[116–125] polymers indicate that such materials show broad optical absorption, high extinction coefficient and high charge mobility.[126,127] On the other hand, benzodithiophene (BDT) is an electron-rich material that has already achieved outstanding PCE in OSCs exceeding 19%.[3,128] BDT exhibits some attractive behaviors that make it a good candidate as photoactive material for OSCs. The planar conjugated structure of benzodithiophene forms $\pi - \pi$ stacking that improves mobility in conjugated polymers. Recently, benzodithiophene-isoindigo (PBDTI-DT) copolymer has been synthesized,[63] the structure of which is displayed in Figure 3.1, and shown to exhibit good photo and thermal stabilities.[129]

In this chapter, we present investigation of the properties of **PBDTI-DT** by examining the

aggregation types into which the copolymer self-assembles. This serves to further guide the synthesis of benzodithiophene-isoindigo for enhanced device performance. The aggregation type of **PBDTI-DT** was investigated by fitting its temperature-dependent PL spectra with a FC analysis. In addition, the evolution of the HR factor with temperature along with the measurement of the relative QY, revealed that the copolymer consists of both H- and J-type aggregates, with H being the dominant aggregation type. The photophysical investigation performed both computationally and experimentally revealed that the $S_0 \rightarrow S_1$ and $S_0 \rightarrow S_7$ transitions are mainly due to intramolecular charge transfer (ICT) and $\pi - \pi^*$ transitions, respectively.

4.2 Result and Discussion

4.2.1 Absorption of PBDTI-DT

Figure 4.1 **A)** shows the absorption spectrum of **PBDTI-DT** in solution and as a spin-coated thin film, displaying the common two-band profile that arises from alternating donor-acceptor bonding.[130] The absorption of **PBDTI-DT** in thin films is somewhat red-shifted from that of the solution-based polymer, indicating aggregate formation in the solid state. To determine the transition types of the absorption bands, the absorption of the uncoupled donor and acceptor units and the polymer were recorded and are shown in Figure 4.2**A)**. The absorption spectra of both the donor (BDT) and acceptor (isoindigo) units peak near the high-energy band of the polymer. This indicates that the absorption band of the polymer above 2.5 eV is a superposition of the local $\pi - \pi^*$ transition of the acceptor and donor units. However, the peak of the polymer below 2.5 eV is observed neither in the spectrum of BDT nor of the isoindigo units, confirming that it has evolved due to ICT between acceptor and donor moieties.

To further elucidate the assignment of the two transition bands, TD-DFT calculations on oligomers up to three repeating units with 50 excited states were computed in the gas phase. The absorption of BDTI was calculated from one to three repeating units as presented in Figure 4.1**B)**. The calculated absorption profile of the trimer resembles the experimental result sufficiently well to use as a basis for studying the transitions in the polymer. The transitions in the four dominant excited states of the trimer are summarized in Table 4.1. Whereas the frontier molecular orbitals

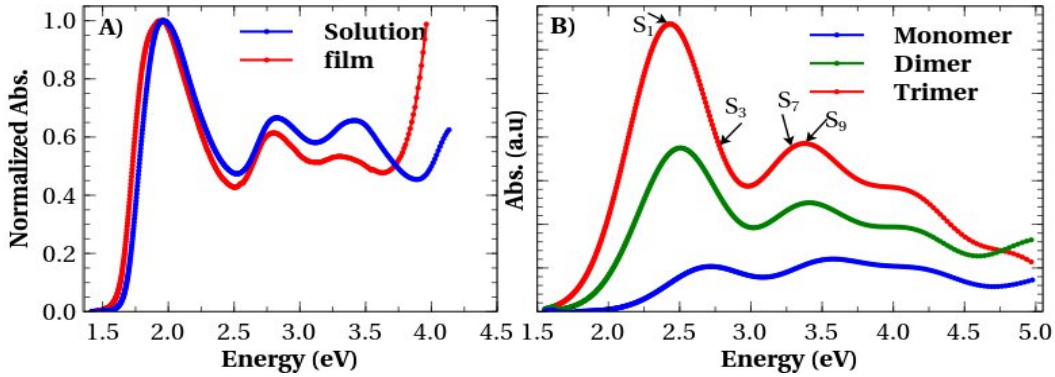

Figure 4.1: **A)** Absorption spectra of **PBDTI-DT** solution and spin-coated film, and **B)** DFT-calculated absorption spectra of BDTI monomer, dimer, and trimer. S_1, S_3, S_7, and S_9 are excited states having strong contributions.

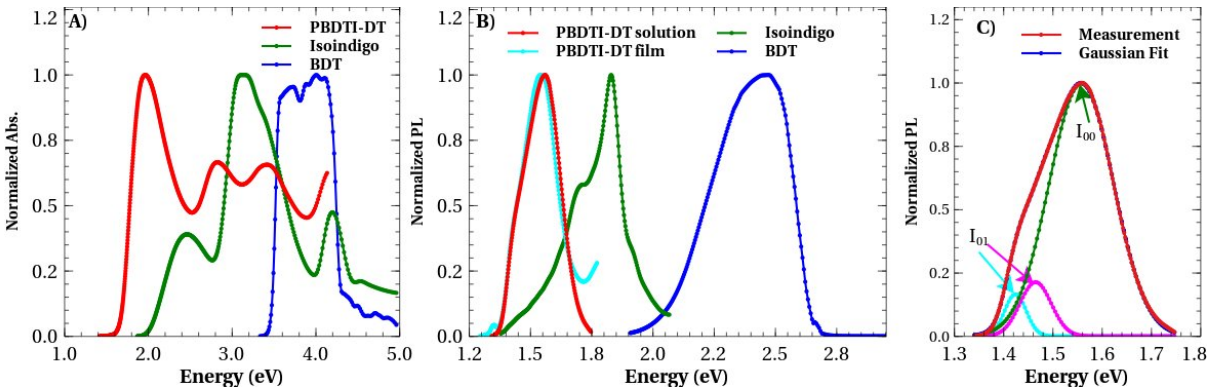

Figure 4.2: **A)** Absorption and **B)** PL spectra of **PBDTI-DT** and its donor (BDT) and acceptor (Isoindigo) units, and **C)** Gaussian fit of **PBDTI-DT** PL spectrum measure at room temperature in solution with pure electronic, I_{00}, and first vibrational, I_{01}, transitions.

Table 4.1: The four most probable excited states of the BDTI trimer with the corresponding dominantly contributing transitions.

Excited State	Excitation Energy (eV)	Oscillator Strength (a.u.)	Transition	Contribution per band (%)
S_1	2.413	3.858	HOMO→LUMO	67
			HOMO-3 →LUMO	11
			HOMO-2 →LUMO+3	9.6
S_3	2.695	0.304	HOMO-1 → LUMO+2	31.4
			HOMO →LUMO+2	31.1
			HOMO-3 →LUMO+1	18.6
S_7	3.280	1.509	HOMO → LUMO	27
			HOMO-3 →LUMO+2	15
			HOMO-3 →LUMO+1	14.3
			HOMO-2 →LUMO+3	12
			HOMO-2 →LUMO	10
S_9	3.412	0.286	HOMO-2 →LUMO	33.2
			HOMO-2 →LUMO+1	22.8
			HOMO-1 →LUMO+1	22.7

of the trimer are displayed in Figure 4.3.

The excited states S_1 and S_7 are the dominant ones lying in the lower and upper energy regions, respectively. The HOMO → LUMO transition contributes to 67% of S_1's oscillator strength. Since the HOMO is spread predominantly over the BDT unit while the LUMO is concentrated in the isoindigo part (Figure 4.3), the HOMO → LUMO transition can be assigned to an ICT state. On the contrary, almost 30% of the transitions in S_7 are due to HOMO-3→ LUMO+1 and HOMO-3→ LUMO+2 transitions, slightly higher than the HOMO → LUMO transition. Interestingly, the three molecular orbitals HOMO-3, LUMO+1, and LUMO+2 are mostly localized on the isoindigo part (Figure 4.3), while the next dominant transition in S_7, the HOMO-2→ LUMO+3 transition, is localized on BDT. Hence, the transitions of S_7 are mainly within localized donor and acceptor units, confirming its local $\pi - \pi^*$ transition.

4.2.2 Temperature-dependent PL of PBDTI-DT

The PL spectra of **PBDTI-DT** and the uncoupled acceptor and donor units were recorded in solution to determine the relaxation channel of the copolymer (see Figure 4.2**B)**). Note here that the emissions were recorded at excitations matching the absorption maximum of each of the polymers. The emission of the copolymer both in film and solution is substantially red-shifted from that of the respective units, confirming its ICT characteristics. The PL spectrum

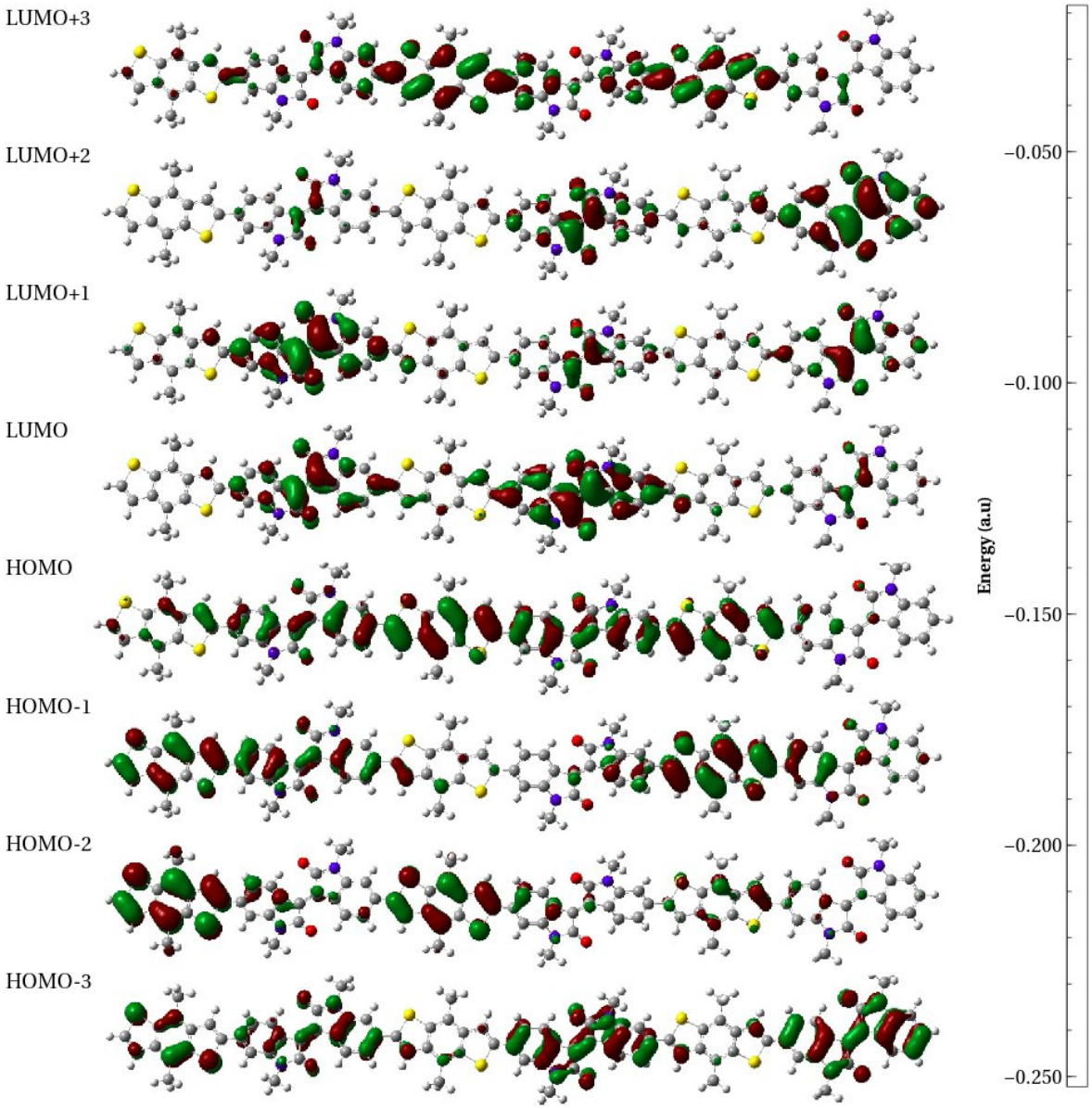

Figure 4.3: Frontier molecular orbitals of the BDTI trimer.

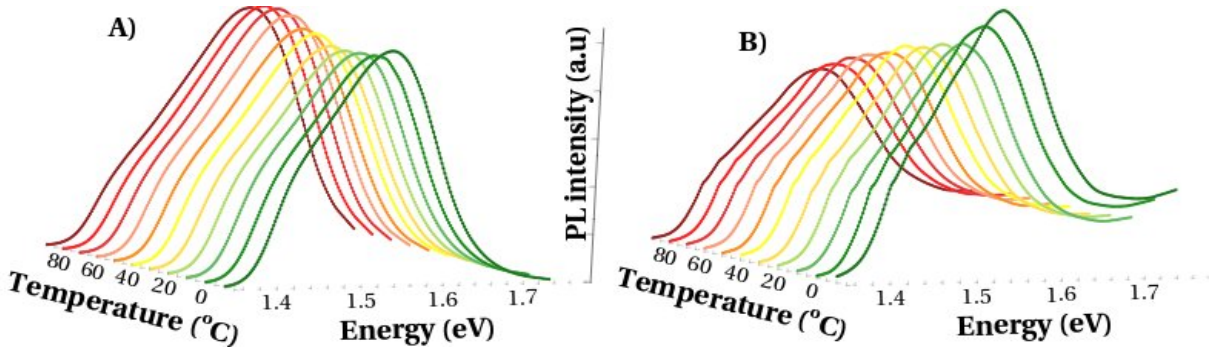

Figure 4.4: Temperature-dependent PL spectra of **PBDTI-DT A)** in solution and **B)** in spin-coated film measured from −10 to 90 ℃ in steps of 10 ℃.

of **PBDTI-DT** in solution shows a red shoulder owing to vibrational transitions. The spectrum can be deconvoluted into three Gaussian envelopes (Figure 4.2**C)**), which we assign to the pure electronic transition (I_{00}), and the the next vibronic transition (I_{01}) with two phonon modes. This Gaussian fit clearly demonstrates that the emission of the copolymer originates from vibronic coupling.

The emission of the polymer was further recorded with increasing temperature both in solution and film, as depicted in Figure 4.4, to investigate the types of aggregates that form in **PBDTI-DT**. As the temperature raised from −10 to 90 ℃ , the PL spectra were blue-shifted by 55.7 meV and 24.8 meV in solution and in film, respectively (see Figures 4.5**A)** and 4.5**B)**, black lines), indicating that the excitonic band edge shifted towards higher energies as the temperature increased. One reason could be that the effective conjugation length of the polymer might have decreased due to heat-induced conformational changes.[56,131] Michelle and Marcelo establish a quantitative relation between lowest-energy transition and effective conjugation length using modified Kuhn equation,

$$E(N) = E_0\sqrt{1 - 2\beta\cos\left(\frac{\pi}{N+1}\right)} - Ae^{-bN} \tag{4.2.1}$$

where E is the lowest-energy transition for the polymer, N number of identical oscillators vibrating with energy E_0, β is a dimensionless parameter related to the force constant of N oscillators, while b and A are free parameters.

Replacing the lowest-energy transition by emission peak energy and using the relation $N =$

$3L_{eff} + 2$,[132] we can relate the PL peak energy (PL_{peak}) to the effective conjugation length L_{eff} as follows,

$$PL_{peak}(L_{eff}) = E_0\sqrt{1 - 2\beta\cos\left(\frac{\pi}{3L_{eff}+3}\right)} - Ae^{-b(3L_{eff}+2)} \tag{4.2.2}$$

This relation supports that as the effective conjugation length decreases the PL peak energy undergoes a blue shift, hence applicable for both thin film and solution provided that the parameters could vary.

Here note that the blue-shift of the **PBDTI-DT** PL spectrum in solution is more than double that of the film. The main difference between the solution and film is the dominant interchain interaction in films.[64] Hence, it is expected that conformational changes in the film need higher thermal energy than in solution, supporting the idea that the blue shift originates from heat-induced conformational changes in the backbone of **PBDTI-DT**.

The PL peak amplitude is displayed in Figure 4.5**A)** and 4.5**B)** (blue lines) against the temperature to better understand the de-excitation photophysics of the polymer both in solution and film. Unlike the peak positions, the PL amplitude reveals different dynamics, viz. an increase in solution but a decrease in the film, confirming two different effects on the emissive species. This change in the emissive species can be observed by integrating the copolymer's emission spectrum, which is shown in Figure 4.5**C)** in relation to temperature. In solution, a temperature increase liberated the emissive states, probably by ordering the polymer chains. However, in the films, the opposite is true, whereby an increasing temperature has reduced the emission yield of the polymer. This may be explained by the interrupted interchain interaction that hampers the planarity of the molecule.[60]

The effect of temperature on the pure electronic transition, I_{00}, and the first side-band transition, I_{01}, can be used to understand the aggregate type in the polymer. In an ideal H-aggregate, the oscillator strength of the free-exciton band is concentrated on top, making the 0-0 transition optically forbidden, while side-band transitions with one or more vibrational phonons are allowed. In contrast, in J-type aggregates, the 0-0 transition is allowed since the oscillator strength is con-

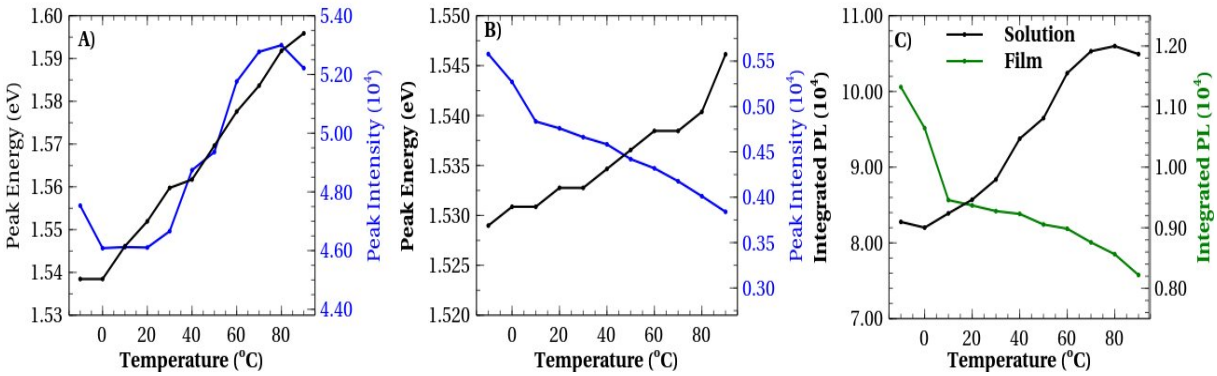

Figure 4.5: PL peak energy (black) and intensity (blue) of **PBDTI-DT A)** in solution and **B)** as spin-coated film as a function of temperature, and **C)** integrated PL of **PBDTI-DT** in solution (black) and as thin film (green).

centrated on the bottom of the free exciton band.[131] Hence, the effect of temperature on the I_{00} is different in H- and J-aggregates: it increases significantly with temperature in H-aggregates as an increasing temperature enhances the amount of disorder that can break the symmetry, while the intensity decreases in J-aggregates because the symmetry breakage may favor the side-band transition.[131]

The electronic-vibrational coupling in a polymer can be quantified by the HR factor, S, which is related to the average number of phonons excited when an electron makes a transition between two electronic states and its value can be obtained by calculating the relative strength of the emission at the 0-1 peak, I_{01}, intensity compared to the 0-0 peak, I_{00}, intensity,[67]

$$S = \frac{I_{01}}{I_{00}}. \tag{4.2.3}$$

The HR factor is a measure of ratio between the potential energy associated with vibrational excitation, $1/2k\Delta Q^2$, and the energy of vibrational quanta, $\hbar\omega_m$, where k is the force constant, ΔQ the change in the equilibrium coordinate, ω_m the angular frequency, and $\hbar$ the reduced Planck constant. In this context, S also yields the number of quanta involved in the vibrational excitation. The HR factor is expressed in Equation 4.2.3 under the assumption of same vibrational frequency, ω, for the excited and ground states, and that the potentials are perfectly parabolic.[133] Due to relaxation transitions are supposed to originate near the bottom where the

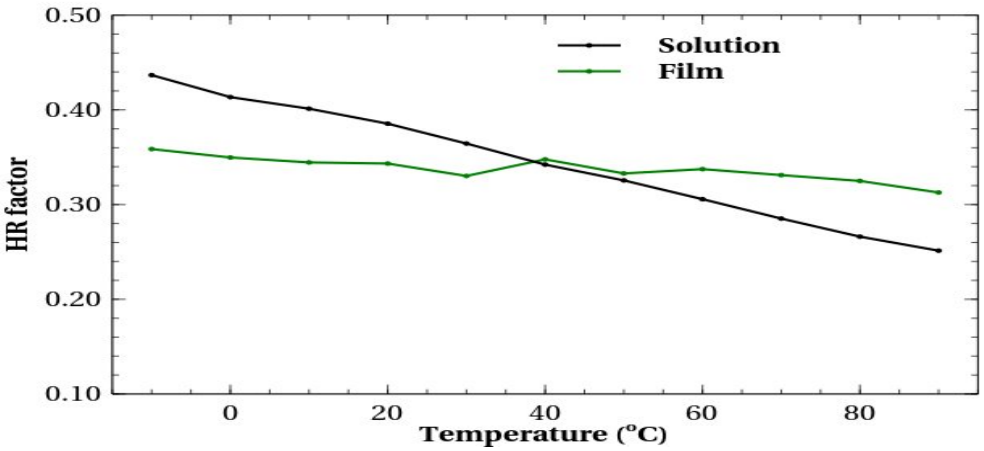

Figure 4.6: HR factor of **PBDTI-DT** in solution (black) and in film (green) as a function of temperature.

potentials are parabolic and the spacing between vibrational levels is equal which supports the above assumption.

The HR factor is sensitive to temperature and/or disorder and can be used to determine the aggregation types formed by polymers. The factor increases (decreases) in J(H) aggregates with increasing temperature/disorder.[131] From the PL spectra of **PBDTI-DT**, both in film and solution, the intensities corresponding to the first vibronic transition, I_{00}, and the second vibronic transition, I_{01}, were extracted for the whole temperature range by taking the maximum amplitude for I_{00}, while I_{01} was determined from the second-order derivative of the spectra. The HR factors of **PBDTI-DT** in solution and film were then calculated and found to decrease, as shown in Figure 4.6, suggesting the presence of H-aggregates. However, the HR factor is significantly smaller than unity due to the highly favored 0-0 transition over 0-1 in the polymer, which is characteristic for J-aggregates.[28,114] However, this does not necessarily assure the presence of J-aggregates rather this might be attributed to disorder even at lower temperatures. This makes the assignment of the aggregates to both H and J-types in the polymer from HR factor insufficient.

4.2.3 Franck-Condon (FC) Analysis

An FC analysis can be used to estimate the spectral intensity distribution of the absorption and PL of polymers.[134–137] An FC analysis assumes all transitions to be vertical and directly related to the square of the overlap integral between the vibrational wavefunctions of the initial and

final states involved in the transition. Using this concept, the vibrational progressions in the PL of the polymer can be used to accurately determine the type of aggregation. In this regard, temperature-dependent PL spectral profiles of **PBDTI-DT** were fitted with two progressions for J- and H-type aggregates given in Equations 3.3.3 and 3.3.4, respectively:[59,114]

Three phonon modes were identified from the measured Raman spectra (Figure 4.7A)) with frequencies of 558 cm^{-1}, 1120 cm^{-1} and 1543 cm^{-1}. The higher two frequencies were also found in the DFT-calculated Raman spectra (Figure 4.7B)), albeit blue-shifted. These two frequencies are connected to carbon-carbon single-bond stretching coupled with carbon-hydrogen bending (C-C/C-H) and carbon-carbon double-bond stretching coupled with carbon-hydrogen bending (C=C/C-H), respectively. Nearly similar phonon mode assignments are also given to MEH-PPV and BEH-PPV in the literature.[138] The DFT calculated Raman spectra did not reveal the low frequency vibration mode. It should be noted that the measured Raman spectrum was obtained in thin film, where torsional disorder is expected, as opposed to the very planar molecule generated in the optimized geometry (See Figure). The main stretching modes are also expected to shift in frequency and fluctuate in intensity with the backbone geometry, as indicated by the small frequency-shifted Raman signal in the trimer compared to the monomer. Furthermore, the effect of side chain length on molecular ordering and hence the frequency of Raman modes could explain the observed variation. For example, Razzell-Hollis *et al.*'s DFT simulation demonstrated that the C=C stretching mode in a poly-3-hexyl telluride (P3HTe) polymer shifts to a higher frequency while the C-C stretching only decreases in intensity with increasing inter-unit torsion angle, confirming the importance of backbone conformation in both the frequency and intensity of the Raman spectra.[139] As a result, the Raman mode at 558 cm^{-1} was assigned to the torsional mode, which is present in the long-chained polymer that is more likely to adopt a non-planar conformation than the three-unit monomer with trimmed side chain to a single methyl unit considered in the calculation, owing to the different molecular conformation.[139,140] In the well-studied MEH-PPV polymer, a similar assignment was used, and a torsional mode was found to rise with increasing temperature.[59]

The PL spectra of the polymer in solution and spin-coated film recorded at temperatures of -10, 30, 60, and 90 ℃ were fitted with the assigned phonon modes, as recorded in Figures 4.8 and

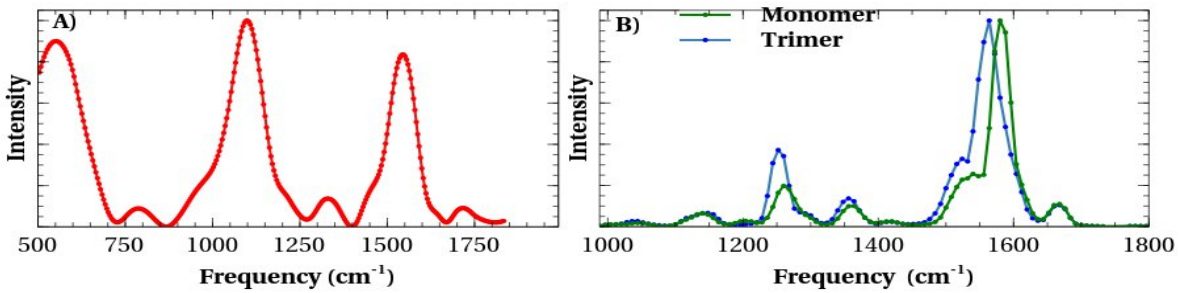

Figure 4.7: Comparison of **A)** experimental and **B)** DFT-calculated monomer (green) and trimer (blue) Raman spectra of **PBDTI-DT.**

4.9. The two modes with higher frequencies were used to fit the PL spectra of **PBDTI-DT** in solution at the two lowest temperatures (−10 and 30 ℃), while at higher temperatures the best fits were obtained only when the third phonon mode was added, which suggests the activation of torsional motion with the $E_p = 558$ cm^{-1} mode.[59] On the contrary, for FC-fitting of the thin film the third phonon mode was activated starting from 30 ℃. The difference in activation temperature of the torsional phonon modes in solution and film suggests that separate mechanisms play a role in polymer planarization. Polymers tend to form large aggregates in solution as the temperature rises due to thermodynamically activated segment diffusion and solvation that eventually isolates the chain leading to self-assembly and thus torsional disorder.[141,142] Polymer conformation in films, on the other hand, is controlled by a variety of factors, including interchain interaction. Heating to a specific temperature below T_g (glass transition temperature), above which the polymer chain start to adopt a new conformation that will result in twisting, can be used to induce the rearrangement of the chains toward an ordered state.[141] As a result, the temperature at which the polymer begins to twist in a film may be lower than the temperature at which it begins to tangle in solution. In addition, Yamagata *et.al* reported the concomitant planarization of polymer chains upon cooling when they are in solution with decreasing temperature.[59]

The FC fitting parameters of **PBDTI-DT** are summarized in Table 4.2. Note here that the two progressions given in Equations 3.3.3 and 3.3.4 were used iteratively to find the best fit that gives physically feasible fitting parameter.

Table 4.2 indicates that the HR factor increased with the temperature for J-aggregates, while it shows a decreasing trend for H-aggregates when considering the activation of the third phonon

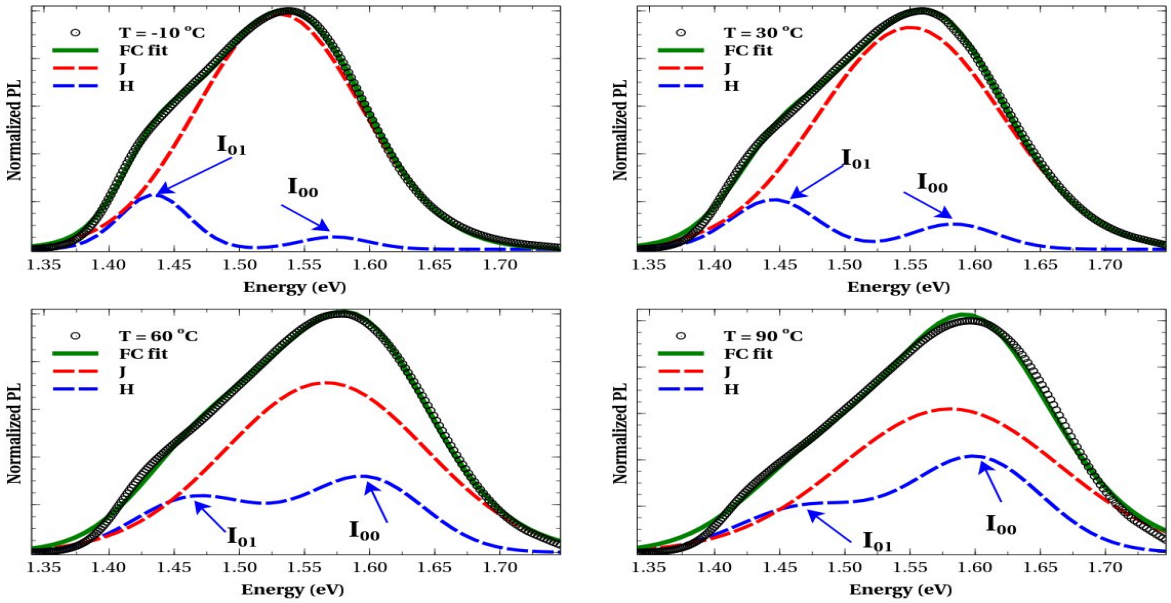

Figure 4.8: FC fit of **PBDTI-DT** in solution at selected temperatures, the green curves (FC fit) are the sum of red (J) and blue (H) curves. The vibronic transitions I_{00} and I_{01} in H-type aggregates are indicated by arrows.

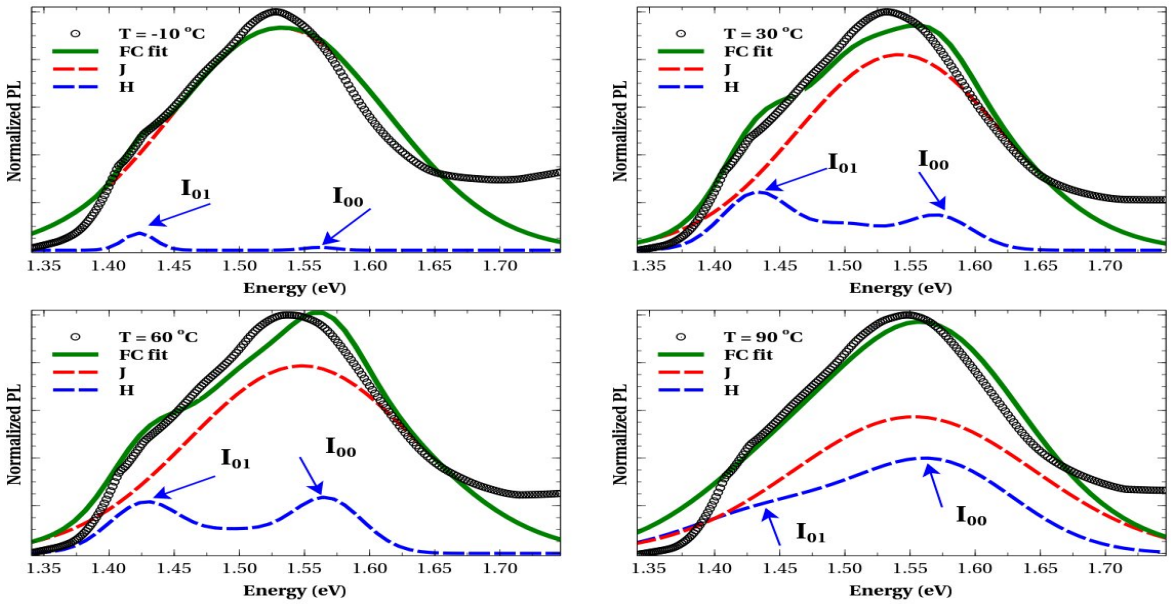

Figure 4.9: FC fit of **PBDTI-DT** in thin film at selected temperatures, the green curves (FC fit) are the sum of red (J) and blue (H) curves. The vibronic transitions I_{00} and I_{01} in H-type aggregates are indicated by arrows.

Table 4.2: Fitting results from FC analysis of **PBDTI-DT**: E_{00} (the 0-0 transition energy), E_{relx} (relaxation energy), S_{total} (HR factor), α (exciton coherence number), and σ (Gaussian line width).

Temperature (℃)			E_{00} (eV)	E_{relx} (meV)	S_{total}	α	σ (meV)
-10	Solution	J	1.5229	0.4220	0.0022	–	63.05
		H	1.5715	59.2619	0.4281	0.0732	26.36
	Film	J	1.5178	0.2954	0.0015	–	84.09
		H	1.5622	14.6846	0.1061	0.01352	12.20
30	Solution	J	1.5406	0.6177	0.0032	–	70.72
		H	1.5813	57.2463	0.4135	0.1597	32.94
	Film	J	1.5297	0.1918	0.001	–	78.90
		H	1.5695	127.8578	1.0009	0.1284	26.46
60	Solution	J	1.5550	0.8556	0.0045	–	77.27
		H	1.5957	133.5390	1.0179	0.2988	43.68
	Film	J	1.5335	0.6810	0.00355	–	87.72
		H	1.5648	99.5562	0.7855	0.2005	27.70
90	Solution	J	1.5674	1.3831	0.0072	–	84.16
		H	1.5978	129.3618	0.9675	0.45276	49.19
	Film	J	1.5364	1.0072	0.0053	–	92.80
		H	1.5657	94.24	0.7391	0.41295	59.92

mode at 60 ℃ and 30 ℃ for polymers in solution and film, respectively. Specifically, the decreasing HR factor for H-aggregates can be observed between −10 and 30 ℃ and between 60 and 90 ℃ for polymers in solution, and between 30 and 90 ℃ for the film-embedded polymers. The large increases at 60 ℃ and 30 ℃ for polymers in solution and film, respectively, are explained by the addition of a third phonon mode to the calculation of the HR factor. Taking this into consideration, the HR factor increases (decreases) for J(H) aggregates in both solution and thin film, as expected, while the total HR factor decreased with temperature, which agrees with the experimental result in section 4.2.2 Figure 4.6. This now leads to the conclusion that both H- and J-aggregates are present and that the fitting results are feasible because the temperature-dependent trends are as expected. Schematic illustration displaying the presence of both H- and J-type aggregates in **BDTI-DT** is shown in Fig 4.10.

The relaxation energy, which measures the strength of the electron-phonon coupling, is related to the HR factor as follows:[143]

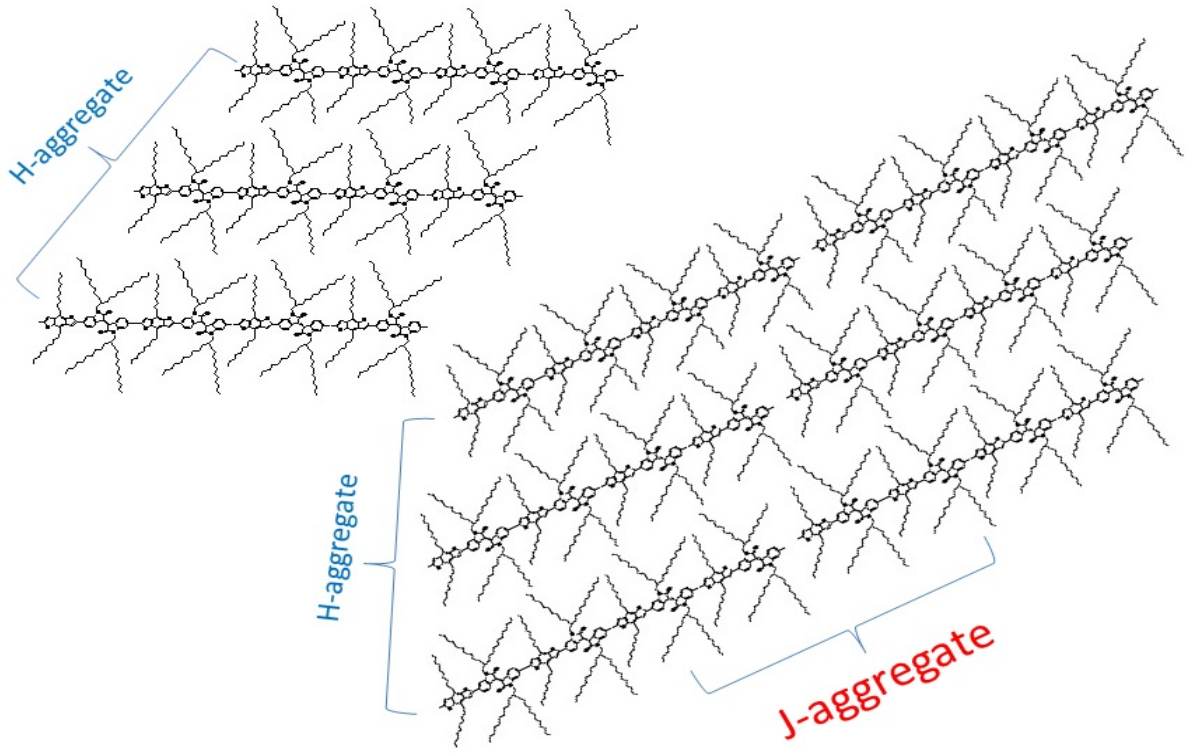

Figure 4.10: Illustration of aggregation types in **PBDTI-DT**.

$$E_{relx} = \sum_i S_i \hbar\omega_i, \tag{4.2.4}$$

where S_i and $\hbar\omega_i$ are respectively the HR factor and energy of the i^{th} phonon.

Table 4.2 shows that the relaxation energy displays the opposite temperature dependence for H- and J-type aggregates. Specifically, it increases for J-aggregates and decreases for H-aggregates with raising temperature. This is expected as disorder favors emission from lower states in H-aggregates, leading to a lowering of the relaxation energy, while it pushes the emissive J-aggregation states away from the lowest state, resulting in a higher relaxation energy. From the fit results, it can also be seen that both σ, which quantifies disorder, and α, the exciton coherence number, increased with temperature, as expected. The energetic disorder, σ, is related to the distance d between accessible excitonic sites through Equation 4.2.5.[144]

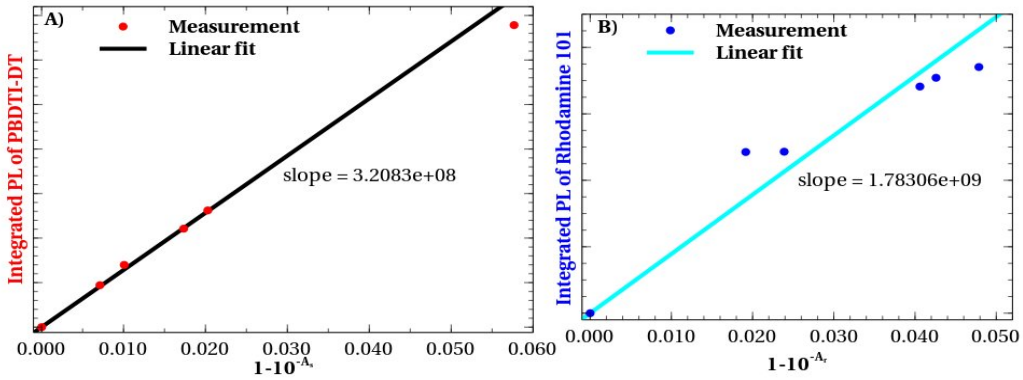

Figure 4.11: Integrated PL of **A) PBDTI-DT** and **B)** rhodamine 101 vs their absorbance ($\mathbf{1-10^{-A}}$) along with corresponding linear fits with R^2 values of 0.9975 and 0.9645, respectively.

$$d = \left[N_0 exp\left(-\frac{1}{2}\frac{\sigma^2}{(kT)^2} \right) \right]^{-1/3}, \tag{4.2.5}$$

where N_0 is the total density of available excitonic states, which is in the order of 10^{21} cm^{-3} for organic semiconductors, and T and k are the absolute temperature and Boltzmann constant, respectively.

The value of d, calculated in the film, shows that important diffusion between two sites takes place at low temperatures due to the reduced energetic disorder σ that leads to a decreasing distance d between accessible excitonic states. At low temperatures, in the thin film, the disorder for H-aggregates is much lower than the disorder in J-aggregates leading to the conclusion that effective diffusion takes place in H-aggregates.

4.2.4 Relative Quantum Yield

Quantum yield indicates how effectively absorbed photons are transformed into emitted photons. It is expected that J-aggregates have a high emission QY while H-aggregates have a lower yield. In this regard, the relative QY of **PBDTI-DT** was calculated using five dilute solutions of rhodamine 101 as a reference. Equation 3.2.1 was used to calculate the relative QY for the five concentrations of the sample and reference by plotting the integrated fluorescence intensity vs $\mathbf{1-10^{-A}}$ at a common excitation energy of 2.10 eV (Figure 4.11).[145] A low QY of approximately 22.43% was found for the copolymer, confirming that most aggregates are of H-type.[30]

4.3 Conclusion

Polymer aggregation has been highlighted to be crucial to the morphology of organic electronics. In this study, computational and experimental techniques were employed to assess the photophysics and aggregate formation of a benzodithiophene-isoindigo copolymer (PBDTI-DT). TD-DFT calculations executed on three units of the copolymer showed that the band-gap transition ($S_0 \rightarrow S_1$) has ICT characteristics while the higher-energy transition ($S_0 \rightarrow S_7$) has $\pi - \pi*$ characteristics, in agreement with the experimental results. An FC analysis was used to fit the temperature-dependent PL spectra, and the appropriate HR factors were computed. The polymer adopts both H- and J-aggregation, according to both the FC simulation and calculation of the HR factors. Furthermore, the H-aggregate is the dominant stacking that the polymer adopts, which confirms that it will be a good candidate for OSCs application, according to the relative QY measurement.

Chapter 5

Conformation-Dictated Aggregation Photophysics in Isoindigo-Based Copolymers

5.1 Introduction

Techniques such as modifying the side chains, molecular weight, and transition temperatures have been employed to tailor the aggregation type of polymers.[146,147] Furthermore, even minor modifications to the polymer backbone have been found to significantly impact the interchain and intrachain excitonic couplings, leading to a transition from H-like to HJ-like aggregation.[34] While structural modification of polymers has been widely used to enhance performance in OSCs, there has been little emphasis on understanding its impact on the molecular aggregation behavior. Donor-acceptor copolymers offer a unique opportunity to tailor the optical and electrical properties of polymers, especially in the context of their application in OSCs. Isoindigo has been successfully introduced as an acceptor unit in well-performing polymers. Evidently, the conformation of isoindigo-based copolymers can be controlled by the selection of the donor unit, through donor-acceptor intramolecular coupling.[130] However, to the best of our knowledge, the effect of the backbone conformation on the aggregation photophysics of isoindigo-based copolymers has not yet been reported.

In this chapter, we studied the effect of conformation on the aggregation photophysics of two isoindigo-based copolymers shown in Figure 3.2. The conformation of the two copolymers was systematically tuned by inserting a thieno[3,2-*b*]thiophene (**TT**) spacer in the bithiophene donor unit. This produced two copolymers, namely **P2TI** and **P2TITT**, synthesises are reported in references. 64 and 65. The backbone of **P2TITT** was found to be more planar compared to **P2TI** due to reduced steric hindrance between the acceptor and donor units. Additionally, the inclusion of the **TT** unit in the donor moiety shifted the HOMO level higher owing to the stronger electron-donating ability of the **TT**-spaced donor. FC analysis, combined with time-resolved PL, was employed to determine the aggregation type. The results indicate that the **TT**-spaced copolymer exhibits more H-type aggregation characteristics. This was further supported by temperature-dependent PL measurements showing stronger interchain interaction in **P2TITT**.

5.2 Results and Discussion

5.2.1 Backbone conformation and electrochemistry

The degree of conjugation and planarity of copolymers are key factors that determine their potential applications as well as their charge-transfer and self-aggregation characteristics.[148,149] The planarity of the copolymers **P2TI** and **P2TITT** was evaluated using the DFT-optimized backbone geometries, which were obtained using the B3LYP functional and 6-31g(d) basis set as displayed in Figure 5.1.

To quantitatively characterize the planarity of the polymers, two metrics were employed: the span of deviation from the plane (SDP) and the molecular planarity parameter (MPP).[150] The MPP reflects the overall deviation of the molecular structure from a fitting plane, while the SDP represents the deviation span of the structure relative to the fitting plane. Generally, a more planar molecular structure is expected to exhibit lower values for both the MPP and the SDP.[151–153] Introducing a thieno[3,2-*b*]thiophene (**TT**) spacer between the two thiophene rings of the donor unit was found to significantly affect the MPP and SDP values resulting in MPP and SDP values, respectively, of 0.91 and 5.25 $\mathring{A}$ in **P2TI**, and 0.73 and 4.07 $\mathring{A}$ in **P2TITT**. Notably,

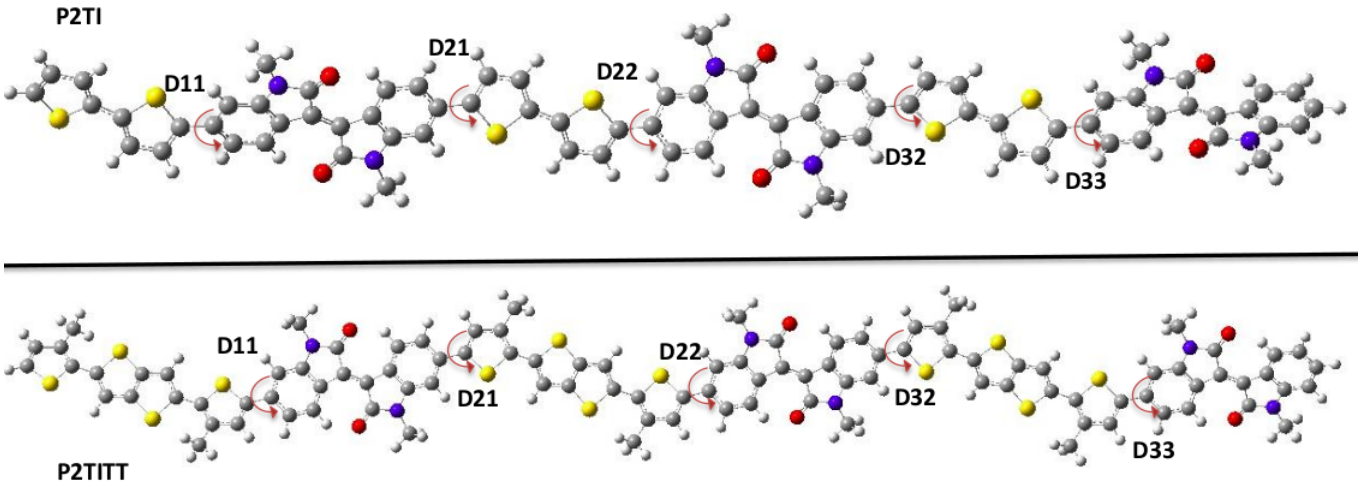

Figure 5.1: Optimized geometries and dihedral angles Dij between the donor and acceptor units for 3-unit oligomers of the two polymers, where h i and j represent the donor and acceptor units, respectively; red (O), blue (N), yellow (S) and gray (C).

the incorporation of a **TT** spacer between the thiophene rings of the donor unit was found to planarize the copolymer by minimizing intramolecular steric hindrance between the acceptor and the donor units. To understand the origin of the backbone twist in **P2TI** the dihedral angles Dij (where i and j represent, respectively, the labels of the donor and acceptor units denoted in Figure 5.1), were measured from the optimized geometries and summarized in Table 5.1. The results indicate that the dihedral angles between the acceptor and donor units of the copolymers were not significantly affected by the spacer. However, the introduction of the TT spacer notably enhanced the overall planarity, as evident from the side views of the optimized trimers of each polymer shown in Figure 5.2.

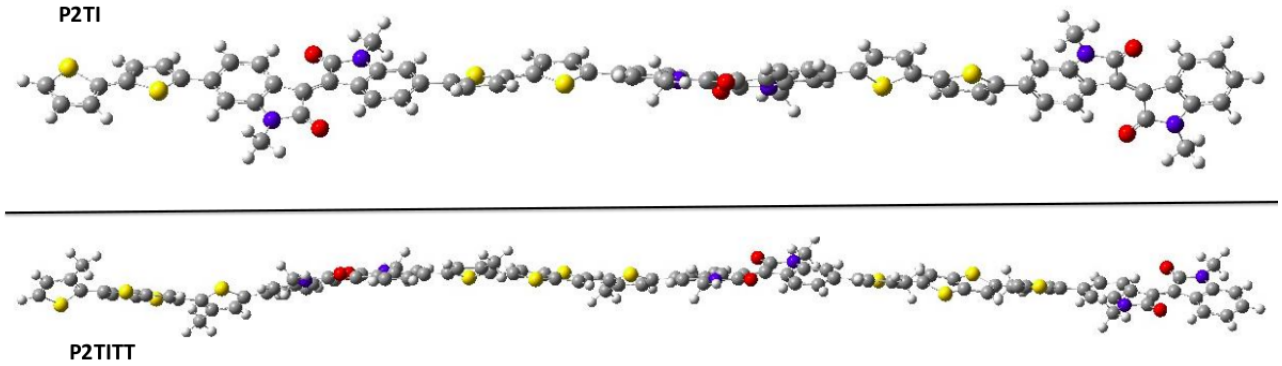

Figure 5.2: Side views of optimized geometries for trimeric units of **P2TI** (top) **P2TITT** (bottom)

In addition to the backbone conformation, π-spacers are also known to affect the electrical

Table 5.1: Dihedral angles (^{o}) between the thiophene and isoindigo units in the trimer units as denoted in Figure 5.1.

Dihedral Angle	**P2TI**	**P2TITT**
D11	158.73	158.94
D21	158.82	158.50
D22	159.04	159.31
D32	159.18	158.38
D33	158.95	158.78

and optical properties of polymers. Thus, the frontier molecular orbitals (FMOs) of **P2TI** and **P2TITT** were computed using the B3LYP functional and 6-31g(d) basis set, and the results are shown in Figure 5.3 along with the experimentally obtained values.[64,65] The experimental LUMO and HOMO energy levels were investigated using squarewave voltammetry (SWV) with their values calculated from the onsets of their reduction and oxidation potentials, respectively, using Equation 5.2.1 as reported by Bekri *et al.* and Desalegn *et al.*[64,65]

$$E_{HOMO/LUMO} = -(E_{ox/red} + 4.4)eV \tag{5.2.1}$$

In addition to determining the energy levels of FMOs, the spatial distribution of the electron density in these FMOs plays a major role in the electron-transfer processes in donor-acceptor copolymer systems. This is because ICT occurs through the transfer of electron density from the donor to the acceptor moieties.[154] The incorporation of **TT** between the two thiophene rings in the donor unit was found to raise the HOMO energy level of the copolymer compared to **P2TI**, indicating an enhanced electron-donating capability, corroborating previous studies.[155,156] In contrast, the introduction of the electron-rich **TT** bridge had only a slight influence on the LUMO energy level, confirming that the LUMO level is primarily determined by the electron-deficient acceptor unit.[157,158] Similar findings were reported by Tao *et al.*[157] who observed that the DFT-calculated LUMO levels of isoindigo-based copolymers were quite comparable. Notably, the DFT-calculated FMO energies closely followed the trend observed in the experimental data, as shown in Figure 5.3.

Furthermore, the electron cloud distribution in the FMO surfaces of **P2TI** and **P2TITT**, depicted in Figures 5.5 and 5.6, reveals that the HOMOs of the two copolymers are delocalized

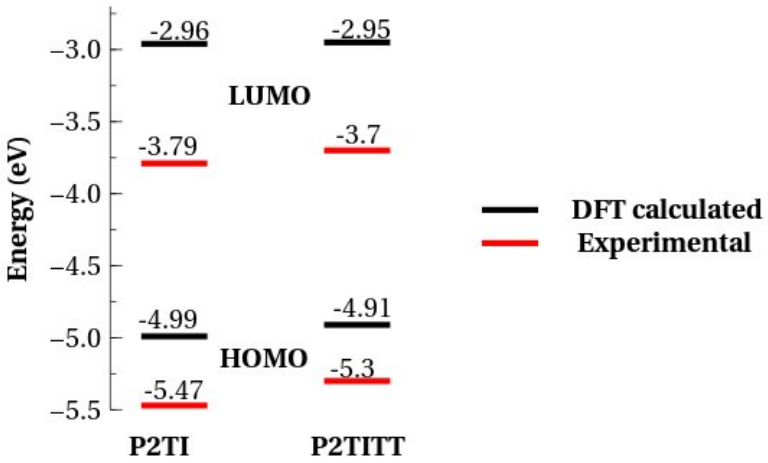

Figure 5.3: Comparison of the DFT-calculated and experimental HOMO - LUMO energy levels of **P2TI** and **P2TITT**.

along the π-conjugated backbone. In contrast, their LUMOs are primarily concentrated on the isoindigo-based acceptor unit, indicating efficient ICT in these D-A copolymers. To further evaluate the contribution of the donor and acceptor units to the electron cloud distribution in the FMOs, we calculated the partial and total density of states (PDOS and TDOS, red in Fig. 5.4) for each copolymer using the CAM-B3LYP/6-31G(d) functional by fragmenting the polymer into a donor (blue) and acceptor (green) components, as shown in Figure 5.4. The density distribution of the HOMO (valence band) and the LUMO (conduction band) are represented by the negative and positive x-axes, respectively. Both in **P2TI** and **P2TITT**, the TDOS occupies more space on the valence band than the conduction band, which supports the donating property of the copolymers. Comparing the TDOS of the two copolymers further reveals **P2TITT** has a stronger donating capacity, as evidenced by a higher TDOS amplitude in the valence band. This finding is analogous to previous studies on acceptors in which the density of state rather occupies more space on the conduction band.[159,160] The analysis reveals that the contribution of the donor unit to the electron density in the HOMO level increased from 47.8% in **P2TI** to 58.4% in **P2TITT** confirming a more localized HOMO in the **TT**-spaced copolymer **P2TITT**. The localization of the HOMO level in **P2TITT** is expected to enhance the ICT in this material. In contrast, the contribution of the acceptor moiety to the LUMO level decreased from 87.3% to 77.5% due to the inclusion of the **TT** spacer.

The copolymers energy levels are a direct result of the electron distribution at each atomic

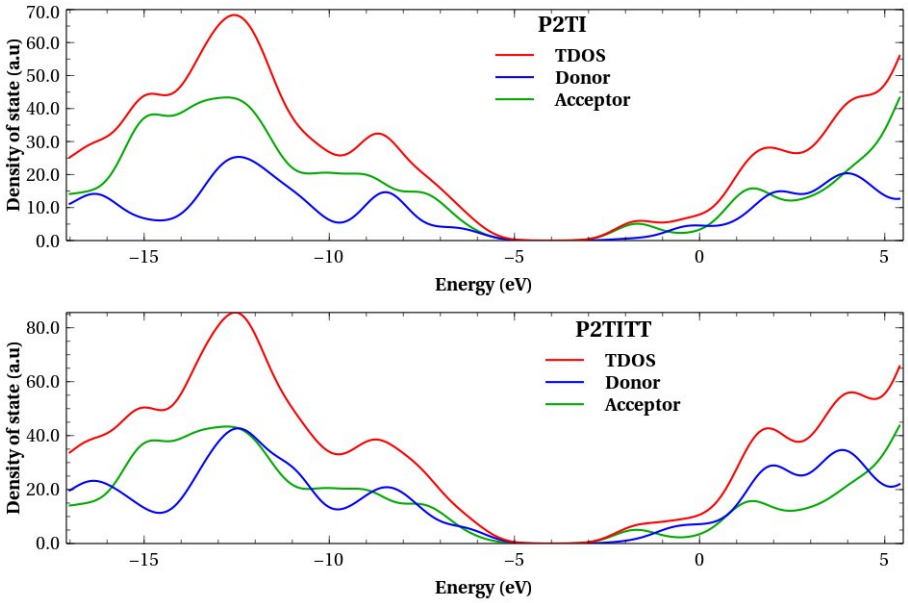

Figure 5.4: Total density of states (TDOS) in trimeric units of **P2TI** and **P2TITT** along with partial density of states of the donor and acceptor moieties, calculated using CAM-B3LYP/6-31g(d).

site within the polymer structure. Therefore, calculating the electrostatic potential (ESP) is an important tool to quantify the differences between the two polymers.[161,162] The ESP surface for three repeat units of **P2TI** and **P2TITT**, calculated at the B3LYP/6-31g(d) level of theory, are shown in Figure 5.7. Interestingly, the ESP values of the donor units were found to be less negative in the **P2TI** copolymer compared to **P2TITT**. This indicates a stronger electron-donating affinity of the **P2TITT** copolymer as a result of incorporating the **TT** spacer units. Consequently, the HOMO level of the **P2TITT** copolymer was found to shift upward as observed in Figure 5.3.[155,163] Intriguingly, the isoindigo units in the two copolymers displayed different ESP values, suggesting that the intramolecular charge-transfer process has modulated the electron distribution along the polymer backbone. This agrees with the electron cloud distribution in the FMO surfaces shown in Figures 5.5 and 5.6.

In summary, the analysis indicates that the **TT** bridges play an important role in imparting increased planarity to the bithiophene-isoindigo-based copolymer **P2TITT**. Moreover, the incorporation of the **TT** spacer enhances the electron-donating strength of the donor units, which increased the energy of the HOMO level compared to the **P2TI** copolymer. This is also supported by a higher density of states in **P2TITT** compared to **P2TI** in the valence band.

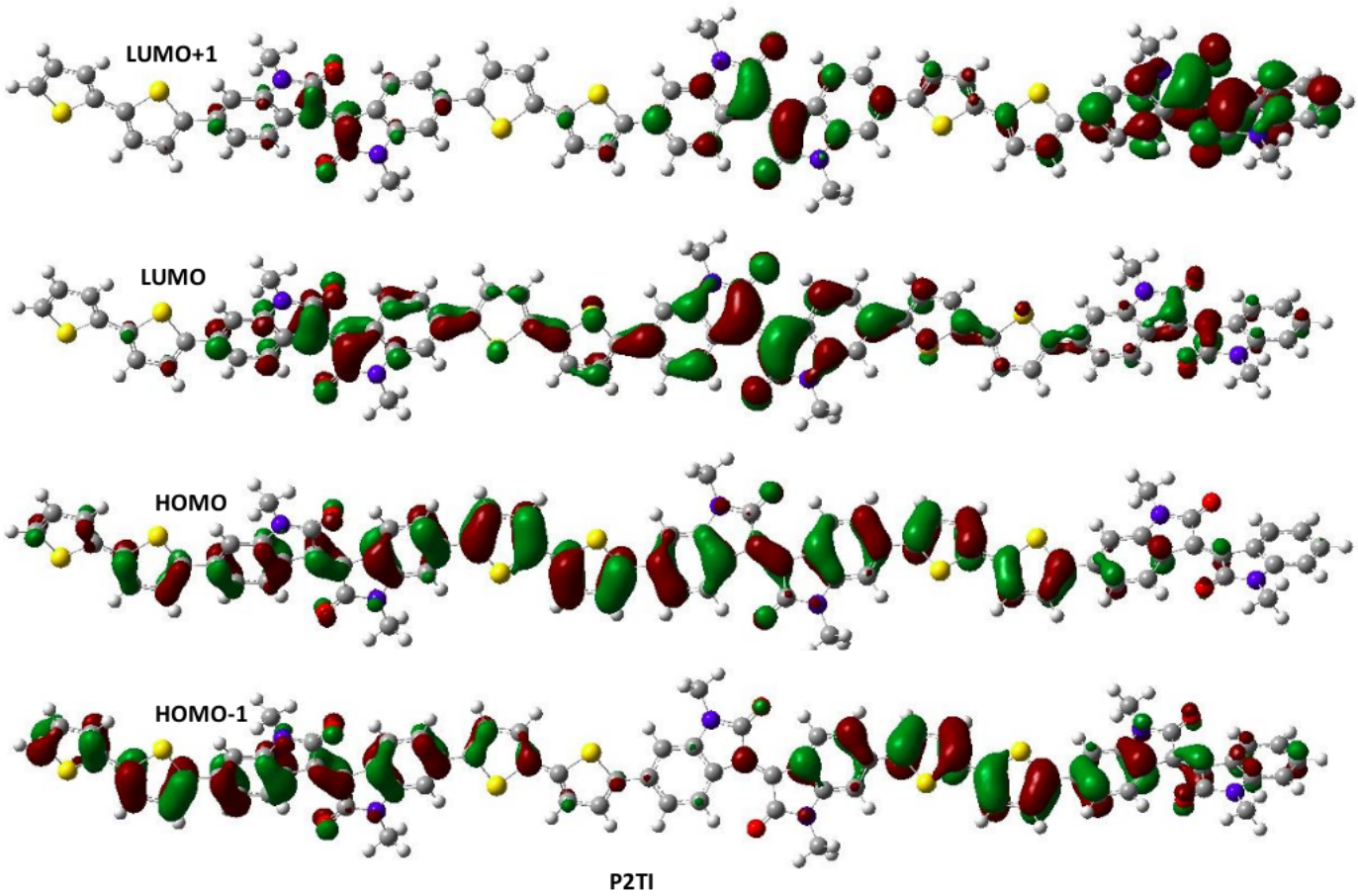

Figure 5.5: Electron cloud distribution in frontier molecular orbitals of **P2TI**.

The more planar molecular geometry facilitated by the **TT**-bridge is anticipated to improve the charge mobility in the **P2TITT** copolymer.

5.2.2 Absorption

To further investigate the optoelectronic properties, TD-DFT calculations were performed on trimer units of **P2TI** and **P2TITT** using the CAM-B3LYP/6-31G(d) functional in the gaseous state. The results are plotted in Figure 5.8(B). The **TT**-spaced copolymer **P2TITT** was found to exhibit a higher oscillator strength than **P2TI**. The $S_0 \rightarrow S_1$ transition occurred at 2.56 eV for **P2TI** and 2.55 eV for **P2TITT** indicating that the **TT** spacer has a negligible effect on the optical bandgap. In contrast, there are clear differences in the electrochemical bandgap calculated from $E_{gap}^{EC} = E_{LUMO} - E_{HOMO}$, where in the case of **P2TI**, the transition to the first excited state consists of H(OMO) $\rightarrow$ L(UMO) and $\mathrm{H}-1 \rightarrow \mathrm{L}+1$ transitions with contributions of 52.5% and 18.2%, respectively, and in **P2TITT**, the H $\rightarrow$ L, $\mathrm{H}-1 \rightarrow \mathrm{L}+1$, and $\mathrm{H}-3 \rightarrow \mathrm{L}+1$ transitions

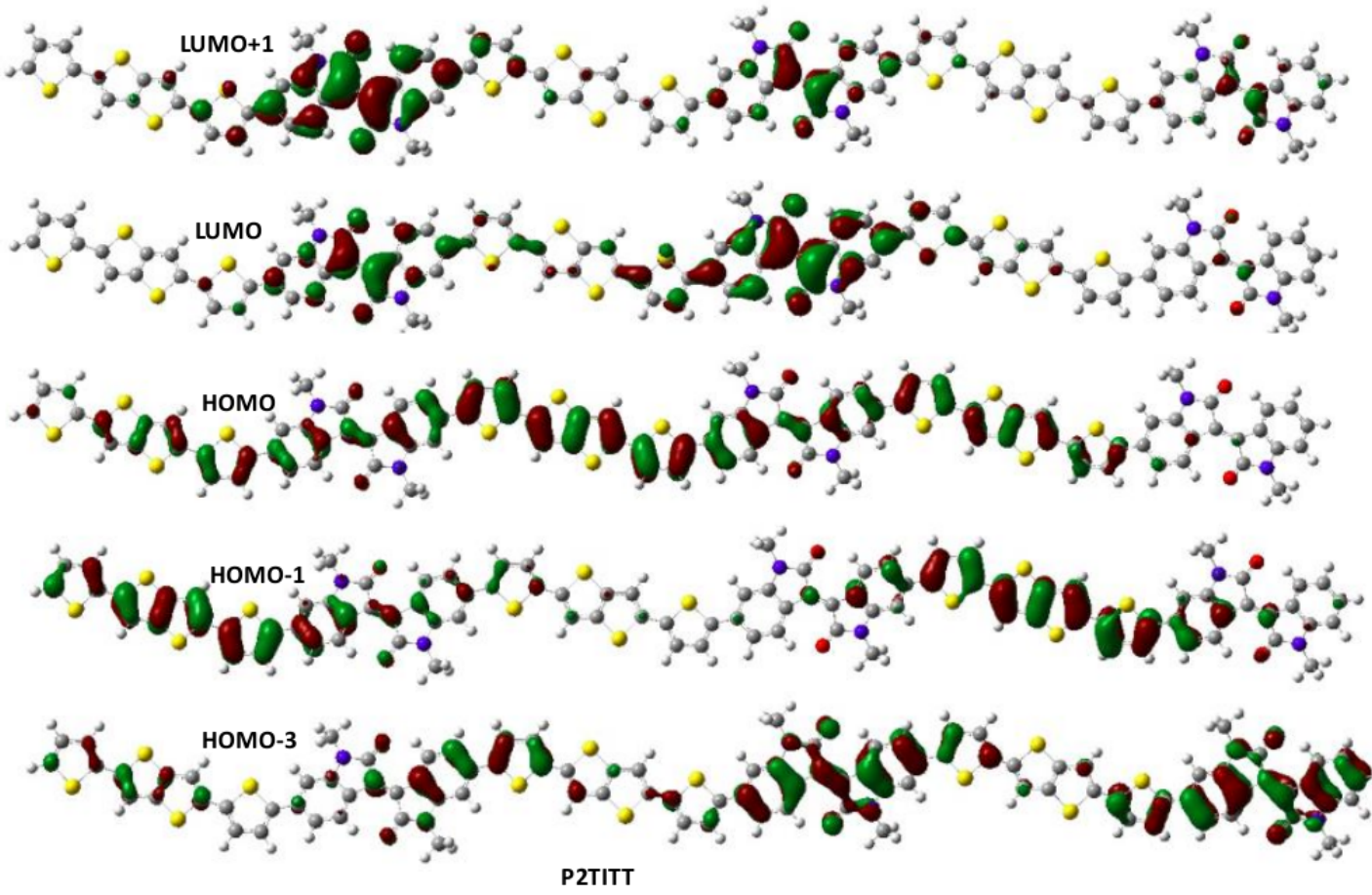

Figure 5.6: Electron cloud distribution in frontier molecular orbitals of **P2TITT**.

comprise the first excited state with respective contributions of 40.7%, 14.7%, and 10.8%. As depicted in Figures 5.5 and 5.6, while the HOMO orbitals are delocalized over the backbone and HOMO−1 is slightly shifted towards the donor units, the LUMO orbital is highly localized on the isoindigo acceptor unit. This confirms that the first excited state in both polymers is predominantly an intramolecular charge-transfer (ICT) state.

The absorption spectra of **P2TI** and **P2TITT** were measured in both solution and thin film, while the PL spectra of the two copolymers were obtained in solution, as shown in Figure 5.8. Both copolymers display the common two-band absorption features that originate from ICT and local $\pi - \pi^*$ transitions. The ICT double-band of the thin film is particularly evident for **P2TI** and indicates the formation of aggregates in the thin films. In solution, the absorption spectrum of **P2TI** is red-shifted compared to **P2TITT**. Conversely, **P2TI**'s thin film absorption spectrum is blue-shifted relative to that of **P2TITT**. Because thin films usually give rise to strong interchain $\pi - \pi$ interaction,[130] the opposite trend between the solution- and thin-film-

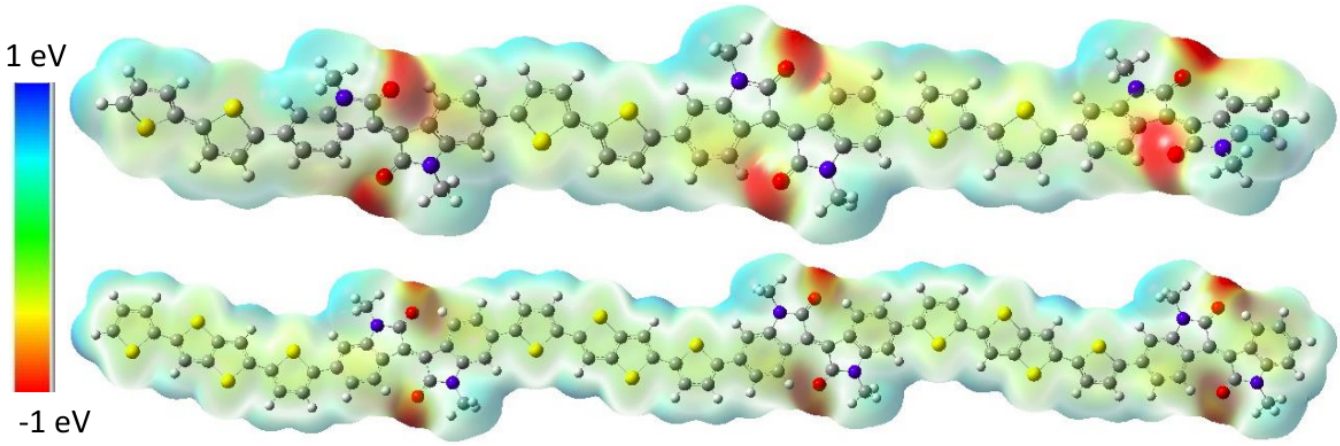

Figure 5.7: Electrostatic potentials surface in trimeric units of **P2TI** (top) and **P2TITT** (bottom).

based absorption spectra can be attributed to the following potential reasons: i) **P2TI** in solution already exhibits strong $\pi - \pi$ stacking, which is negligibly enhanced in the thin film, leading to a negligible additional red-shift, whereas in **P2TITT**, the thin film produces stronger aggregation, resulting in a more pronounced red shift. ii) The trend observed in thin films agrees with the DFT-calculated results, confirming that the **TT** spacer narrows the band gap in **P2TITT**. The opposite trend in solution could be related to solvation effects.

The PL spectra of the two copolymers in solution (Figure 5.8) reveal broader and more red-shifted emission for **P2TITT** compared to **P2TI**. This may arise from additional vibrational modes introduced by the **TT** spacer.

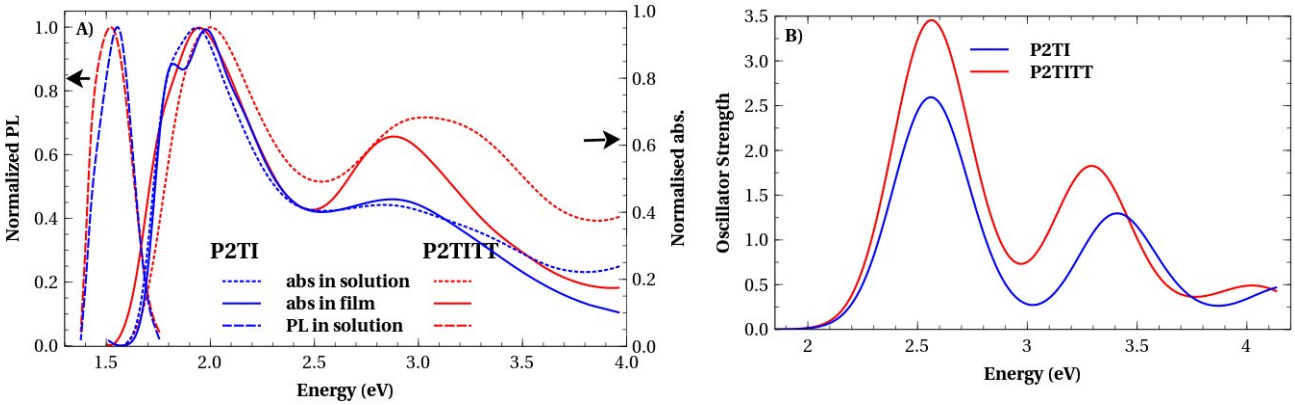

Figure 5.8: (A) Experimental absorption spectra in solution (dotted lines) and thin films (solid lines), PL spectra (dashed lines) in solution of **P2TI** (blue) and **P2TITT** (red) and (B) TD/DFT-calculated absorption of the copolymers in 3 units.

Furthermore, the Stokes shifts were calculated to be 0.38 eV for **P2TI** and 0.47 eV for **P2TITT**. The larger Stokes shift of **P2TITT** suggests that it undergoes more intraband relaxation prior to emission compared to **P2TI**. According to Kasha's model, emission comes out from the minimum band, where the band has necessarily positive curvature.[15,18] To distinguish between J- and H-type aggregation, the band curvature of free-exciton at the minimum band can be evaluated from the second derivative of the energy using Equation 5.2.2,[32]

$$\omega_c \equiv \frac{1}{2}\frac{d^2E_k}{dk^2}\bigg|_{k=k_{min}} \tag{5.2.2}$$

where ω_c is the band curvature, k is the wave number, and E_k the energy at the k^{th} exciton.

In J-aggregates, since the $k = 0$ exciton represents the minimum band, the free-exciton curvature is positive at the bottom band. Hence, emission originates directly from the $k = 0$ exciton with negligible Stokes shift. In contrast, the $k = 0$ state in H-aggregates resides at the top of the band resulting in a negative curvature. Therefore, in H-aggregates, emission will be possible only when there is symmetry-breaking disorder or vibronic coupling due to intraband relaxation that populates excitons from the $k = 0$ to the $k = \pi$ band. In this regard, the chromophores in both **P2TI** and **P2TITT** might assemble preferably in an H-type aggregate form, with the symmetry-breaking disorder potentially being greater in **P2TI**. Alternatively, the shift in the potential wells between the ground state and excited states could be more substantial in **P2TITT** than **P2TI** leading to the observed larger Stokes shift for **P2TITT**.

5.2.3 Temperature-dependent photoluminescence

The aggregation type of polymers can be determined by analyzing the evolution of the 0–0 and 0–1 emission peaks (I_{00} and (I_{01}), respectively) as a function of temperature. To this end, the temperature-dependent PL spectra of the two copolymers were recorded in solution over the temperature range of -5 ℃ to 85 ℃ in steps of 10 ℃ as depicted in Figure 5.9. To assess the effect of temperature on the vibronic peak energy and intensity, a two-peak Gaussian fit was carried out at the end temperatures, $T = -5$ and $T = 80$ ℃, as shown in the bottom panels

of Figure 5.9. As the temperature increased from −5 ℃ to 85 ℃, the main emission peak (I_{00}) of both **P2TI** and **P2TITT** exhibited a blue-shift by 51.54 and 49.15 meV, respectively, accompanied by spectral broadening and increased intensity. The blue-shift of the emission peak can be attributed to a decrease in the effective conjugation length due to thermally-induced dissociation of interchain couplings, while the broadening and intensity increase are likely due to the liberation of new emissive states facilitated by the elevated temperature.[164–166]

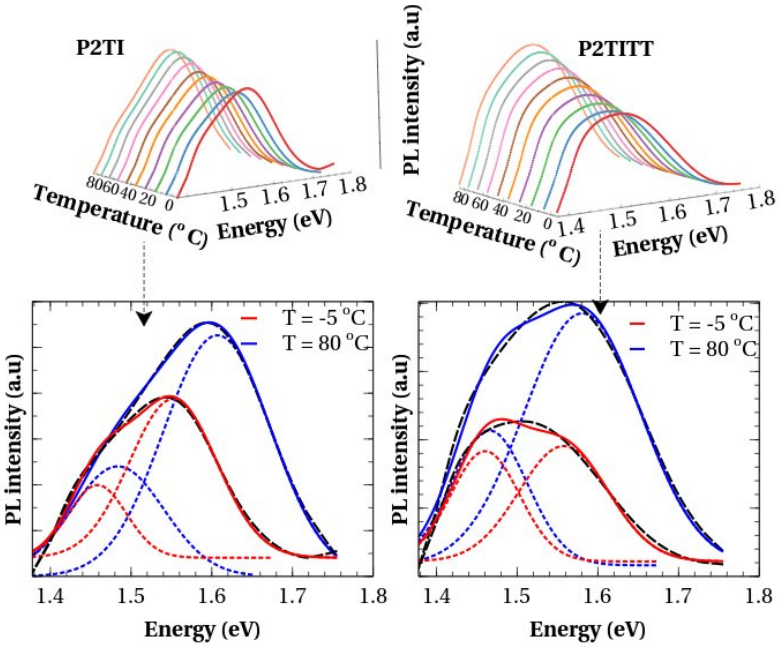

Figure 5.9: Temperature-dependent PL spectra over a temperature range of −5 ℃ to 85 ℃ (top panels) and two-peak Gaussian fit (bottom panels) at −5 (red) and 80 ℃ (blue) of **P2TI** (left) and **P2TITT** (right). The dashed, solid, and dotted lines represent the measured data, the cumulative fit, and the two distinct bands, respectively.

A cursory examination of the PL spectra reveals that the I_{00} peak intensity dominates over the I_{01} peak intensity, characteristic of J-aggregate formation. However, the observation that the I_{00} intensity increases with rising temperature also suggests H-aggregate characteristics, because the 0–0 transition is optically forbidden in an ideal H-aggregate, but as temperature increases, the amount of disorder increases and the transition becomes more likely. To gain deeper insight into the aggregation behavior, a FC analysis was employed to curve-fit the temperature-dependent PL spectra. This analysis utilized two FC progressions to account for the potential co-existence of both J- and H-type aggregates in the copolymers, as given by Equations 3.3.3 and 3.3.4.[59,114]

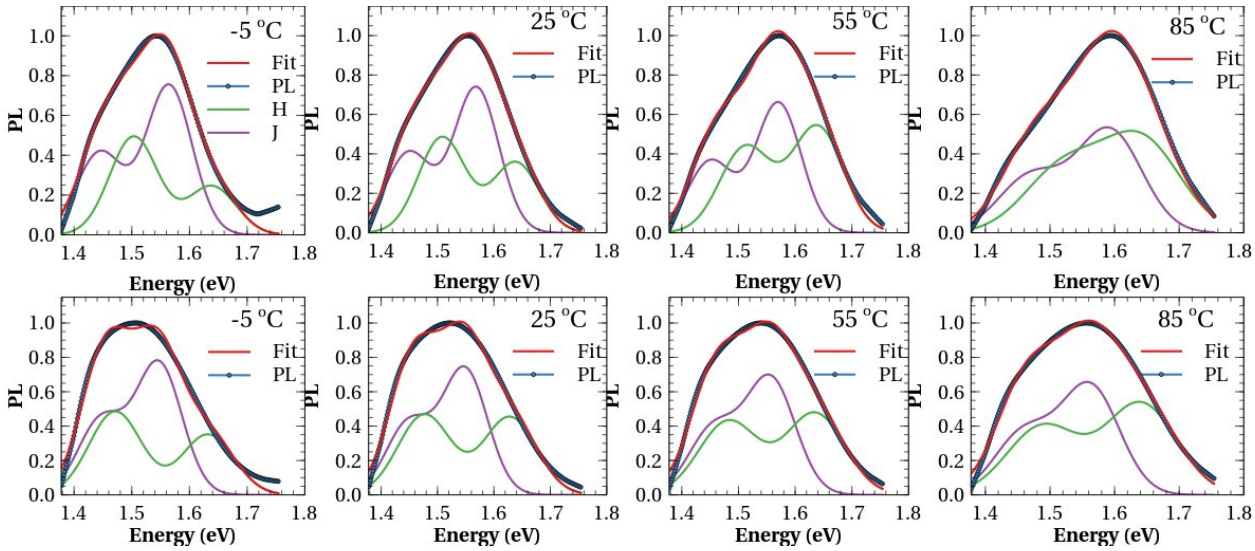

Figure 5.10: Franck-Condon curve fits at selected temperatures of **P2TI** (top) and **P2TITT** (bottom) PL spectra in solution.

As shown in Figure 5.10, the PL spectra of **P2TI** and **P2TITT** were successfully fitted with H-type and J-type FC progressions at some representative temperatures. This suggests that both H- and J-type aggregates are present in the polymers. Upon increasing temperature, an enhancement in the 0–0 peak emission intensity occurred, particularly for the H-type spectral component. This is likely due to thermal disorder-induced relaxation of the selection rules, which makes the 0–0 transition more allowed. In other words, an enhanced I_{00} intensity can be attributed to a decrease in interchain interaction.[60] The PL peak ratio (I_{00}/I_{01}) calculated from the curve fits is plotted in Figure 5.11. This ratio is lower for **P2TITT** than for **P2TI**, indicating higher temperatures are required to break the symmetry in **P2TITT**, consistent with the greater Stokes shift of **P2TITT** in Figure 5.8. A similar study on anthracene-containing statistical poly(phenylene ethynylene)-*alt*-(phenylene vinylene) (AnE-PVstat) copolymers in solution revealed an increase in the I_{00}/I_{01} ratio with increasing temperature which the authors attributed to a reduction in the interchain interaction potentially leading to a breakdown of H-aggregates.[60]

Figure 5.11 also indicates a more gradual increase in the PL peak ratio with temperature for **P2TITT** than for **P2TI**, from which it can be inferred that the **TT**-spaced copolymer **P2TITT** exhibits stronger interchain interactions than **P2TI**. This could be due to the more planar geometry of **P2TITT**, which would suppress molecular torsion upon increasing temperature.[60]

As pointed out in the work of Kanemoto *et al.* on 16-mer oligothiophene (16 T),[166] the full

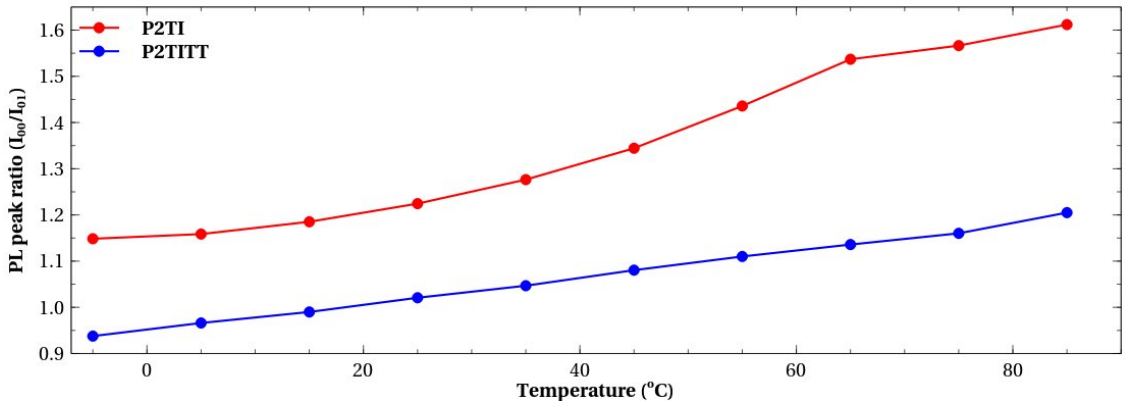

Figure 5.11: Temperature-dependent PL peak ratios calculated after Franck-Condon curve fits.

width at half maximum (FWHM) of the emission spectra can be used to assess conformational changes induced by temperature. In this regard, the FWHM values were extracted from the FC fits of the PL spectra. The results show that **P2TITT** exhibits higher FWHM values than **P2TI**, supporting the broader PL spectra of **P2TITT** due to the presence of additional phonon modes. Moreover, the FWHM increases with rising temperature for both **P2TI** and **P2TITT**, as higher temperatures lead to increased conformational disorder. Specifically, the FWHM of **P2TI** increased from 40.80 to 45.90 meV (a 12.50% increase), while for **P2TITT** it increased from 42.60 to 46.10 meV (an 8.22% increase), over the measured temperature range. These results suggest that the temperature-induced conformational changes are more pronounced in **P2TI** than in **P2TITT**.

Another parameter used to compare the exciton interchain coupling in the copolymers is α, which dictates the intensity of the I_{00} peak as described in Equation 3.3.4. The value of α can range from 0 to 1, with 0 indicating complete dominance of interchain interaction and perfect H-aggregate formation, while 1 would suggest the dominance of intrachain interaction. Over the measured temperature range, the value of α increased from 0.46 to 0.98 for **P2TI** and from 0.35 to 0.87 for **P2TITT**. Smaller values of α for **P2TITT** than **P2TI** at any temperature further supports the notion that interchain exciton coupling is stronger in **P2TITT** than in **P2TI**.[114]

5.2.4 Emission lifetimes

Time-resolved PL measurements were performed on diluted solutions and films of **P2TI** and **P2TITT**. The emission decay profiles were best fitted using bi-exponential functions convolved

Table 5.2: Lifetimes and corresponding amplitudes of the copolymers.

		τ_1 (ns)	A_1 (%)	τ_2 (ns)	A_2 (%)	average τ (ns)
P2TI	Solution	0.34	66	1.01	34	0.57
	Film	0.30	50	1.10	50	0.70
P2TITT	Solution	0.46	80	1.01	20	0.57
	Film	0.26	47	1.09	53	0.70

with a simulated instrument response function (IRF) using the software described in Ref.[167] The fitted function is of the form

$$IRF \otimes (A_1 e^{-t/\tau_1} + A_2 e^{-t/\tau_2}), \tag{5.2.3}$$

where A_i and τ_i (with i =1,2) are fitting parameters representing the fraction of molecules decaying and the corresponding PL lifetime, respectively.

The experimental PL decay curves along with their corresponding bi-exponential fits are presented in Figure 5.12. Small values of χ^2 close to unity and lack of structure in the residuals were used to confirm the goodness of the fits. The extracted lifetime values are also summarized in Table 5.2. As far as we are considering donor copolymers, and not blends, factors such as bimolecular recombination and carrier traps may not have significant effects because we do not expect free charge carriers and carrier traps, especially in solution. Hence, the presence of two distinct lifetimes in the decay profile may suggest the coexistence of two different types of aggregation species, namely H- and J-aggregates, within the polymers. However, as mentioned in the experimental section, the polymer solutions were prepared at a relatively low concentration of approximately 0.02 mg/mL, which is unlikely to promote significant aggregation. Therefore, the two observed lifetime components in the solution-phase measurement can be more appropriately assigned to isolated (non-aggregated) polymer chains for fast decaying and H-aggregated polymer chains for long-lived components.

A closer examination of the relative amplitudes of the two lifetime components revealed that the faster decays tend to dominate over the longer lifetimes in the solution state as evidenced by the higher pre-exponential factors ($A_1 > A_2$) associated with the shorter lifetime species. Attributing the longer lifetimes to H-aggregated species[57] and the shorter lifetimes to isolated

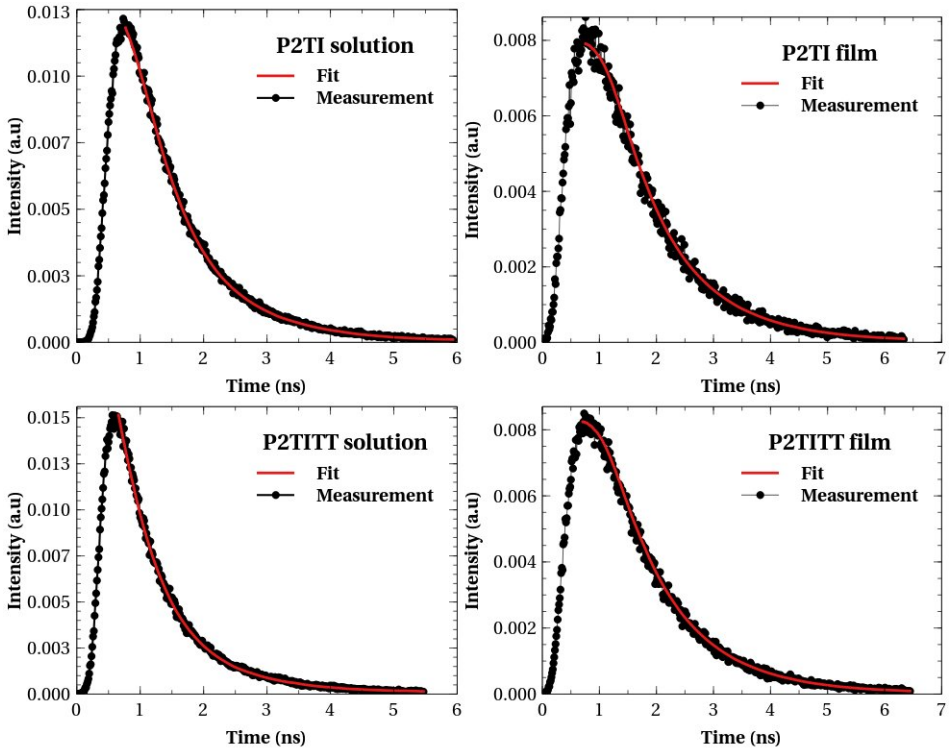

Figure 5.12: Emission decay curves fitted with two exponential functions.

chain segments, the increase in the amplitude of longer lifetime component in the thin films compared to solution suggests that the proportion of aggregated species increases in the solid state.

Similar assignments of longer lifetimes to aggregated species and shorter lifetimes to non-aggregated chain segments have been reported in the literature for other polymer systems.[168–170] For example, in poly(*p*-pyridyl vinylene) (PPyV), the solution-phase PL decay was found to be nearly mono-exponential while the film emission consisted of both very fast and long-lived species.[168] Likewise, in PPE-PPV copolymers, the emission lifetimes in solution were well-described by single-exponential decays assigned to H-aggregated species, whereas the lifetimes in the film were better fitted using a bi-exponential function, with the longer lifetime component attributed to H-aggregate and the shorter lifetime to J-aggregated chain segments.[169,170]

The need to employ a bi-exponential function to fit the PL decay profiles of **P2TI** and **P2TITT** copolymers further supports the presence of two distinct emissive species, likely corresponding to H-aggregated and isolated chain segments in the solution state or H-aggregated and J-aggregated (isolated chain) segments in the thin film as the photophysical properties of single

conjugated polymer chains and J-aggregates are similar.[29] The notion of two distinct emissive species is in agreement with the FC analysis of the temperature-dependent PL spectra.

5.3 Conclusion

In this part of the work, we have studied the effect backbone conformation has on aggregation-induced photophysics of two isoindigo-based bithiophene-isoindigo copolymers with (**P2TITT**) and without (**P2TI**) **TT** spacer. The introduction of a **TT** spacer in **P2TITT** improved the planarity of the copolymer backbone and shifted the HOMO energy level upward due to the stronger electron-donating nature of the **TT** moiety. These structural and electronic changes also affected the extent of HOMO–LUMO delocalization in the two copolymers. To probe the aggregation behavior of these materials, temperature-dependent PL measurements were conducted. The temperature-dependent evolution of the key parameters such as the first two vibronic peaks intensity ratio, the peak positions, and spectral broadening provided insights into the temperature-induced changes in the effective conjugation length and the activation of more emissive conformational species due to the dissociation of interchain couplings. Interestingly, a comparison of the temperature-dependent PL peak ratios between the two copolymers revealed stronger interchain interaction in the **TT**-containing **P2TITT**. Furthermore, the PL spectra were best fitted using two FC progressions suggesting the coexistence of two distinct aggregation types, which was further supported by the observation of two emission lifetime components in the time-resolved PL measurements. The longer lifetime component was attributed to H-aggregate species, while the shorter lifetime was assigned to J-aggregate (isolated) chain segments. The relative contributions of these lifetime components, as reflected in the pre-exponential factors, indicated that the proportion of aggregated species increases in the thin films compared to the dilute solutions. These observations give important insights into the role of the backbone conformation and interchain interaction in modulating the aggregation-induced photophysical properties of conjugated polymers, which is crucial for their optimization in optoelectronic applications.

Chapter 6

Summary and Outlook

Polymer aggregation has been highlighted to be crucial to the morphology of organic electronics which has a direct bearing on device performance. In this study, computational and experimental techniques were used to assess the photophysics and aggregate formation of a benzodithiophene-isoindigo copolymer (**PBDTI-DT**) and two bithiophene-isoindigo copolymers with (**P2TITT**) and without (**P2TI**) **TT** spacer. In the study on **PBDTI-DT**, FC analysis show the polymer adopts both J- and H-aggregation, the H-aggregate being the dominant stacking according to the relative QY measurement. In the second work, we have studied the effect of backbone conformation on aggregation-induced photophysics of **P2TITT** and **P2TI**. The introduction of a **TT** spacer in **P2TITT** improved the planarity of the copolymer backbone and shifted the HOMO energy level upward due to the stronger electron-donating nature of the **TT** moiety. These structural and electronic changes also affected the extent of HOMO–LUMO delocalization in the two copolymers. Interestingly, a comparison of the temperature-dependent PL peak ratios between the two copolymers revealed stronger interchain interaction in the **TT**-containing **P2TITT**. Furthermore, the PL spectra were best fitted using two FC progressions suggesting the coexistence of two distinct aggregation types, which was further supported by the observation of two emission lifetime components in the time-resolved PL measurements. These results provide important insights into the role of the backbone conformation and interchain interaction in modulating the aggregation-induced photophysical properties of conjugated polymers, which is crucial for their optimization in optoelectronic applications.

In molecules that have two or more molecules in a unit cell packing arrangements, the absorption/emission spectrum depends on the polarization of the excitation source. In this regard, we recommend polarized absorption/emission spectra measurement to be carried out in addition to the other experimental techniques used in this study to have a more reliable assignment of the aggregation types. The study of photophysics would be complete if the excited state dynamics were investigated with transient absorption spectroscopy. We also recommend contrasting device performances from these polymers with the identified photophysical properties and aggregation types.

Acknowledgment

In one way or another a number of people have played a role in this PhD work. This work has been supervised by Newayemedhin Aberra and co-supervised by Tjaart P. J. Krüger. I am thankful for their encouragement, guidance and constructive comments throughout the development of this study. They have been a model of scientific excellence and generous mentorship. I deeply appreciate their dedicated guidance, support, patience, and understanding. The polymers used in this study are synthesized from Prof. Wendimagegn Mammo's lab, and I want to say thank you to Prof. Wendimagegn Mammo for providing us with the polymers. The laboratory facilities for the polymer physics lab in the Department of Physics at Addis Abeba University are provided by the International Science Program (ISP), Uppsala University, Sweden. I am happy to thank Addis Abeba University (AAU) for hosting me to peruse my PhD study. Particularly, I would like to thank the Physics Department head and leader of our research group, Prof. Fekadu Gashaw Hone for the efforts and the facilitation he did to finalize this PhD study. I am also thankful to all members of our research group. The heart felt thanks of mine are again stretched out to AAU, Department of Physics staff members, especially, Prof. Teshime Senbeta (former head of the department), Dr. Mulugeta Bekele and Dr. Desalegn Ayehu. Moreover, I want to thank W/ro Tsilat Adinew and Yeshi Gezaghegn for their encouragement and motherly approach. I would also like to thank Wollo University for sponsoring this PhD study. I am indebted to my colleagues and friends from Wollo University, especially Ashenafi Admasu (head of the department), Sintayehu Yigzaw and Tegenu Argaw. My special thank goes to Dr. Nika Bekri for his uninterrupted followups. I also want to say thank you to Leonato Tambua Nchinda. My elderly parents whom I was supposed to visit on a regular basis which I did not do during the last three years deserve my apology. I am also thankful to my little sister, Wubit Asmare, my life partner, Hana Tegen and my sister-in-law, Helen Tegen. Thank you to everyone!

Bibliography

[1] Lucas RF Henneman, Peter Rafaj, Harold J Annegarn, and Carmen Klausbruckner. Assessing emissions levels and costs associated with climate and air pollution policies in south africa. *Energy Policy*, 89:160–170, 2016.

[2] Pavlos Nikolaidis. Solar energy harnessing technologies towards de-carbonization: A systematic review of processes and systems. *Energies*, 16(17):6153, 2023.

[3] Lei Zhu, Ming Zhang, Jinqiu Xu, Chao Li, Jun Yan, Guanqing Zhou, Wenkai Zhong, Tianyu Hao, Jiali Song, Xiaonan Xue, et al. Single-junction organic solar cells with over 19% efficiency enabled by a refined double-fibril network morphology. *Nature Materials*, 21(6):656–663, 2022.

[4] Jinhua Gao, Na Yu, Zhihao Chen, Yanan Wei, Congqi Li, Tianhua Liu, Xiaobin Gu, Jianqi Zhang, Zhixiang Wei, Zheng Tang, et al. Over 19.2% efficiency of organic solar cells enabled by precisely tuning the charge transfer state via donor alloy strategy. *Advanced Science*, 9(30):2203606, 2022.

[5] Hu Chen, Sang Young Jeong, Junfu Tian, Yadong Zhang, Dipti R Naphade, Maryam Alsufyani, Weimin Zhang, Sophie Griggs, Hanlin Hu, Stephen Barlow, et al. A 19% efficient and stable organic photovoltaic device enabled by a guest nonfullerene acceptor with fibril-like morphology. *Energy & Environmental Science*, 16(3):1062–1070, 2023.

[6] Kerui Liu, Yuanyuan Jiang, Feng Liu, Guangliu Ran, Fei Huang, Wenxuan Wang, Wenkai Zhang, Cheng Zhang, Jianhui Hou, and Xiaozhang Zhu. Organic solar cells with over 19% efficiency enabled by a 2d-conjugated non-fullerene acceptor featuring favorable electronic and aggregation structures. *Advanced Materials*, 35(32):2300363, 2023.

[7] Chenyu Han, Jianxiao Wang, Shuai Zhang, Liangliang Chen, Fuzhen Bi, Junjie Wang, Chunming Yang, Pengchao Wang, Yonghai Li, and Xichang Bao. Over 19% efficiency organic solar cells by regulating multidimensional intermolecular interactions. *Advanced Materials*, 35(10):2208986, 2023.

[8] Hongyue Tian, Mingxin Zhao, Xiaoling Ma, Chunyu Xu, Wenjing Xu, Zhongyuan Liu, Miao Zhang, and Fujun Zhang. Critical progress of polymer solar cells with a power conversion efficiency over 18%. *Energies*, 16(11):4494, 2023.

[9] Guanyu Ding, Tianyi Chen, Mengting Wang, Xinxin Xia, Chengliang He, Xiangjun Zheng, Yaokai Li, Di Zhou, Xinhui Lu, Lijian Zuo, et al. Solid additive-assisted layer-by-layer processing for 19% efficiency binary organic solar cells. *Nano-Micro Letters*, 15(1):92, 2023.

[10] Jiehao Fu, Patrick WK Fong, Heng Liu, Chieh-Szu Huang, Xinhui Lu, Shirong Lu, Maged Abdelsamie, Tim Kodalle, Carolin M Sutter-Fella, Yang Yang, et al. 19.31% binary organic solar cell and low non-radiative recombination enabled by non-monotonic intermediate state transition. *Nature communications*, 14(1):1760, 2023.

[11] Chengliang He, Zhaozhao Bi, Zeng Chen, Jing Guo, Xinxin Xia, Xinhui Lu, Jie Min, Haiming Zhu, Wei Ma, Lijian Zuo, et al. Compromising charge generation and recombination with asymmetric molecule for high-performance binary organic photovoltaics with over 18% certified efficiency. *Advanced Functional Materials*, 32(18):2112511, 2022.

[12] Mengyuan Gao, Wenxuan Wang, Jianhui Hou, and Long Ye. Control of aggregated structure of photovoltaic polymers for high-efficiency solar cells. *Aggregate*, 2(5):e46, 2021.

[13] Michael Kasha. Characterization of electronic transitions in complex molecules. *Discussions of the Faraday society*, 9:14–19, 1950.

[14] Michael Kasha. Relation between exciton bands and conduction bands in molecular lamellar systems. *Reviews of Modern Physics*, 31(1):162, 1959.

[15] Michael Kasha. Energy transfer mechanisms and the molecular exciton model for molecular aggregates. *Radiation research*, 20(1):55–70, 1963.

[16] Robin M Hochstrasser and Michael Kasha. Application of the exciton model to monomolecular lamellar systems. *Photochemistry and Photobiology*, 3(4):317–331, 1964.

[17] Michael Kasha, Henry R Rawls, and M Ashraf El-Bayoumi. The exciton model in molecular spectroscopy. *Pure and Applied Chemistry VIIIth*, 11(3-4):371–392, 1965.

[18] Eion G McRae and Michael Kasha. Enhancement of phosphorescence ability upon aggregation of dye molecules. *The Journal of Chemical Physics*, 28(4):721–722, 1958.

[19] Edwin E Jelley. Spectral absorption and fluorescence of dyes in the molecular state. *Nature*, 138(3502):1009–1010, 1936.

[20] Edwin E Jelley. Molecular, nematic and crystal states of i: I-diethyl–cyanine chloride. *Nature*, 139(3519):631–631, 1937.

[21] E Daltrozzo, G Scheibe, K Gschwind, and F Haiment. On the structure of the j-aggregates of pseudocyanine. 1973.

[22] Dietmar Möbius. Scheibe aggregates. *Advanced materials*, 7(5):437–444, 1995.

[23] GV Zakharova, AR Kombaev, and AK Chibisov. J aggregation of meso-ethylsubstituted carbocyanine dyes in polymer films. *High Energy Chemistry*, 38:180–183, 2004.

[24] Seul-ong Kim, Tae Kyu An, Jun Chen, Il Kang, So Hee Kang, Dae Sung Chung, Chan Eon Park, Yun-Hi Kim, and Soon-Ki Kwon. H-aggregation strategy in the design of molecular semiconductors for highly reliable organic thin film transistors. *Advanced Functional Materials*, 21(9):1616–1623, 2011.

[25] Hajime Yamagata, Chris M Pochas, and Frank C Spano. Designing j-and h-aggregates through wave function overlap engineering: applications to poly (3-hexylthiophene). *The Journal of Physical Chemistry B*, 116(49):14494–14503, 2012.

[26] Mina Baghgar, Joelle A Labastide, Felicia Bokel, Ryan C Hayward, and Michael D Barnes. Effect of polymer chain folding on the transition from h-to j-aggregate behavior in p3ht nanofibers. *The Journal of Physical Chemistry C*, 118(4):2229–2235, 2014.

[27] Yonghong Deng, Wen Yuan, Zhe Jia, and Gao Liu. H-and j-aggregation of fluorene-based chromophores. *The Journal of Physical Chemistry B*, 118(49):14536–14545, 2014.

[28] Frank C Spano and Carlos Silva. H-and j-aggregate behavior in polymeric semiconductors. *Annual review of physical chemistry*, 65:477–500, 2014.

[29] Hajime Yamagata and Frank C Spano. Strong photophysical similarities between conjugated polymers and j-aggregates. *The journal of physical chemistry letters*, 5(3):622–632, 2014.

[30] Theresa Eder, Thomas Stangl, Max Gmelch, Klaas Remmerssen, Dirk Laux, Sigurd Höger, John M Lupton, and Jan Vogelsang. Switching between h-and j-type electronic coupling in single conjugated polymer aggregates. *Nature communications*, 8(1):1641, 2017.

[31] Chien-You Su and Chi-Chung Hua. Aggregation properties of meh-ppv/pmma blends in solution and thin film. *Journal of Polymer Research*, 24:1–11, 2017.

[32] Nicholas J Hestand and Frank C Spano. Expanded theory of h-and j-molecular aggregates: the effects of vibronic coupling and intermolecular charge transfer. *Chemical reviews*, 118(15):7069–7163, 2018.

[33] Brenden McDearmon, Eunhee Lim, In-Hwan Lee, Lisa M Kozycz, Kathryn O'Hara, P Isaac Robledo, Naveen R Venkatesan, Michael L Chabinyc, and Craig J Hawker. Effects of side-chain topology on aggregation of conjugated polymers. *Macromolecules*, 51(7):2580–2590, 2018.

[34] Mark E Ziffer, Sae Byeok Jo, Yun Liu, Hongliang Zhong, Joseph C Mohammed, Jeffrey S Harrison, Alex K-Y Jen, and David S Ginger. Tuning h-and j-aggregate behavior in π-conjugated polymers via noncovalent interactions. *The Journal of Physical Chemistry C*, 122(33):18860–18869, 2018.

[35] Theresa Eder, Jan Vogelsang, Sebastian Bange, Klaas Remmerssen, Daniela Schmitz, Stefan-S Jester, Tristan J Keller, Sigurd Höger, and John M Lupton. Interplay between j-and h-type coupling in aggregates of π-conjugated polymers: A single-molecule perspective. *Angewandte Chemie International Edition*, 58(52):18898–18902, 2019.

[36] Minjun Kim, Won-Tae Park, Seung Un Ryu, Sung Y Son, Junwoo Lee, Tae Joo Shin, Yong-Young Noh, and Taiho Park. Improving the electrical connection of n-type conjugated polymers through fluorine-induced robust aggregation. *Chemistry of Materials*, 31(13):4864–4872, 2019.

[37] Qi-Yi Li, Ze-Fan Yao, Jie-Yu Wang, and Jian Pei. Multi-level aggregation of conjugated small molecules and polymers: from morphology control to physical insights. *Reports on Progress in Physics*, 84(7):076601, 2021.

[38] Antonio Sánchez-Ruiz, Ana Sousa-Herves, Juan Tolosa, Amparo Navarro, and Joaquín C García-Martínez. Aggregation-induced emission properties in fully π-conjugated polymers, dendrimers, and oligomers. *Polymers*, 13(2):213, 2021.

[39] Justin J Kwok, Giridar Vishwanathan, Kyung Sun Park, Bijal B Patel, Dongqi Zhao, Gabriel Juarez, and Ying Diao. Understanding the aggregation and flow response of donor–acceptor conjugated polymers. *Macromolecules*, 55(22):10153–10166, 2022.

[40] Hao-Tian Wu, Ze-Fan Yao, Zhe Xu, Hua-Kang Kong, Xin-Yi Wang, Qi-Yi Li, Jie-Yu Wang, and Jian Pei. Controlling solution-state aggregation and solid-state microstructures of conjugated polymers by tuning backbone conformation. *Macromolecular Rapid Communications*, 43(16):2200069, 2022.

[41] Jinyue Zhu, Yanfang Liu, Shaohua Huang, Shuguang Wen, Xichang Bao, Mian Cai, and Jingwen Li. Impact of backbone linkage positions on the molecular aggregation behavior of polymer photovoltaic materials. *Physical Chemistry Chemical Physics*, 24(29):17462–17470, 2022.

[42] Chanwoo Kim, Hyeyoung Joung, Hyung Jun Kim, Keewook Paeng, Laura J Kaufman, and Jaesung Yang. Aggregates of conjugated polymers: bottom-up control of mesoscopic morphology and photophysics. *NPG Asia Materials*, 15(1):32, 2023.

[43] Frank Würthner, Theo E Kaiser, and Chantu R Saha-Möller. J-aggregates: from serendipitous discovery to supramolecular engineering of functional dye materials. *Angewandte Chemie International Edition*, 50(15):3376–3410, 2011.

[44] Frank C Spano and Hajime Yamagata. Vibronic coupling in j-aggregates and beyond: a direct means of determining the exciton coherence length from the photoluminescence spectrum. *The Journal of Physical Chemistry B*, 115(18):5133–5143, 2011.

[45] G De Miguel, M Ziółek, M Zitnan, JA Organero, SS Pandey, S Hayase, and A Douhal. Photophysics of h-and j-aggregates of indole-based squaraines in solid state. *The Journal of Physical Chemistry C*, 116(17):9379–9389, 2012.

[46] Julia L Bricks, Yuri L Slominskii, Ihor D Panas, and Alexander P Demchenko. Fluorescent j-aggregates of cyanine dyes: basic research and applications review. *Methods and applications in fluorescence*, 6(1):012001, 2017.

[47] Miriam Más-Montoya and René AJ Janssen. The effect of h-and j-aggregation on the photophysical and photovoltaic properties of small thiophene–pyridine–dpp molecules for bulk-heterojunction solar cells. *Advanced Functional Materials*, 27(16):1605779, 2017.

[48] Suqian Ma, Sijia Du, Guocui Pan, Shuting Dai, Bin Xu, and Wenjing Tian. Organic molecular aggregates: From aggregation structure to emission property. *Aggregate*, 2(4):e96, 2021.

[49] Ferenc Zsila, Zsolt Bikadi, Zsofia Keresztes, Jozsef Deli, and Miklos Simonyi. Investigation of the self-organization of lutein and lutein diacetate by electronic absorption, circular dichroism spectroscopy, and atomic force microscopy. *The Journal of Physical Chemistry B*, 105(39):9413–9421, 2001.

[50] Sebastian Westenhoff, Agnese Abrusci, W James Feast, Oliver Henze, Andreas FM Kilbinger, Albertus PHJ Schenning, and Carlos Silva. Supramolecular electronic coupling in chiral oligothiophene nanostructures. *Advanced Materials*, 18(10):1281–1285, 2006.

[51] Frank C Spano. Analysis of the uv/vis and cd spectral line shapes of carotenoid assemblies: spectral signatures of chiral h-aggregates. *Journal of the American Chemical Society*, 131(12):4267–4278, 2009.

[52] Alexei Halpin, Philip JM Johnson, Roel Tempelaar, R Scott Murphy, Jasper Knoester, Thomas LC Jansen, and RJ Dwayne Miller. Two-dimensional spectroscopy of a molecu-

lar dimer unveils the effects of vibronic coupling on exciton coherences. *Nature chemistry*, 6(3):196–201, 2014.

[53] Hong-Guang Duan, Peter Nalbach, Valentyn I Prokhorenko, Shaul Mukamel, and Michael Thorwart. On the origin of oscillations in two-dimensional spectra of excitonically-coupled molecular systems. *New Journal of Physics*, 17(7):072002, 2015.

[54] Fabian Panzer, Michael Sommer, Heinz Bassler, Mukundan Thelakkat, and Anna Kohler. Spectroscopic signature of two distinct h-aggregate species in poly (3-hexylthiophene). *Macromolecules*, 48(5):1543–1553, 2015.

[55] Hajime Yamagata and Frank C Spano. Interplay between intrachain and interchain interactions in semiconducting polymer assemblies: The hj-aggregate model. *The Journal of chemical physics*, 136(18), 2012.

[56] Jiemei Ou, Yuzhao Yang, Wensheng Lin, Zhongke Yuan, Lin Gan, Xiaofeng Lin, Xudong Chen, and Yujie Chen. Connection between the conformation and emission properties of poly [2-methoxy-5-(2-ethyl-hexyloxy)-1, 4-phenylene vinylene] single molecules during thermal annealing. *Applied Physics Letters*, 106(12), 2015.

[57] Qiaoqiao Zhao, Jiangang Liu, Haiyang Wang, Mingguang Li, Ke Zhou, Hua Yang, and Yanchun Han. Balancing the h-and j-aggregation in dts (ptth 2) 2/pc 70 bm to yield a high photovoltaic efficiency. *Journal of Materials Chemistry C*, 3(31):8183–8192, 2015.

[58] Ruizhi Wang, Xiao Yang, Shu Hu, Yang Zhang, Xiaoliang Yan, Yuchen Wang, Chuang Zhang, and ChuanXiang Sheng. Effect of thermal annealing on aggregations in meh-ppv films. *The Journal of Physical Chemistry C*, 123(17):11055–11062, 2019.

[59] Hajime Yamagata, Nicholas J Hestand, Frank C Spano, Anna Köhler, Christina Scharsich, Sebastian T Hoffmann, and Heinz Bässler. The red-phase of poly [2-methoxy-5-(2-ethylhexyloxy)-1, 4-phenylenevinylene](meh-ppv): A disordered hj-aggregate. *The Journal of chemical physics*, 139(11), 2013.

[60] A Saaidia, MA Saidani, E Hleli, S Alam, C Ulbricht, S Romdhane, A Ben Fredj, C Kastner, DAM Egbe, US Schubert, et al. Temperature-tuning of optical properties and molecular aggregation in ane-pvstat copolymer solution. *The Journal of Physical Chemistry C*, 122(7):3965–3969, 2018.

[61] Shu Hu, Yang Liao, Yang Zhang, Xiaoliang Yan, Zhenlu Zhao, Weiqiang Chen, Xin Zhang, Hongxing Liu, Heng Li, Li Li, et al. Effect of thermal annealing on conformation of meh-ppv chains in polymer matrix: Coexistence of h-and j-aggregates. *Polymers*, 12(8):1771, 2020.

[62] Xin Chang, Mohammad Balooch Qarai, and Frank C Spano. Hj-aggregates of donor–acceptor–donor oligomers and polymers. *The Journal of Chemical Physics*, 155(3), 2021.

[63] Newayemedhin A Tegegne, Zelalem Abdissa, and Wendimagegn Mammo. Photophysical, thermal and structural properties of thiophene and benzodithiophene-based copolymers synthesized by direct arylation polycondensation method. *Polymers*, 13(7):1151, 2021.

[64] Nika Bekri, Eninges Asmare, Zelalem Abdissa, Wendimagegn Mammo, and Newayemedhin A Tegegne. Photophysics and thermally-induced degradation of p2ti-dd, a polymer synthesized by direct arylation reaction. *Journal of Materials Science: Materials in Electronics*, 33(20):16066–16076, 2022.

[65] Behayilu S Desalegn, Nika Bekri, Fekadu G Hone, Dinsefa M Andoshe, Wendimagegn Mammo, Zelalem Abdissa, Gurthwin Bosman, and Newayemedhin A Tegegne. One-pot synthesis and thermal stability of thiophene-bridged thieno [3, 2-b] thiophene donor-based copolymers. *Materials Today Communications*, 29:102803, 2021.

[66] Hideki Shirakawa, Edwin J Louis, Alan G MacDiarmid, Chwan K Chiang, and Alan J Heeger. Synthesis of electrically conducting organic polymers: halogen derivatives of polyacetylene,(ch) x. *Journal of the Chemical Society, Chemical Communications*, (16):578–580, 1977.

[67] Anna Köhler and Heinz Bässler. *Electronic processes in organic semiconductors: An introduction*. John Wiley & Sons, 2015.

[68] John Betteley Birks. Photophysics of aromatic molecules. *(No Title)*, 1970.

[69] Antonio Facchetti. π-conjugated polymers for organic electronics and photovoltaic cell applications. *Chemistry of Materials*, 23(3):733–758, 2011.

[70] Bernard Valeur and Mario Nuno Berberan-Santos. *Molecular fluorescence: principles and applications*. John Wiley & Sons, 2013.

[71] Frédéric Laquai, Young-Seo Park, Jang-Joo Kim, and Thomas Basché. Excitation energy transfer in organic materials: from fundamentals to optoelectronic devices. *Macromolecular rapid communications*, 30(14):1203–1231, 2009.

[72] Paulus Albertus Van Hal. Photophysics of molecules and materials for polymer solar cells. 2003.

[73] Robert A Scott, A Grant Mauk, and Harry B Gray. Experimental approaches to studying biological electron transfer, 1985.

[74] Tracey M Clarke and James R Durrant. Charge photogeneration in organic solar cells. *Chemical reviews*, 110(11):6736–6767, 2010.

[75] Qianqian Li and Zhen Li. Molecular packing: another key point for the performance of organic and polymeric optoelectronic materials. *Accounts of chemical research*, 53(4):962–973, 2020.

[76] Glenn P Bartholomew, Guillermo C Bazan, Xianhui Bu, and Rene J Lachicotte. Packing modes of distyrylbenzene derivatives. *Chemistry of materials*, 12(5):1422–1430, 2000.

[77] Peter J Brown, D Steve Thomas, Anna Köhler, Joanne S Wilson, Ji-Seon Kim, Catherine M Ramsdale, Henning Sirringhaus, and Richard H Friend. Effect of interchain interactions on the absorption and emission of poly (3-hexylthiophene). *Physical Review B*, 67(6):064203, 2003.

[78] Ferenc Zsila, József Deli, Zsolt Bikádi, and Miklós Simonyi. Supramolecular assemblies of carotenoids. *Chirality: The Pharmacological, Biological, and Chemical Consequences of Molecular Asymmetry*, 13(10):739–744, 2001.

[79] Eric A Margulies, Leah E Shoer, Samuel W Eaton, and Michael R Wasielewski. Excimer formation in cofacial and slip-stacked perylene-3, 4: 9, 10-bis (dicarboximide) dimers on a redox-inactive triptycene scaffold. *Physical Chemistry Chemical Physics*, 16(43):23735–23742, 2014.

[80] Yuanwei Zhang, Bosung Kim, Sheng Yao, Mykhailo V Bondar, and Kevin D Belfield. Controlled aggregation and enhanced two-photon absorption of a water-soluble squaraine dye with a poly (acrylic acid) template. *Langmuir*, 29(35):11005–11012, 2013.

[81] Somananda Sanyal, Anna Painelli, Swapan Kumar Pati, Francesca Terenziani, and Cristina Sissa. Aggregates of quadrupolar dyes for two-photon absorption: the role of intermolecular interactions. *Physical Chemistry Chemical Physics*, 18(40):28198–28208, 2016.

[82] Shiki Yagai, Tomohiro Seki, Takashi Karatsu, Akihide Kitamura, and Frank Würthner. Transformation from h-to j-aggregated perylene bisimide dyes by complexation with cyanurates. *Angewandte Chemie International Edition*, 47(18):3367–3371, 2008.

[83] Alexandru Sarbu, Laure Biniek, Jean-Michel Guenet, Philippe J Mésini, and Martin Brinkmann. Reversible j-to h-aggregate transformation in thin films of a perylenebisimide organogelator. *Journal of Materials Chemistry C*, 3(6):1235–1242, 2015.

[84] H Yamagata, DS Maxwell, J Fan, KR Kittilstved, AL Briseno, MD Barnes, and FC Spano. Hj-aggregate behavior of crystalline 7, 8, 15, 16-tetraazaterrylene: Introducing a new design paradigm for organic materials. *The Journal of Physical Chemistry C*, 118(49):28842–28854, 2014.

[85] Nicholas J Hestand, Roel Tempelaar, Jasper Knoester, Thomas LC Jansen, and Frank C Spano. Exciton mobility control through sub- å packing modifications in molecular crystals. *Physical Review B*, 91(19):195315, 2015.

[86] SM Vlaming, R Augulis, MCA Stuart, Jasper Knoester, and PHM Van Loosdrecht. Exciton spectra and the microscopic structure of self-assembled porphyrin nanotubes. *The journal of physical chemistry B*, 113(8):2273–2283, 2009.

[87] Osamu Ohno, Youkoh Kaizu, and Hiroshi Kobayashi. J-aggregate formation of a water-soluble porphyrin in acidic aqueous media. *The Journal of chemical physics*, 99(5):4128–4139, 1993.

[88] IG Scheblykin, OP Varnavsky, W Verbouwe, S De Backer, Mark Van der Auweraer, and AG Vitukhnovsky. Relaxation dynamics of excitons in j-aggregates revealing a two-component davydov splitting. *Chemical physics letters*, 282(3-4):250–256, 1998.

[89] Ashli Austin, Nicholas J Hestand, Ian G McKendry, Chuwei Zhong, Xuanyu Zhu, Michael J Zdilla, Frank C Spano, and Jodi M Szarko. Enhanced davydov splitting in crystals of a perylene diimide derivative. *The Journal of Physical Chemistry Letters*, 8(6):1118–1123, 2017.

[90] Daniel A Higgins, Philip J Reid, and Paul F Barbara. Structure and exciton dynamics in j-aggregates studied by polarization-dependent near-field scanning optical microscopy. *The Journal of Physical Chemistry*, 100(4):1174–1180, 1996.

[91] Kazuhiko Misawa, Hiroshi Ono, Kaoru Minoshima, and Takayoshi Kobayashi. New model of excitonic bands and molecular arrangement of highly oriented j-aggregates in polymer films prepared by a novel method. *Journal of luminescence*, 60:812–815, 1994.

[92] Kazuhiko Misawa, Hiroshi Ono, Kaoru Minoshima, and Takayoshi Kobayashi. New fabrication method for highly oriented j aggregates dispersed in polymer films. *Applied physics letters*, 63(5):577–579, 1993.

[93] Hans von Berlepsch, Sven Möller, and Lars Dähne. Optical properties of crystalline pseudoisocyanine (pic). *The Journal of Physical Chemistry B*, 105(24):5689–5699, 2001.

[94] Frank Balzer, Heiko Kollmann, Matthias Schulz, Gregor Schnakenburg, Arne Lutzen, Marc Schmidtmann, Christoph Lienau, Martin Silies, and Manuela Schiek. Spotlight on excitonic coupling in polymorphic and textured anilino squaraine thin films. *Crystal Growth & Design*, 17(12):6455–6466, 2017.

[95] M Muccini, E Lunedei, C Taliani, D Beljonne, J Cornil, and JL Brédas. Interchain interaction in a prototypical conjugated oligomer from polarized absorption at 4.2 k: α-sexithienyl single crystal. *The Journal of chemical physics*, 109(23):10513–10520, 1998.

[96] Michael Wykes, R Parambil, David Beljonne, and Johannes Gierschner. Vibronic coupling in molecular crystals: A franck-condon herzberg-teller model of h-aggregate fluorescence based on quantum chemical cluster calculations. *The Journal of Chemical Physics*, 143(11), 2015.

[97] Qiaoqiao Zhao, Hanjian Lai, Hui Chen, Heng Li, and Feng He. H-and j-aggregation inspiring efficient solar conversion. *Journal of Materials Chemistry A*, 9(2):1119–1126, 2021.

[98] Meng-Huan Jao, Hsueh-Chung Liao, and Wei-Fang Su. Achieving a high fill factor for organic solar cells. *Journal of Materials Chemistry A*, 4(16):5784–5801, 2016.

[99] Jianqi Zhang, Yajie Zhang, Jin Fang, Kun Lu, Zaiyu Wang, Wei Ma, and Zhixiang Wei. Conjugated polymer–small molecule alloy leads to high efficient ternary organic solar cells. *Journal of the American Chemical Society*, 137(25):8176–8183, 2015.

[100] Yaokai Li, Yuan Guo, Zeng Chen, Lingling Zhan, Chengliang He, Zhaozhao Bi, Nannan Yao, Shuixing Li, Guanqing Zhou, Yuanping Yi, et al. Mechanism study on organic ternary photovoltaics with 18.3% certified efficiency: from molecule to device. *Energy & Environmental Science*, 15(2):855–865, 2022.

[101] Chengliang He, Zeng Chen, Tonghui Wang, Ziqiu Shen, Yaokai Li, Jiadong Zhou, Jianwei Yu, Huiyu Fang, Yuhao Li, Shuixing Li, et al. Asymmetric electron acceptor enables highly luminescent organic solar cells with certified efficiency over 18%. *Nature Communications*, 13(1):2598, 2022.

[102] Thuc-Quyen Nguyen, Ignacio B Martini, Jei Liu, and Benjamin J Schwartz. Controlling interchain interactions in conjugated polymers: the effects of chain morphology on exciton-exciton annihilation and aggregation in meh- ppv films. *The Journal of Physical Chemistry B*, 104(2):237–255, 2000.

[103] Haridas Kar, Dominik W Gehrig, Frédéric Laquai, and Suhrit Ghosh. J-aggregation, its impact on excited state dynamics and unique solvent effects on macroscopic assembly of a core-substituted naphthalenediimide. *Nanoscale*, 7(15):6729–6736, 2015.

[104] Xinyu Jiang, Pauline Chotard, Kexun Luo, Felix Eckmann, Suo Tu, Manuel A Reus, Shanshan Yin, Julija Reitenbach, Christian L Weindl, Matthias Schwartzkopf, et al. Revealing donor–acceptor interaction on the printed active layer morphology and the formation kinetics for nonfullerene organic solar cells at ambient conditions. *Advanced Energy Materials*, 12(14):2103977, 2022.

[105] Sylvia J Lou, Jodi M Szarko, Tao Xu, Luping Yu, Tobin J Marks, and Lin X Chen. Effects of additives on the morphology of solution phase aggregates formed by active layer components of high-efficiency organic solar cells. *Journal of the American Chemical Society*, 133(51):20661–20663, 2011.

[106] Tonghui Wang and Jean-Luc Bredas. Organic photovoltaics: understanding the preaggregation of polymer donors in solution and its morphological impact. *Journal of the American Chemical Society*, 143(4):1822–1835, 2021.

[107] Farooq Kyeyune, Joshua L Botha, Bertus Van Heerden, Pavel Malỳ, Rienk Van Grondelle, Mmantsae Diale, and Tjaart PJ Krüger. Strong plasmonic fluorescence enhancement of individual plant light-harvesting complexes. *Nanoscale*, 11(32):15139–15146, 2019.

[108] Kyle A Baseden and Jesse W Tye. Introduction to density functional theory: Calculations by hand on the helium atom. *Journal of chemical education*, 91(12):2116–2123, 2014.

[109] Muhammad Ramzan Saeed Ashraf Janjua. Structural properties and nonlinear optical responses of halogenated compounds: a dft investigation on molecular modelling. *Open Chemistry*, 16(1):978–985, 2018.

[110] Mohamed Bourass, Adil Touimi Benjelloun, Mohammed Benzakour, Mohammed Mcharfi, Fayssal Jhilal, Françoise Serein-Spirau, Jean Marc Sotiropoulos, and Mohammed Bouachrine. Dft/td-dft characterization of conjugational electronic structures and spectral properties of materials based on thieno [3, 2-b][1] benzothiophene for organic photovoltaic and solar cell applications. *Journal of Saudi Chemical Society*, 21(5):563–574, 2017.

[111] M. J. Frisch, G. W. Trucks, H. B. Schlegel, G. E. Scuseria, M. A. Robb, J. R. Cheeseman, G. Scalmani, V. Barone, G. A. Petersson, H. Nakatsuji, X. Li, M. Caricato, A. V. Marenich,

J. Bloino, B. G. Janesko, R. Gomperts, B. Mennucci, H. P. Hratchian, J. V. Ortiz, A. F. Izmaylov, J. L. Sonnenberg, D. Williams-Young, F. Ding, F. Lipparini, F. Egidi, J. Goings, B. Peng, A. Petrone, T. Henderson, D. Ranasinghe, V. G. Zakrzewski, J. Gao, N. Rega, G. Zheng, W. Liang, M. Hada, M. Ehara, K. Toyota, R. Fukuda, J. Hasegawa, M. Ishida, T. Nakajima, Y. Honda, O. Kitao, H. Nakai, T. Vreven, K. Throssell, J. A. Montgomery, Jr., J. E. Peralta, F. Ogliaro, M. J. Bearpark, J. J. Heyd, E. N. Brothers, K. N. Kudin, V. N. Staroverov, T. A. Keith, R. Kobayashi, J. Normand, K. Raghavachari, A. P. Rendell, J. C. Burant, S. S. Iyengar, J. Tomasi, M. Cossi, J. M. Millam, M. Klene, C. Adamo, R. Cammi, J. W. Ochterski, R. L. Martin, K. Morokuma, O. Farkas, J. B. Foresman, and D. J. Fox. Gaussian˜16 Revision C.01. 2016. Gaussian Inc. Wallingford CT.

[112] Zhiying Ma, Hua Geng, Dong Wang, and Zhigang Shuai. Influence of alkyl side-chain length on the carrier mobility in organic semiconductors: herringbone vs. pi–pi stacking. *Journal of Materials Chemistry C*, 4(20):4546–4555, 2016.

[113] Guglielmo Lanzani. *The photophysics behind photovoltaics and photonics*. John Wiley & Sons, 2012.

[114] Jenny Clark, Carlos Silva, Richard H Friend, and Frank C Spano. Role of intermolecular coupling in the photophysics of disordered organic semiconductors: aggregate emission in regioregular polythiophene. *Physical review letters*, 98(20):206406, 2007.

[115] M Guesmi, MA Saidani, A Ben Fredj, S Romdhane, DAM Egbe, R Chtourou, and H Bouchriha. Temperature-dependent intermolecular coupling and exciton migration in an anthracene containing ppe-ppv copolymer. *Synthetic Metals*, 220:221–226, 2016.

[116] Yu Wang, Hongsen Wang, Jinni Deng, Yi Pan, Zhaohui Zheng, and Xiaobin Ding. Isoindigo-based dual-acceptor conjugated polymers incorporated conjugation length and intramolecular charge transfer for high-efficient photothermal conversion. *Macromolecular Rapid Communications*, 44(19):2300244, 2023.

[117] Yi Ren, Anna M Hiszpanski, Luisa Whittaker-Brooks, and Yueh-Lin Loo. Structure–property relationship study of substitution effects on isoindigo-based model compounds as electron donors in organic solar cells. *ACS Applied Materials & Interfaces*, 6(16):14533–14542, 2014.

[118] Leandro A Estrada, Romain Stalder, Khalil A Abboud, Chad Risko, Jean-Luc Bredas, and John R Reynolds. Understanding the electronic structure of isoindigo in conjugated systems: A combined theoretical and experimental approach. *Macromolecules*, 46(22):8832–8844, 2013.

[119] Paolo Salvatori, Edoardo Mosconi, Ergang Wang, Mats Andersson, Michele Muccini, and Filippo De Angelis. Computational modeling of isoindigo-based polymers used in organic solar cells. *The Journal of Physical Chemistry C*, 117(35):17940–17954, 2013.

[120] Aristide Gumyusenge, Xuyi Luo, Hongyi Zhang, Gregory M Pitch, Alexander L Ayzner, and Jianguo Mei. Isoindigo-based binary polymer blends for solution-processing of semiconducting nanofiber networks. *ACS Applied Polymer Materials*, 1(7):1778–1786, 2019.

[121] Jie Cao, Xiaoyu Luo, Shenglong Zhou, Zhixin Wu, Qi Zhao, Hua Gu, Wen Wang, Zhilin Zhang, Kaiyue Zhang, Kaiyun Li, et al. Isoindigo–thiophene d–a–d–type conjugated polymers: Electrosynthesis and electrochromic performances. *International Journal of Molecular Sciences*, 24(3):2219, 2023.

[122] Dorine Ameline, Stéphane Diring, Yoann Farre, Yann Pellegrin, Gaia Naponiello, Errol Blart, Benoît Charrier, Danilo Dini, Denis Jacquemin, and Fabrice Odobel. Isoindigo derivatives for application in p-type dye sensitized solar cells. *RSC Advances*, 5(104):85530–85539, 2015.

[123] Romain Stalder, Jianguo Mei, Kenneth R Graham, Leandro A Estrada, and John R Reynolds. Isoindigo, a versatile electron-deficient unit for high-performance organic electronics. *Chemistry of Materials*, 26(1):664–678, 2014.

[124] Wenliu Zhuang, Margherita Bolognesi, Mirko Seri, Patrik Henriksson, Desta Gedefaw, Renee Kroon, Markus Jarvid, Angelica Lundin, Ergang Wang, Michele Muccini, et al. Influence of incorporating different electron-rich thiophene-based units on the photovoltaic properties of isoindigo-based conjugated polymers: an experimental and dft study. *Macromolecules*, 46(21):8488–8499, 2013.

[125] Iqra Shafiq, Gang Wu, Mashal Khan, Muhammad Usman Khan, Saad M Alshehri, and Ke Chen. Exploration of promising photovoltaic properties of bisisoindigo-based heterocyclic chromophores for organic solar cells: A dft/td-dft study. *Journal of Saudi Chemical Society*, page 101878, 2024.

[126] Chun-Chih Ho, Sheng-Yung Chang, Tzu-Chia Huang, Chien-Ann Chen, Hsueh-Chung Liao, Yang-Fang Chen, and Wei-Fang Su. Synthesis, characterization and photovoltaic properties of poly (cyclopentadithiophene-alt-isoindigo). *Polymer Chemistry*, 4(20):5351–5360, 2013.

[127] Ergang Wang, Zaifei Ma, Zhen Zhang, Patrik Henriksson, Olle Inganäs, Fengling Zhang, and Mats R Andersson. An isoindigo-based low band gap polymer for efficient polymer solar cells with high photo-voltage. *Chemical Communications*, 47(17):4908–4910, 2011.

[128] Rui Sun, Yao Wu, Xinrong Yang, Yuan Gao, Zeng Chen, Kai Li, Jiawei Qiao, Tao Wang, Jing Guo, Chao Liu, et al. Single-junction organic solar cells with 19.17% efficiency enabled by introducing one asymmetric guest acceptor. *Advanced Materials*, 34(26):2110147, 2022.

[129] Nika Bekri, Eninges Asmare, Wendimagegn Mammo, and Newayemedhin A Tegegne. Photostability of benzodithiophene based polymer: effect of pc60bm and intermolecular interactions. *Materials Research Express*, 9(5):055502, 2022.

[130] Newayemedhin A Tegegne, Zelalem Abdissa, Wendimagegn Mammo, Takayuki Uchiyama, Yoshiko Okada-Shudo, Francesco Galeotti, William Porzio, Mats R Andersson, Derck Schlettwein, Varun Vohra, et al. Effect of alkyl side chain length on intra-and intermolecular interactions of terthiophene–isoindigo copolymers. *The Journal of Physical Chemistry C*, 124(18):9644–9655, 2020.

[131] Frank C Spano. The spectral signatures of frenkel polarons in h-and j-aggregates. *Accounts of chemical research*, 43(3):429–439, 2010.

[132] Michelle Leifeld Raicoski and Marcelo Goncalves Vivas. Photobleaching kinetics of meh-ppv in solution: the role of conformational disorder. *The Journal of Physical Chemistry B*, 125(34):9887–9894, 2021.

[133] Suchi Guha, JD Rice, YT Yau, Christopher M Martin, Meera Chandrasekhar, Holalkere R Chandrasekhar, R Guentner, P Scanduicci De Freitas, and Ullrich Scherf. Temperature-dependent photoluminescence of organic semiconductors with varying backbone conformation. *Physical Review B*, 67(12):125204, 2003.

[134] Edward Condon. A theory of intensity distribution in band systems. *Physical Review*, 28(6):1182, 1926.

[135] Edward U Condon. Nuclear motions associated with electron transitions in diatomic molecules. *Physical Review*, 32(6):858, 1928.

[136] Hao Tang, Chen Wen Wang, Feng Long Gu, and Chaoyuan Zhu. Absorption and fluorescence spectra of conjugated polymers poly (propylene oxide)–poly (phenylene ethynylene) interpreted by franck–condon simulation. *Journal of Physical Organic Chemistry*, 34(11):e4261, 2021.

[137] Takao Itoh. Franck-condon analysis of the absorption and fluorescence spectra of all trans α, ω-diphenylpolyenes with one to seven polyene double bonds. *The Journal of chemical physics*, 123(6), 2005.

[138] FAC Oliveira, LA Cury, A Righi, RL Moreira, PSS Guimaraes, FM Matinaga, MA Pimenta, and RA Nogueira. Temperature effects on the vibronic spectra of beh–ppv conjugated polymer films. *The Journal of chemical physics*, 119(18):9777–9782, 2003.

[139] Joseph Razzell-Hollis, Franziska Fleischli, Ashlee A Jahnke, Natalie Stingelin, Dwight S Seferos, and Ji-Seon Kim. Effects of side-chain length and shape on polytellurophene molecular order and blend morphology. *The Journal of Physical Chemistry C*, 121(4):2088–2098, 2017.

[140] Henrik Tylli, Henrik Konschin, and Birgitta Fagerström. The methyl and methoxyl torsional modes and the lattice vibration in the low-frequency raman spectrum of 1, 4-dimethoxybenzene. *Journal of molecular structure*, 128(4):297–304, 1985.

[141] Baocai Du, Jicheng Yi, He Yan, and Tao Wang. Temperature induced aggregation of organic semiconductors. *Chemistry–A European Journal*, 27(9):2908–2919, 2021.

[142] I Bitsanis, HT Davis, and M Tirrell. Brownian dynamics of nondilute solutions of rodlike polymers. 1. low concentrations. *Macromolecules*, 21(9):2824–2835, 1988.

[143] Katsuichi Kanemoto, Tatsuji Sudo, Ichiro Akai, Hideki Hashimoto, Tsutomu Karasawa, Yoshio Aso, and Tetsuo Otsubo. Intrachain photoluminescence properties of conjugated polymers as revealed by long oligothiophenes and polythiophenes diluted in an inactive solid matrix. *Physical Review B*, 73(23):235203, 2006.

[144] Oleksandr V Mikhnenko, Paul WM Blom, and Thuc-Quyen Nguyen. Exciton diffusion in organic semiconductors. *Energy & Environmental Science*, 8(7):1867–1888, 2015.

[145] Christian Würth, Markus Grabolle, Jutta Pauli, Monika Spieles, and Ute Resch-Genger. Relative and absolute determination of fluorescence quantum yields of transparent samples. *Nature protocols*, 8(8):1535–1550, 2013.

[146] Shuang Pan, Mingjing Zhu, Luze He, Hongdong Zhang, Feng Qiu, Zhiqun Lin, and Juan Peng. Transformation from nanofibers to nanoribbons in poly (3-hexylthiophene) solution by adding alkylthiols. *Macromolecular Rapid Communications*, 39(11):1800048, 2018.

[147] Mincheol Chang, Jiho Lee, Nabil Kleinhenz, Boyi Fu, and Elsa Reichmanis. Photoinduced anisotropic supramolecular assembly and enhanced charge transport of poly (3-hexylthiophene) thin films. *Advanced Functional Materials*, 24(28):4457–4465, 2014.

[148] Benedetta Carlotti, Zhengxu Cai, Hyungjun Kim, Valerii Sharapov, Ifeanyi Kizito Madu, Donglin Zhao, Wei Chen, Paul M Zimmerman, Luping Yu, and Theodore Goodson III. Charge transfer and aggregation effects on the performance of planar vs twisted nonfullerene acceptor isomers for organic solar cells. *Chemistry of Materials*, 30(13):4263–4276, 2018.

[149] Muhammad Umar Saeed, NMA Hadia, Javed Iqbal, MM Hessien, Ahmed M Shawky, Muhammad Ans, Naifa S Alatawi, and Rasheed Ahmad Khera. Impact of end-group modifications and planarity on bdp-based non-fullerene acceptors for high-performance organic solar cells by using dft approach. *Journal of Molecular Modeling*, 28(12):397, 2022.

[150] Tian Lu. Simple, reliable, and universal metrics of molecular planarity. *Journal of molecular modeling*, 27(9):263, 2021.

[151] Mariam Ishtiaq, Muhammad Waqas, Hira Zubair, Rana Farhat Mehmood, Nabil Al-Zaqri, Rasheed Ahmad Khera, Mahmoud AA Ibrahim, and Javed Iqbal. Theoretical designing of symmetrical non-fullerene acceptor molecules by end-capped modification for promising photovoltaic properties of organic solar cells. *Journal of Molecular Liquids*, 386:122473, 2023.

[152] Shihan Zhao, Jiameng Cao, Qian Liu, and Xianbin Zhang. Fine-tuning the π bridge of organic dye molecules with triarylamino as an electron donor by using electron-rich/deficient groups for more efficient dye-sensitized solar cells. *Molecular Physics*, 120(13):e2093286, 2022.

[153] Rania Zaier, Arnaud Martel, and Tomasz J Antosiewicz. Effect of benzothiadiazole-based π-spacers on fine-tuning of optoelectronic properties of oligothiophene-core donor materials for efficient organic solar cells: A dft study. *The Journal of Physical Chemistry A*, 127(50):10555–10569, 2023.

[154] Tridip Chutia, Shahnaz Ahmed, and Dhruba Jyoti Kalita. A rational design of dithieno-benzodithiophene based acceptors for organic solar cells. *Computational and Theoretical Chemistry*, 1228:114282, 2023.

[155] Newayemedhin A Tegegne, Asfaw Negash, Desalegn Yilma, Kidan G Gebremariam, Zewdneh Genene, Wendimagegn Mammo, and Neill J Goosen. Tailoring intra-molecular coupling in bdt-based copolymers to enhance their performance in fullerene-free organic solar cells. *Materials Advances*, 4(24):6694–6703, 2023.

[156] Nanjia Zhou, Xugang Guo, Rocio Ponce Ortiz, Tobias Harschneck, Eric F Manley, Sylvia J Lou, Patrick E Hartnett, Xinge Yu, Noah E Horwitz, Paula Mayorga Burrezo, et al. Marked consequences of systematic oligothiophene catenation in thieno [3, 4-c] pyrrole-4, 6-dione and bithiopheneimide photovoltaic copolymers. *Journal of the American Chemical Society*, 137(39):12565–12579, 2015.

[157] Qiang Tao, Yuxin Xia, Xiaofeng Xu, Svante Hedstrom, Olof Backe, David I James, Petter Persson, Eva Olsson, Olle Inganas, Lintao Hou, et al. D–a1–d–a2 copolymers with extended donor segments for efficient polymer solar cells. *Macromolecules*, 48(4):1009–1016, 2015.

[158] Nicolas Blouin, Alexandre Michaud, David Gendron, Salem Wakim, Emily Blair, Rodica Neagu-Plesu, Michel Belletete, Gilles Durocher, Ye Tao, and Mario Leclerc. Toward a rational design of poly (2, 7-carbazole) derivatives for solar cells. *Journal of the American Chemical Society*, 130(2):732–742, 2008.

[159] Ghulam Bary, Lubna Ghani, Muhammad Imran Jamil, Muhammad Arslan, Waqar Ahmed, Anees Ahmad, Muhammad Sajid, Riaz Ahmad, and Duohui Huang. Designing small organic non-fullerene acceptor molecules with diflorobenzene or quinoline core and dithiophene donor moiety through density functional theory. *Scientific Reports*, 11(1):19683, 2021.

[160] Rudranarayan Khatua, Bibhas Das, and Anirban Mondal. Rational design of non-fullerene acceptors via side-chain and terminal group engineering: a computational study. *Physical Chemistry Chemical Physics*, 25(11):7994–8004, 2023.

[161] Smiti Rani Bora and Dhruba Jyoti Kalita. End group modulation of a–d–a type small donor molecules for dtp based organic photovoltaic solar cells: a dft approach. *RSC advances*, 13(38):26418–26429, 2023.

[162] Cansu Zeytun Karaman, Seza Göker, Ümmügülsüm Şahin, Serife O Hacioglu, Sultan Taşkaya Aslan, Tuğba Hacıefendioğlu, Gonul Hizalan, Erol Yıldırım, Ali Çırpan, and Levent Toppare. Effect of thiophene, 3-hexylthiophene, selenophene, and thieno [3, 2-b] thiophene spacers on opv device performance of novel 2, 1, 3-benzothiadiazole based alternating copolymers. *Journal of Electroanalytical Chemistry*, 895:115483, 2021.

[163] Dandan Tu, Yu Qiao, Yongfeng Ni, Xin Guo, and Can Li. Structural engineering of anthracene diimide polymers for molecular ordering manipulation. *Macromolecules*, 55(10):4102–4110, 2022.

[164] Fatima Bencheikh, David Duché, Carmen M Ruiz, Jean-Jacques Simon, and Ludovic Escoubas. Study of optical properties and molecular aggregation of conjugated low band gap

copolymers: Ptb7 and ptb7-th. *The Journal of Physical Chemistry C*, 119(43):24643–24648, 2015.

[165] Linlin Liu, Tao Han, Xiaoyan Wu, Song Qiu, Baoling Wang, Muddasir Hanif, Zengqi Xie, and Yuguang Ma. Aggregation behaviors of ladder-type poly (p-phenylene) in dilute solutions and spin-coated films. *The Journal of Physical Chemistry C*, 119(21):11833–11838, 2015.

[166] Katsuichi Kanemoto, Ichiro Akai, Mitsuru Sugisaki, Hideki Hashimoto, Tsutomu Karasawa, Nobukazu Negishi, and Yoshio Aso. Temperature effects on quasi-isolated conjugated polymers as revealed by temperature-dependent optical spectra of 16-mer oligothiophene diluted in a sold matrix. *The Journal of chemical physics*, 130(23), 2009.

[167] Joshua L. Botha, Bertus van Heerden, and Tjaart P.J. Krüger. Advanced analysis of single-molecule spectroscopic data. *Biophysical Reports*, 4(3):100173, 2024.

[168] JW Blatchford, TL Gustafson, AJ Epstein, DA Vanden Bout, J Kerimo, DA Higgins, PF Barbara, D-K Fu, T Mo Swager, and AG MacDiarmid. Spatially and temporally resolved emission from aggregates in conjugated polymers. *Physical Review B*, 54(6):R3683, 1996.

[169] M Guesmi, A Ben Fredj, S Romdhane, N Bouguerra, DAM Egbe, RW Lang, M Havlicek, NS Sariciftci, and H Bouchriha. Effect of alkoxy side chains on intra and interchain exciton coupling in ppe-ppv copolymers solution. *Synthetic Metals*, 224:72–79, 2017.

[170] M Guesmi, A Ben Fredj, S Romdhane, N Bouguerra, DAM Egbe, RW Lang, M Havlicek, and H Bouchriha. Impact of alkoxy side chains on morphology and excitonic coupling in ppe-ppv copolymer thin films. *Journal of Luminescence*, 203:447–454, 2018.